Relating Cardiac Electrical and Mechanical Alternans to Ventricular Stability

by

Edward Arthur Clancy

B.S., Worcester Polytechnic Institute
(1983)

SUBMITTED IN PARTIAL FULFILLMENT

OF THE REQUIREMENTS OF THE

DEGREE OF

MASTER OF SCIENCE

IN ELECTRICAL ENGINEERING AND COMPUTER SCIENCE

at the

MASSACHUSETTS INSTITUTE OF TECHNOLOGY

January 1987

Signature of Author _____
Department of Electrical Engineering and Computer Science
January 16, 1987

Certified by _____
Richard J. Cohen
Thesis Supervisor

Accepted by _____
Arthur C. Smith
Chairman, Department Committee on Graduate Students

Relating Cardiac Electrical and Mechanical Alternans to Ventricular Stability

by

Edward Arthur Clancy

Submitted to the Department of Electrical Engineering and Computer Science on January 16, 1987 in partial fulfillment of the requirements for the Degree of Master of Science in Electrical Engineering and Computer Science

Abstract

The prevention of sudden cardiac death (SCD) remains a challenge to contemporary medicine. SCD is often thought to be the result of a malignant cardiac rhythm known as ventricular fibrillation (VF). A non-invasive measure of the stability of the cardiac rhythm (susceptibility of the heart to VF) has long been sought as a means to identify and prospectively treat the individual at risk for SCD. Smith and Cohen (1984) and Smith et al. (1985) have found that a subtle alternation in the surface ECG (electrical alternans) may provide a measure of ventricular stability. In both finite-element and physiologic models, they found that the degree of electrical alternans detected in the surface ECG was correlated with the instability of the cardiac rhythm. Electrical alternans is an every other beat variation in the contour of the ECG waveform. Thus, beat 1 is similar to beats 3,5,7... and beat 2 is similar to beats 4,6,8,..., but the odd and even beats are dissimilar. The source of the alternation was theorized to be a spatial-temporal alternation in the contour of the heart beat. This thesis proposes that if alternation occurs via the above mechanism, then the spatial-temporal alternation will also cause a mechanical alternation in the heart beat (mechanical alternans). The mechanical alternans, reflected in the contour of the blood pressure and volume waveforms, may provide additional information as to the stability of the heart. A computer model, similar to that of the above authors, and a physiologic model of the heart were constructed to test the theory of combined electrical-mechanical alternans. Both models found 1) a regime of combined electrical-mechanical alternans during the transition from a normal rhythm towards a fibrillatory rhythm, 2) the detected degree of alternation to be correlated with the relative instability of the rhythm, and 3) that the electrical and mechanical alternans may be the result of a single underlying mechanism consistent with the theory of a spatial-temporal alternation in the contour of the heart beat.

Thesis Supervisor: Richard J. Cohen
Title: Associate Professor of Health Sciences and Technology

Acknowledgements

This work was supported by ONR grant #N0014-80-C-0520, award #F33615-84-C-0601 from USAF School of Aerospace Medicine, NASA grants #NAG-327 and #NAGW-988, ONR contract #N0014-79-C-0168 to the Naval Blood Research Laboratory, Boston University School of Medicine, and a grant from the RJR-Nabisco Company.

This thesis represents the culmination of three and one half years of graduate study - one half year in the General Electric Company A Course, one year part-time at M.I.T., and two years full-time at M.I.T. I wish to thank all of the people who have been a part of my growth during this time.

Thanks to Buddy Gregory, Harvey Dragoon and Bob Bianchi at General Electric for supporting me professionally, academically and personally during my year and one half stay at General Electric. Thanks to Samir Sayegh for his great "vigor for the intellect" which he instilled throughout the A Course.

My jump to full-time status at M.I.T. was made possible by the invite of Richard Cohen. Thank you, Richard, for opening this path and for guiding me along it. Thanks to Joe Smith who served as my mentor here at M.I.T. and taught me much of which is reported herein.

Thanks to Terry Sylvina for her support in the animal work, and for always teaching and encouraging the proper place of animals in research. Thanks to Dr. Valeri and Joe Polumba of the Naval Blood Research Laboratory for all of their support.

Thanks to all the members of the Cohen lab for their exchange of ideas, and, more importantly, for their friendship.

Thanks to Mary Tosches for opening so many doors of my imagination.

Thanks to the whole Clancy gang - Jack, Ann, Jen, Sean, Bob, Carol, Paul, Diane, Mary, Kathy, Mom and Dad. Thanks especially to Mom and Dad.

Finally, I give thanks to my God. I hope that He has been and continues to be the Heart and Soul of all that I do.

Table of Contents

List of Figures

Chapter I

Introduction

Sudden Cardiac Death (SCD) claims close to 500,000 lives annually in the United States (Horowitz and Morganroth, 1982). The majority of these deaths occur outside the hospital setting and represent the first symptom of any cardiac disease. Lown (1979) termed SCD "...the major challenge confronting contemporary cardiology." Presently, there exists no screening technique available to the general public for confident identification of the individual specifically at risk for SCD. An ability to non-invasively assess susceptibility to SCD would facilitate identification of the individual at risk as well as provide a tool for monitoring corrective therapy.

The majority of SCD's are thought to be the result of a cardiac rhythm disturbance known as ventricular fibrillation (VF). In VF, the normally synchronous contraction of the ventricles degenerates into a chaotic contraction which yields no net flow of blood out of the heart. Death ensues rapidly. The initiation of VF is often thought to be facilitated by a fractionation, or breaking-up, in the propagation of the cardiac action potential. Normally, an electrical wave of depolarization spreads throughout the resting (or repolarized) heart in one fluent sweep. Figure 1.1 depicts the flow of the normal depolarization wave through a region of the heart. Each element in the figure represents a local macroscopic region of the heart. After a time period governed by local biological clocks, individual elements within the heart repolarize. Figure 1.2 depicts this asynchronous nature of repolarization. During the time from depolarization to repolarization, the element is refractory to further depolarization. Thus, if, as shown in Figure 1.3, a second depolarization wave enters a refractory (or partially refractory) region, the wave will be forced to travel around

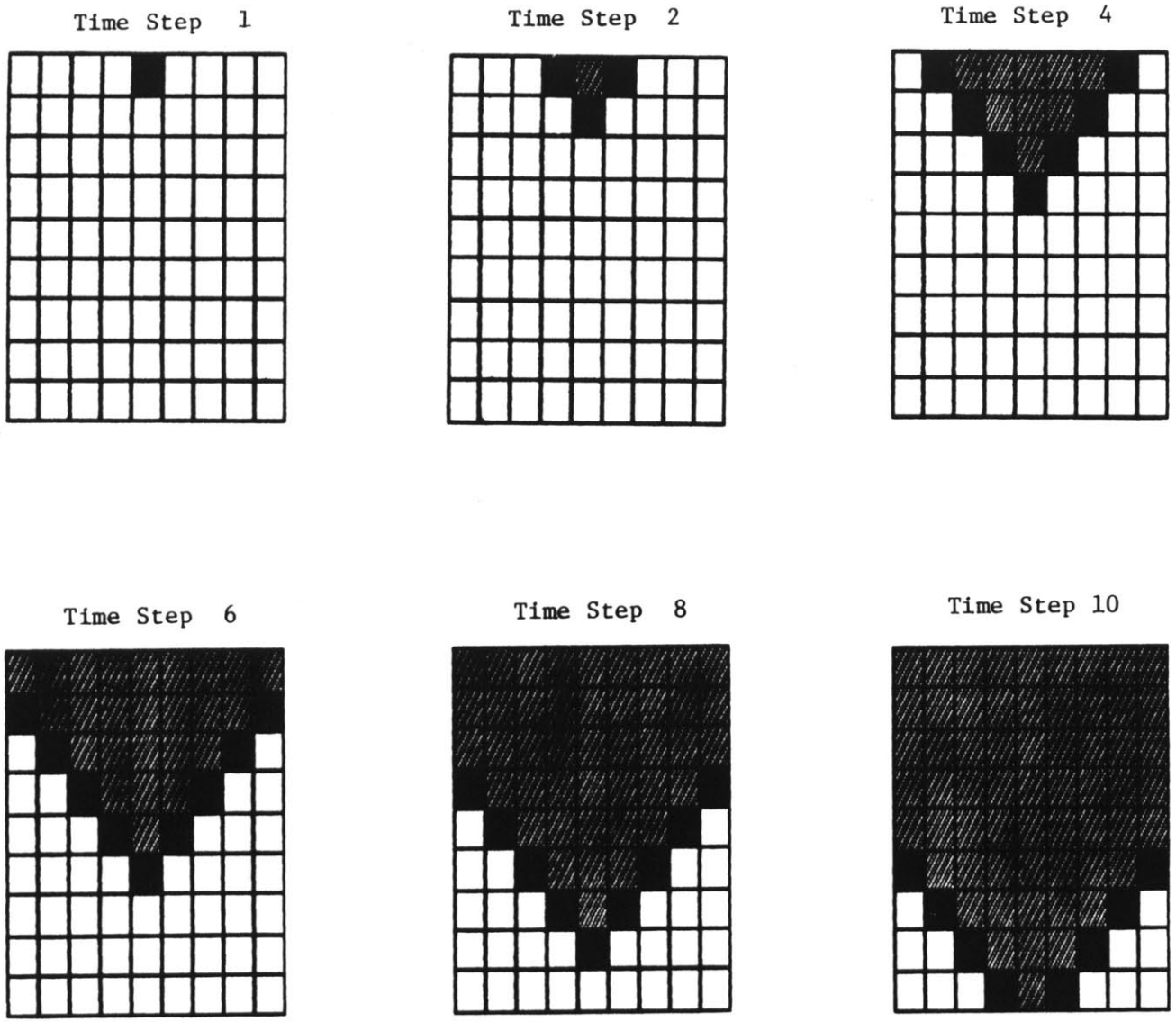

Figure 1.1: Schematic of a Normal Depolarizing Wave

Figure depicts the fluent flow (from top to bottom during time steps 0-10) of a normal depolarizing wave through a region of the heart. A white box represents a repolarized area. A gray box represents a depolarized area. A black box represents a recently depolarized area and shows the front of the depolarizing wave.

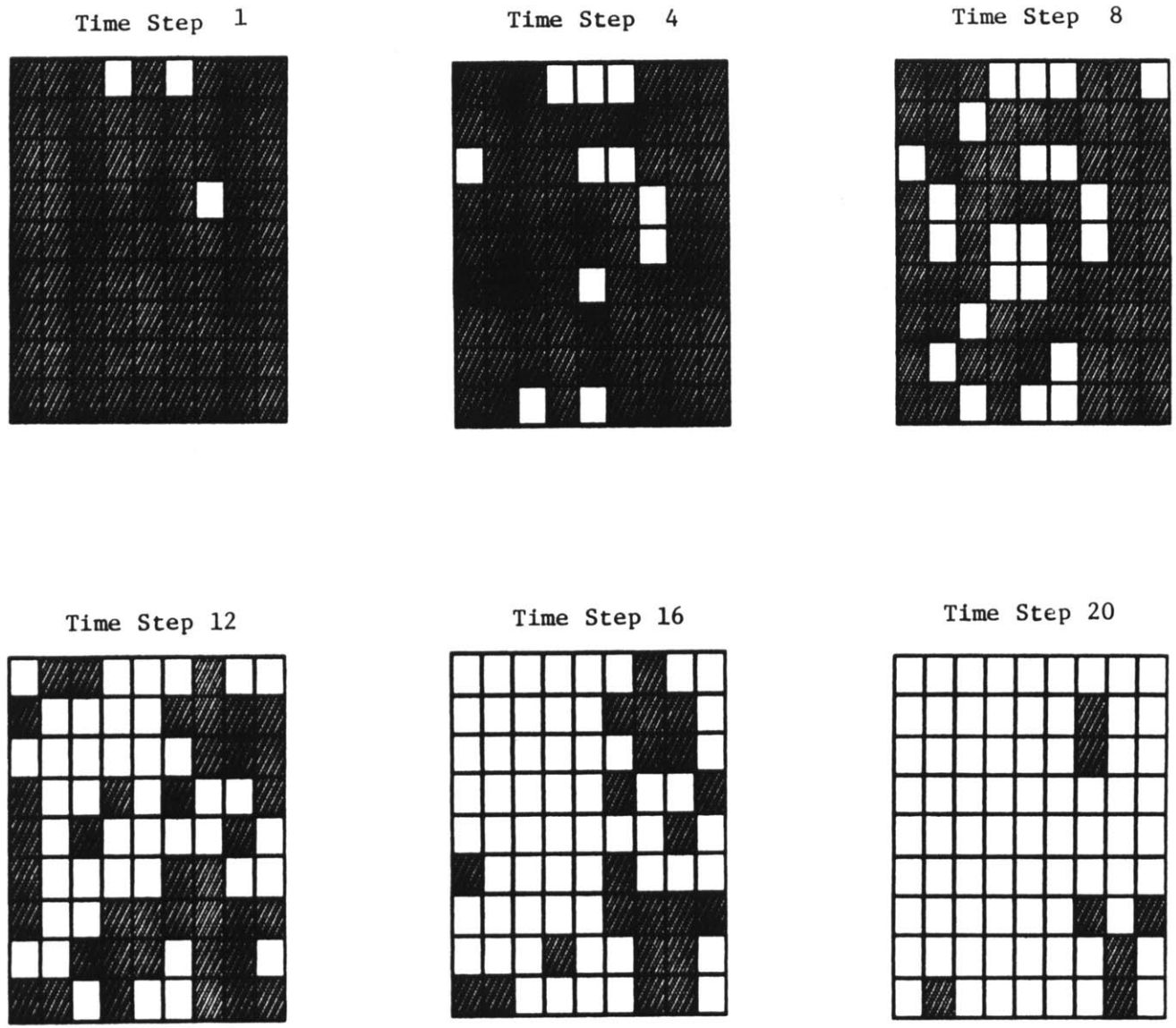

Figure 1.2: Schematic of Normal Repolarization

The asynchronous nature of repolarization is pictured in time steps 0-20. A white box represents a repolarized area. A gray box represents a depolarized area.

the refractory regions. This process is wavefront fractionation. The synchrony of the beat has been degraded. Increased fractionation can lead to VF - a totally chaotic self-sustained activation of the ventricles.

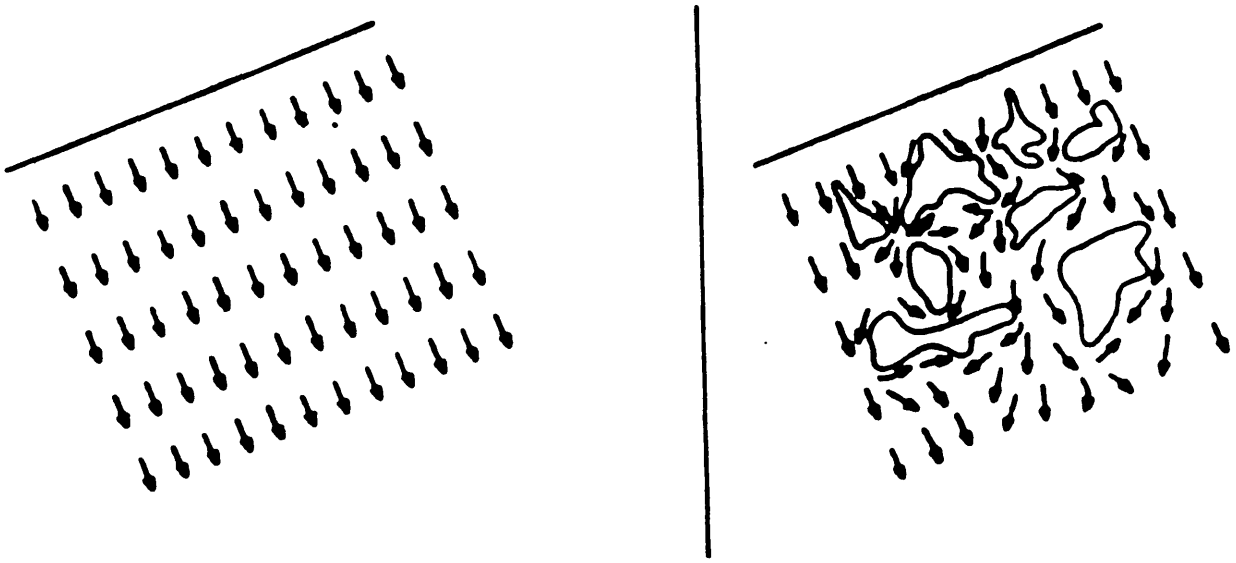

Figure 1.3 Fractionation of the Depolarizing Wavefront

Islands of refractory tissue serve to fractionate the impinging wavefronts of excitation. (From Smith and Cohen, 1984)

Smith and Cohen (1984) constructed a simple finite-element computer model of ventricular conduction. This model incorporated the asynchronous nature of repolarization via the spatial dispersion in cellular refractory periods noted by Han and Moe (1964) and Han et al. (1966). The model displayed a wide range of ventricular rhythm disturbances including VF. Smith and Cohen (1984) found that a region of surface electrical alternans was consistently encountered during the

transition from a normal rhythm to a chaotic rhythm. Surface electrical alternans is a disturbance of the electrical activity of the heart, noted at the body surface, such that every second beat looks the same, but adjacent beats look different (see Figure 1.4).

Figure 1.4: Schematic Drawing of Surface Electrical Alternans

Surface electrical alternans is a disturbance of the electrical activity of the heart such that every second beat looks the same, but adjacent beats look different. In the above figure, both the height and the shape of the waveform alternate.

Smith and Cohen (1984) claimed that a spatial-temporal alternation in the contour of the heart beat developed from a population of elements whose long refractory periods prohibited them from being depolarized every heart beat. Adam et al. (1984), Smith (1985), and Smith et al. (1985) further showed in an animal model an inverse correlation between the degree of electrical alternation present at the body surface and the susceptibility of the ventricles to fibrillate. Thus, electrical alternans may serve as a measure of the susceptibility of the heart to VF.

This thesis develops this theory of alternation of the heart to hypothesize that an alternation in the mechanical activity of the heart accompanies electrical alternation. The mechanism of the mechanical alternans is attributed to the spatial-temporal alternation in the contour of the heart beat. The hypothesis is examined in a finite-element electrical-mechanical model of the heart and in an animal model. The finite-element model incorporates the dispersion of cellular refractory period principle as well as some of the salient mechanical attributes of the heart and peripheral circulation. The animal model consisted of acute dog preparations in which a decrease in ventricular stability was induced via rapid atrial pacing and systemic hypothermia. Results from both models will seek to define a relationship between electrical-mechanical alternation of the heart and ventricular stability.

The Chapters Which Follow:

Chapter II: Anatomy and Physiology of the Cardiovascular System

This chapter presents background information on the anatomy and physiology of the cardiovascular system. The electrical and mechanical activity of individual cardiac cells, as well as the composite heart is described. Mathematical models of components of the cardiovascular system are introduced.

Chapter III: Sudden Cardiac Death

Chapter III illuminates the extent of the problem of SCD. The mechanisms of VF (the malignant rhythm disturbance thought to be responsible for the majority of SCD's) are reviewed. An association between the spatial dispersion in the properties of individual myocardial cells and the susceptibility to VF is made.

Chapter IV: Dispersion of Refractoriness and Alternation of the Heart

A mathematical model of the electrical properties of the heart which includes a spatial dispersion in the electrical properties of individual myocardial elements (Smith and Cohen, 1984) is reviewed. A region of alternation in the electrical activity of the model occurs during the transition from normal model behavior to chaotic (resembling VF) model behavior. The mechanism for this alternation is attributed to the element dispersion. Physiologic data is presented which further supports the development of electrical alternans as a precursor to VF. It is then predicted that an alternation in mechanical activity should

accompany the electrical alternans.

Chapter V: Mechanisms of Electrical and Mechanical Alternans

This chapter is a literature review of the present understanding of the mechanisms of electrical alternans and mechanical alternans. Note that, in general, these two forms of alternans are studied independently.

Chapter VI: A Finite-Element Electrical-Mechanical Model of the Heart

The heart model of Smith and Cohen (1984) is incorporated into an electrical-mechanical model of the heart. The model is exercised and the transition between a normal rhythm and a chaotic rhythm studied. Alternation in the electrical and mechanical response of the model is quantified and compared to the degree of dispersion in element properties.

Chapter VII: A Physiologic Model of Electrical-Mechanical Alternans

A physiologic model of electrical-mechanical alternans is developed in the anesthetized dog. Systemic hypothermia and rapid atrial pacing are employed to alter the relative electrical stability of the ventricles. Electrical and mechanical alternation is quantified and correlated to the hypothermia and pacing interventions.

Chapter VIII: Final Discussion

Chapter VIII is a final discussion which relates the major themes presented in the finite-element model, the physiologic model and throughout the thesis.

Chapter IX: Conclusion

Chapter X: References

Chapter II

Anatomy and Physiology of the Cardiovascular System

2.1 Gross Cardiovascular Anatomy and Function

The heart, arteries and veins form the cardiovascular system. The heart is a hollow, muscular, valved pump which cyclically contracts and relaxes, propelling blood throughout the cardiovascular system. The arteries and veins form a complete closed-loop system in which essential nutrients are transported to and removes wastes from all regions of the body. An adequate flow of blood to the body tissues is essential to the sustenance of life.

The heart is comprised of a right side and a left side with a total of four pumping chambers and four valves as shown in Figure 2.1. The right side of the heart pumps blood returned from the veins into the pulmonary circulation. The left side of the heart pumps blood from the pulmonary circulation into the systemic circulation. Venous blood enters the right atrium of the heart from the inferior vena cava, superior vena cava and the coronary sinus. Blood from the right atrium flows unidirectionally through the tricuspid valve into the right ventricle. Blood from the right ventricle is propelled through the pulmonic valve and into the pulmonary circulation to be oxygenated. This completes the pumping circuit in the right heart. Similarly, in the left heart, blood flows from the pulmonary circulation into the left atrium, through the mitral valve into the left ventricle, and then through the aortic valve into the systemic circulation. The blood circuit is completed through the arteries and veins.

The atrial chambers are thin-walled, reflecting the normally low pressures (less than 10 mmHg) developed in these cavities. The ventricles are thick-walled chambers. The left ventricular muscle (or

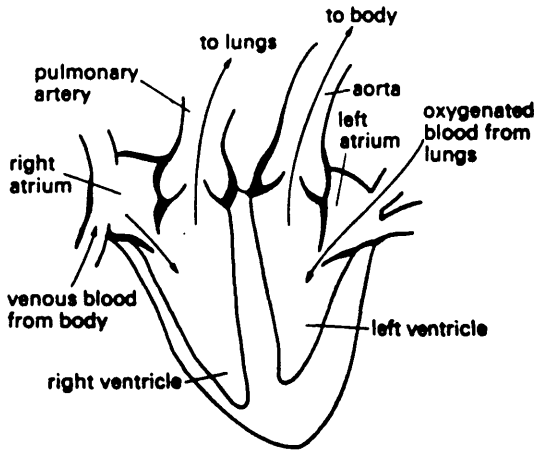

Figure 2.1: Basic Anatomy of the Heart

Diagrammatic representation of anatomy and directions of blood flow in the heart. (From Caro et al., 1978)

myocardium) is the thickest and most massive chamber. The left ventricle performs the major portion of the pumping work of the heart.

The cardiac valves passively open and close to limit the flow of blood in the heart to one direction. The valves are comprised of extremely thin (about 0.1 mm) durable cusps. The tricuspid, pulmonic and aortic valves contain three cusps, while the mitral valve contains only two cusps. The tricuspid and mitral valves are termed the atrioventricular valves, while the pulmonic and aortic valves are termed the semilunar valves.

The entire heart is encased within a thin fibrous tissue sac termed the pericardium. The moist inner lining of the pericardium allows the heart to rotate within the thorax without producing friction between

itself and other internal organs. The pericardial sac stretches easily to accommodate normal heart volumes, but is quite unyielding to above normal volumes.

The systemic arteries and veins form the vascular system. As blood leaves the outflow tract of the left ventricle, it enters the aorta. The aorta branches into numerous arteries. These arteries, in turn, branch into arterioles and then capillaries. The capillaries lead to the venules. The major exchange of cellular substances with the blood is made in the arterioles, capillaries and venules (together these vessels are termed the microcirculation). From the venules, blood travels through veins to the superior and inferior venae cavae. The venae cavae then lead to the right atrium of the heart.

2.2 Mechanics of the Cardiac Cycle

Figure 2.2 shows a diagrammatic illustration of the mechanical

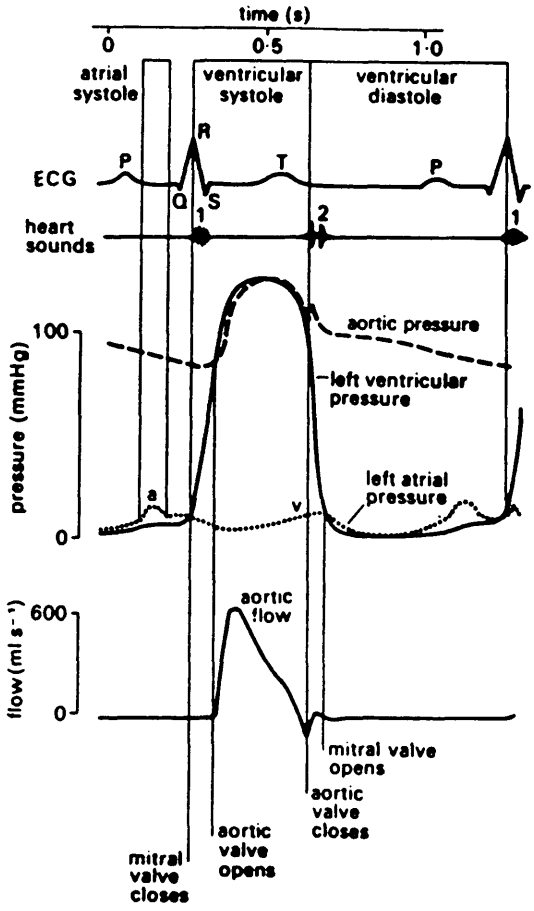

Figure 2.2: Diagrammatic Illustration of the Mechanical Events in the Cardiac Cycle

Mechanical activity in the left side of the heart is drawn as a function of time. (From Caro el al., 1978)

events in the cardiac cycle. Initially, the heart is relaxed. Both sides of the heart fill with blood due to a passive pressure gradient existing from the filling blood (venae cavae and coronary sinus for the

right heart and pulmonary veins for the left heart) to the atria to the ventricles. The transmural pressure exerted in the atria and ventricles by the filling blood is termed the preload. This preload is a relatively constant venous pressure for the right side of the heart and a relatively constant pulmonary vein pressure for the left side of the heart. Contraction begins as both atria squeeze to force blood into their respective ventricles. The atria serve as "booster pumps" to augment the filling volume of the ventricular chambers. Following a short delay, the ventricular myocardium contracts. This time delay of approximately 0.2 seconds synchronizes atrioventricular contraction to maximize the volume of blood boosted into the ventricle by the atria. As the ventricle contracts, ventricular pressure rises until the flow through the atrioventricular valves is reversed in direction and the valves close. Ventricular pressure continues to rise during the ensuing period of isovolumic contraction. When ventricular pressure exceeds the pressure beyond the semilunar valve (ventricular outflow valve), the valve opens. The pressure which exists beyond the semilunar valve (pulmonary artery pressure for the case of the right heart and aortic pressure for the case of the left heart) is termed the afterload. Frank (1888) modeled left ventricular afterload as a vascular compliance shunted by a vascular resistance, connected to a flow sink (mechanical flow "ground"). This is a popular model which is known as the Windkessel model.

The opening of the semilunar valves signals the start of the ejection phase. Blood is ejected through the outflow tract of the ventricle. Eventually, the ventricle empties sufficiently and begins to relax. When ventricular pressure falls below the afterload pressure the

semilunar valves close and the ejection phase is complete. The ventricles now enter a period of isovolumic relaxation. Isovolumic relaxation continues until the ventricular pressure falls below the atrial pressure. At this point the atrioventricular valves open and diastolic filling commences. The four phases- diastolic filling, isovolumic contraction, ejection and isovolumic relaxation- repeat to form the mechanical events of the cardiac cycle. A typical healthy adult will maintain a peak (systolic) arterial pressure of 120 mmHg and a minimum (diastolic) arterial pressure of 80 mmHg.

The ability of the heart to contract is termed "myocardial contractility." The measurement of myocardial contractility has received considerable attention and debate in the literature. Recent evidence, derived from physiologic modeling of the in vitro dog left ventricle (Suga and Sagawa, 1974; Suga et al., 1973; Sunagawa et al., 1982; Sunagawa and Sagawa, 1982) suggests that the instantaneous volume-pressure ratio provides a reliable measure of instantaneous myocardial contractility. The volume-pressure ratio, Q(t)/P(t), is termed the capacitance, C(t). These investigators demonstrated that C(t) is an instantaneous intrinsic measure of cardiac contractility independent of ventricular volume or outflow impedance. The ventricle is thus viewed as a volume storage device. The pumping action of the heart is achieved by cyclically altering is storage capability. In the context of the cardiac cycle, C(t) is at a maximum during diastolic filling, decreases during isovolumic contraction and ejection, finds its minimum value, and then increases during isovolumic relaxation.

2.3 Electrophysiology of the Heart

Cardiac mechanical activity is triggered by an electrical action potential which originates from a focus within the heart. The electrical activity traverses the entire heart in a synchronous fashion to elicit a coordinated mechanical contraction. An understanding of this process is derived from the cellular electrical and mechanical physiology. From the knowledge of cellular electrophysiology, the specialized electrical conduction system can be introduced and the normal sequence of myocardial excitation presented. A theoretical model for understanding the surface electrocardiogram (ECG) - the electrical activity of the heart which is observable at the body surface - will then be reviewed.

2.3.1 Cellular Electrophysiology

The membrane of the cardiac cell is semi-permeable to potassium (K), sodium (Na), chloride (Cl), calcium (Ca) ions and other less significant ions. Ions flow across the cell membrane through numerous functionally independent channels. Gradients of these ionic species are maintained across the cell membrane by ionic pumps. For each ion, an equilibrium potential, E_i, between the inside and the outside of the cell is established according to the Nernst equilibrium equation;

$$E_i = \frac{R\,T}{Z_i F} \ln\left[\frac{C_{out_i}}{C_{in_i}}\right] \qquad (2.1)$$

where

R = gas constant (8.2 joules/(mole*degree K)),

T = absolute temperature in degrees K,

F = Faraday's constant (9.65×10^4 coul/mole),

Z_i = valence of the i^{th} ion,

C_{out_i} = molar concentration of the i^{th} ion outside of the cell,

C_{in_i} = molar concentration of the i^{th} ion inside of the cell.

Figure 2.3 gives an electrical circuit model of a unit area of the cell membrane. V_M is the transmembrane potential (potential inside the cell - potential outside the cell), C_M is the membrane capacitance, J_M is the membrane current density, and g_i is the membrane conductance of the i^{th} ionic species. The membrane conductance, g_i, is an index of the ability of the membrane to carry the flow of the i^{th} ionic species across the membrane. From Figure 2.3 an expression for the transmembrane potential can be written as;

$$J_M = C_M \frac{dV_M}{dt} + \sum_i g_i (V_M - E_i) \qquad (2.2)$$

If the cell is at rest ($dV_M/dt = 0$) and there is no externally applied current ($J_M = 0$), then the transmembrane potential is given by;

$$V_M^o = \frac{g_K}{g_M} E_K + \frac{g_{Na}}{g_M} E_{Na} + \frac{g_{Ca}}{g_M} E_{Ca} + \frac{g_{Cl}}{g_M} E_{Cl} + \ldots \qquad (2.3)$$

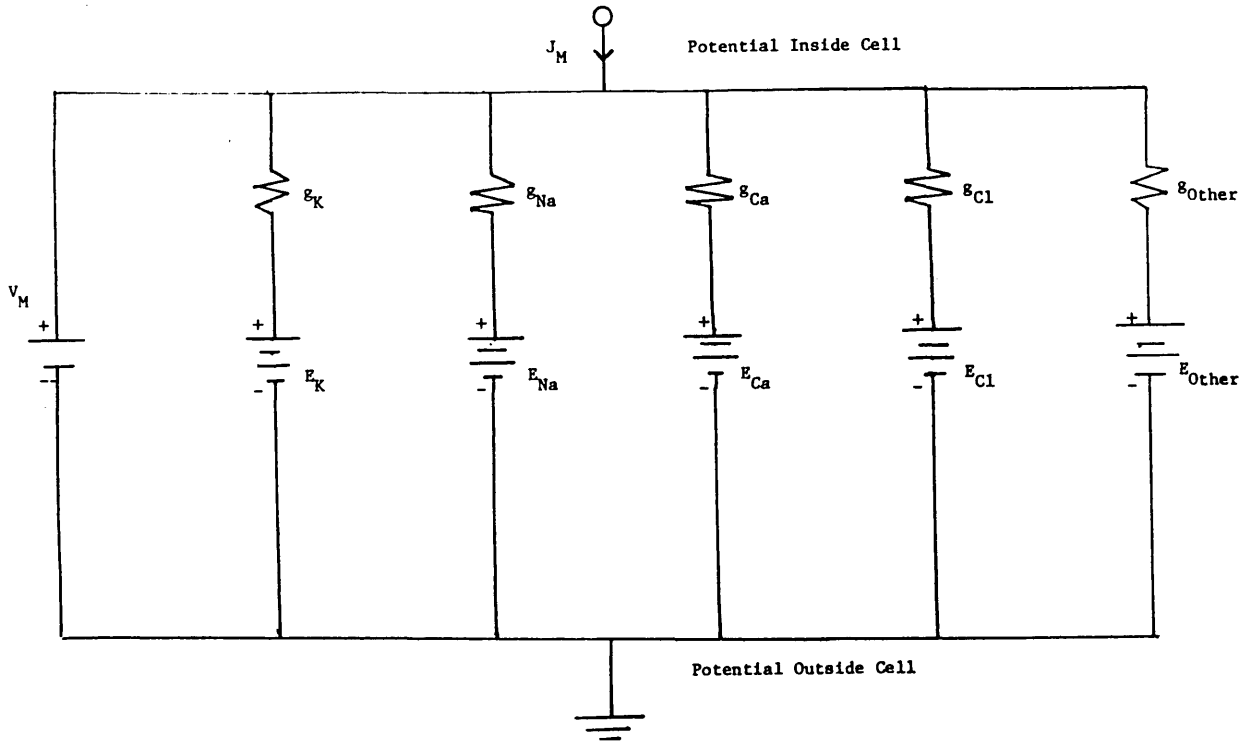

Figure 2.3: Electrical Circuit Model of a Unit Area of the Cell Membrane

Symbols are defined in the text. (Modified from HST090 Class Notes, 1985)

where

V_M^o = resting transmembrane potential,

and

$$g_M = \sum_i g_i \tag{2.4}$$

In the resting state, the membrane is principally permeable to the potassium ion only, thus, the predicted transmembrane potential is $V_M = E_K = -90mV$. A typical resting cell exhibits an actual resting transmembrane potential, denoted V_R, of -80 to -90 mV (the inside of the cell is negative with respect to the outside). The cell is said to be

"polarized" (also termed "repolarized"). If the transmembrane potential is less than this normal resting potential ($V_M<V_R$), then the cell is "hyperpolarized". (Katz, 1983; HST090 Class Notes, 1985)

As current from an external source enters the cell, the transmembrane potential increases. At a threshold level, V_T, the external source can be removed and the transmembrane potential will continue to increase. The characteristic time-course of the transmembrane potential, termed the action potential, results. Figure 2.4 shows the action potential for a typical ventricular cell.

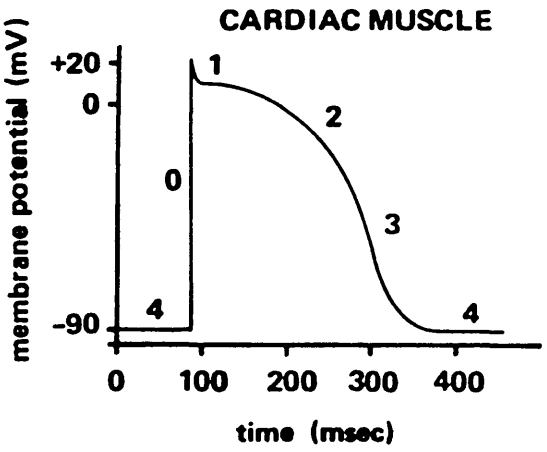

Figure 2.4: The Cardiac Action Potential

The cardiac action potential (shown here for a Purkinje fiber) consists of five phases. Phase 0 is the upstroke phase, phase 1 is early repolarization, phase 2 is the plateau phase, phase 3 corresponds to repolarization, and phase 4 (diastole) corresponds to the resting potential. (From Katz, 1983)

Figure 2.5 shows the corresponding changes in ionic conductances. The action potential has five characteristic phases. In the upstroke phase, phase 0, the cellular potential changes rapidly from the resting

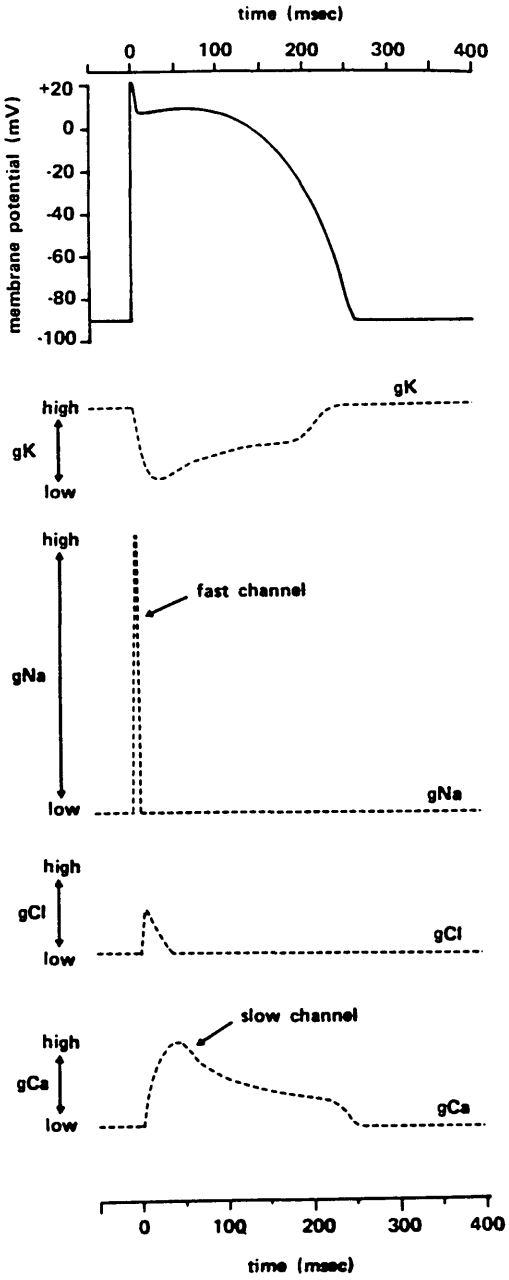

Figure 2.5: Changes in Ionic Conductances During the Action Potential in a Purkinje Fiber

Note the typical action potential (top) and, reading from top to bottom, the accompanying changes in conductance for potassium (gK), sodium (gNa), chloride (gCl), and calcium (gCa). (From Katz, 1983)

potential to a value of approximately +20 millivolts. The cell is said to be "depolarized" because V_M is no longer equal to the resting polarized value V_R. The sharp, transient increase in sodium conductance, causing an inward flow of the sodium ion (E_{Na} = +40 mV), is principally responsible for the depolarization of the resting potential. This rapid flow of ions is associated with the "fast channel". The brief period of rapid repolarization which follows the upstroke phase is the early repolarization phase (phase 1). A sharp decrease in sodium conductance leads to a fall in the membrane potential. The inward flow of the chloride ion (E_{Cl} = -28 mV), due to an increase in chloride conductance, contributes to the return of the membrane potential to a plateau level. Phase 2, the plateau phase, is characterized by a prolongation of the action potential. A decrease in the inward flow of the potassium and chloride ions (E_K = -90 mV, E_{Cl} = -28 mV) is balanced by a decrease in the inward flow of calcium ions (E_{Ca} = +205 mV). Over the time course of the plateau phase, the calcium conductance decreases. The calcium-related current, termed the slow inward current, is associated with the "slow channel". During phase 3, the repolarization phase, the membrane potential returns to its resting, or repolarized, state. This repolarization occurs when the conductance of potassium returns to a high state. The final phase, phase 4, is the resting potential. If the phase 4 membrane potential is less than the normal resting potential (i.e. $V_M < V_R$), then the cell is hyperpolarized.

Depolarization of a myocardial cell begins in one region of a cell's membrane and then quickly spreads throughout the cell. Once a given cell is depolarized it can, for a short time, stimulate a neighboring cell. The cell is said to have propagated an action

potential to its neighbor. In this manner, excitation spreads throughout the heart on a cell to cell basis. The rate at which the action potential spreads, either within a cell or on a cell to cell basis, is termed the conduction velocity.

Immediately after depolarization there exists an effective refractory period (ERP) during which electrical stimulation of the cell can produce no propagated action potential. This time period is shown in Figure 2.6. During the ERP the cell is oblivious to its surrounding environment. The cell next exhibits a relative refractory period (RRP). An abnormally strong stimulus can initiate a propagated action potential. The refractory periods are followed by a supernormal period (SNP) in which a weaker than normal stimulus can elicit a propagated response. The responses elicited during the RRP and SNP tend to be altered in form and have a slower conduction velocity with respect to normal activation. The time period from depolarization until completion of the SNP is the full recovery time (FRT). A normal stimulus received after the FRT will generate a normal action potential.

The duration of the refractory period varies monotonically with the length of the cardiac cycle. As the interstimulus interval decreases (increases) the duration of the refractory period decreases (increases). This relationship prohibits the heart muscle from being tetanized. A protective feature results, as tetany would prevent any effective pumping action. Changes in the refractory period also contribute toward preventing conduction block. If the refractory periods did not change (decrease), then at fast heart rates (i.e. for interstimulus intervals less than the ERP) the wavefront of the propagating action potential would meet refractory cells and become blocked. During abnormal

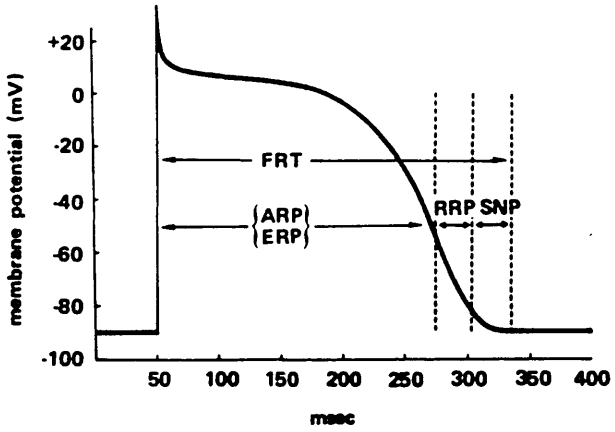

Figure 2.6: Excitability During the Cardiac Action Potential

The effective refractory period (ERP or ARP), during which stimuli of any strength are unable to initiate a propagated action potential, is followed by the relative refractory period (RRP), during which only stimuli greater than those which normally reach threshold can cause a propagated action potential. The RRP is followed by the supernormal period (SNP), during which stimuli slightly less than those which normally reach threshold can cause a propagated action potential. The action potentials generated during the RRP and SNP usually propagate slowly, so full recovery time (FRT) is the interval following depolarization after which threshold returns to normal and stimulation produces a normally propagated action potential. (Figure from Hoffman and Cranefield, 1960; Caption from Katz, 1983)

conditions, the decrease in the duration of the ERP is not sufficient and conduction block results.

Han and Moe (1964) and Han et al. (1966) have provided evidence for the existence of a spatial dispersion in ERP's. Spatially separated cells recover non-uniformly after excitation. Thus, in contrast to the cell to cell activation process, repolarization is an asynchronous process.

2.3.2 Excitation-Contraction Coupling

The electrical depolarization of a myocardial cell triggers the initiation of mechanical contraction. Figure 2.7 shows the time course of cellular depolarization superimposed on the time course of developed isometric force of a small segment of human heart muscle. Tension in the muscle strip is developed shortly after depolarization and reaches a peak prior to completion of the ERP.

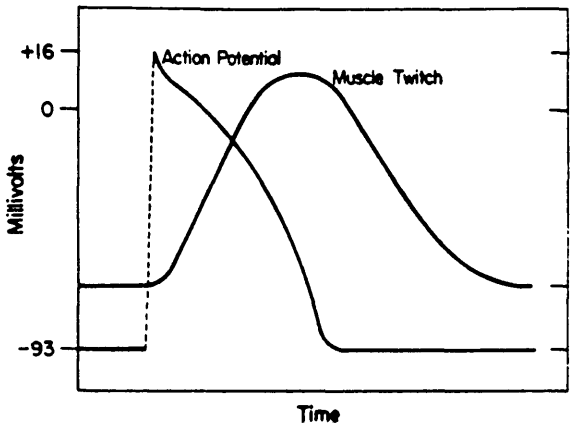

Figure 2.7: Time Relationship of the Action Potential and Muscle Twitch

Figure shows the time relationships between the mechanical tension developed by a thin strip of ventricular muscle and the changes in transmembrane potential. (From Berne and Levy, 1981)

The basics of cellular excitation-contraction coupling have been modeled by Morgan et al. (1984) as shown in Figure 2.8. The slow inward current of the cardiac action potential permits a small amount of calcium to enter the cell. This calcium triggers the release of large

amounts of intracellular calcium (stored in the sarcoplasmic reticulum) which interact with the myofilaments to induce contraction. Relaxation occurs when calcium diffuses back into the sarcoplasmic reticulum from its binding sites on the myofilaments. The trigger calcium exits the cell via a sodium-calcium exchange mechanism and (recent evidence suggests) through a calcium pump. In general, interventions that decrease (increase) the contractile force of the heart do so by decreasing (increasing) the availability of intracellular calcium for activation of the myofilaments.

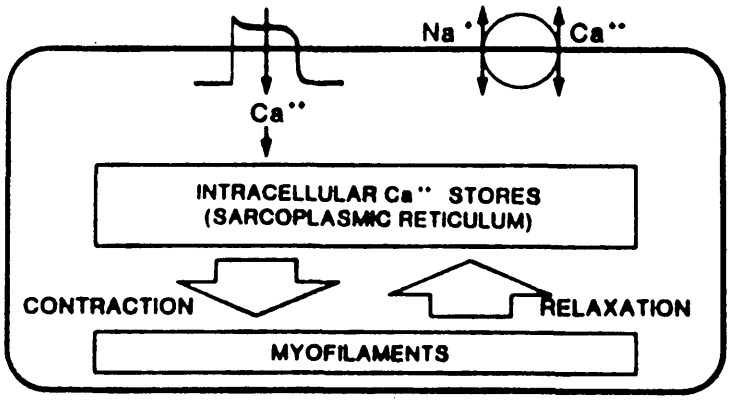

Figure 2.8: Major Steps of Excitation-Contraction Coupling

(From Morgan et al., 1984)

The strength and duration of contraction derived dynamically from an excitation are a complex function of (at least) the following variables: the force or load which the muscle is acting against, the initial length of the muscle fibers prior to contraction, the frequency of muscle contraction and the pharmacologic state of the muscle. Sonnenblick et al. (1965) have, however, shown that a simple static relationship exists between muscle length and tension. Figure 2.9 shows

this relation for both resting and active excised human heart papillary muscle.

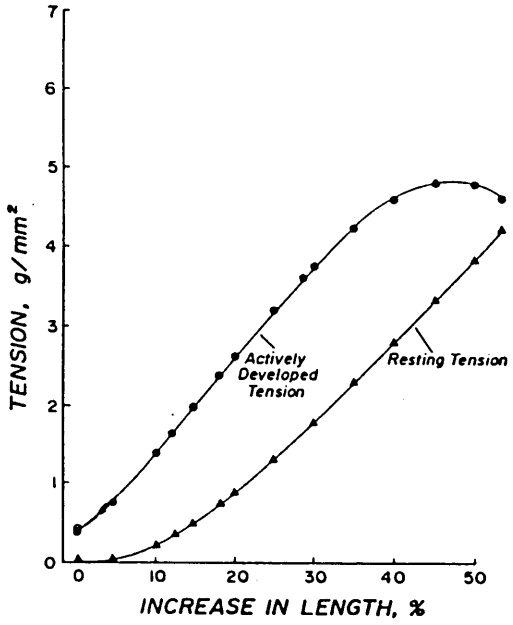

Figure 2.9: Resting and Active Papillary Muscle Length-Tension Relationship

A 3.6 mm^2 cross-sectional area of human papillary muscle was stimulated at a rate of twelve contractions per minute to obtain the above curves. (Modified from Sonnenblick et al., 1965)

2.3.3 Initiation and Propagation of Electrical Excitation

Certain cells within the myocardium display a resting potential, V_M, which is not constant in time. The resting potential rises as is shown in Figure 2.10. At the threshold level, V_T, the cell depolarizes. Such cells display the property of automaticity - they can function as pacemaker cells to spontaneously initiate a propagated action potential.

These cells may be found in the SA node, the specialized conduction system of the ventricles (discussed below) and in the AV node.

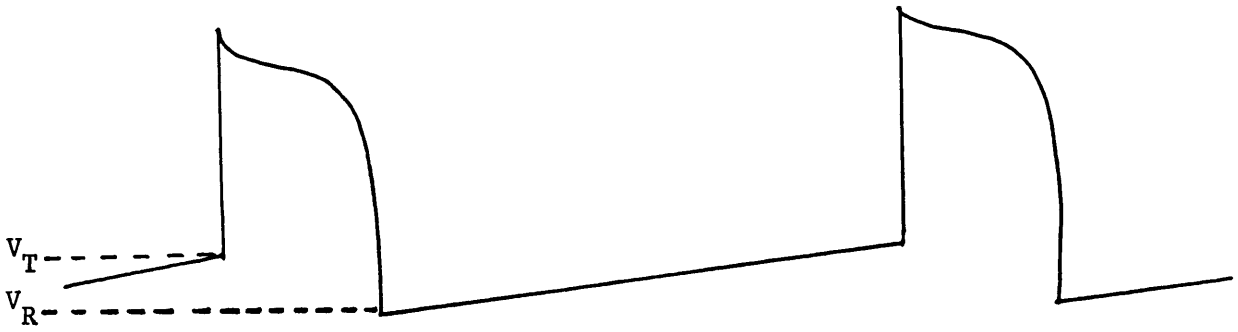

Figure 2.10: Diagram of the Transmembrane Potential of an Automatic Cell

The phase 4 resting membrane potential is not constant in time. (Modified from HST090 Class Notes, 1985)

A normal heart beat is initiated from cells within the SA node 60–100 times each minute. The action potential traverses the atria and ventricles utilizing specialized conduction pathways and cell to cell activation. Figure 2.11 shows the conduction system drawn onto the cardiac anatomy. The SA node is a small cluster of cells located in the right atrium near the entrance of the venae cavae. From the SA node, excitation spreads slowly throughout the atria principally by cell to cell conduction. A group of preferred conduction pathways, collectively called internodal tracts, may help to channel the action potential to the AV node. The AV node represents the only normal electrical junction

between the atria and ventricles. Propagation through the AV node is slow, causing a time delay of approximately 0.2 seconds between atrial and ventricular activation. The bundle of His arises directly from the AV bundle. The His bundle and Purkinje network (including the major bundle branches shown in Figure 2.11) form a rapid network of fibers which conduct the action potential throughout the ventricle. Excitation spreads from the Purkinje fibers throughout the ventricular muscle by cell to cell conduction. The His-Purkinje system synchronizes a wavefront of ventricular activation to spread, in general, from endocardium (inner surface) to epicardium (outer surface), and from apex (inferior portion) to base (superior portion). Figure 2.12 outlines the normal activation sequence. Note that the entire process of depolarizing the ventricular muscle mass takes only about 80 milliseconds.

Figure 2.12 also details the rate of pacemaker discharge from various regions of the heart. Cells in the SA node discharge at the fastest rate. Other regions along the conduction pathway discharge at progressively slower rates. During a normal beat, the action potential originating from the SA node will reach all regions of the heart prior to any other spontaneously generated action potential. This activation will reset the respective pacemaker clocks. Thus, the lower order pacemaker sites are normally dormant. During pathologic conditions(i.e. impaired higher order automaticity, conduction defects or advanced lower order automaticity) the lower order cells may initiate the heart beat.

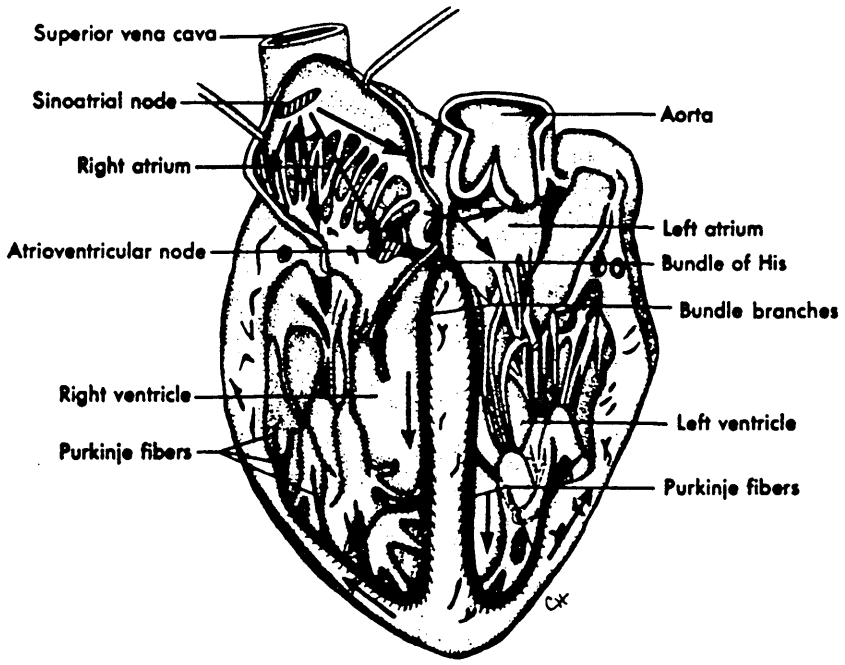

Figure 2.11: Schematic Representation of the Conduction System of the Heart

Conduction starts from the Sinoatrial node, spreads throughout the atrium, conducts across the Atrioventricular node, and is dispersed throughout the ventricles via the ventricular conduction system. (From Berne and Levy, 1981)

2.3.4 The Surface Electrocardiogram

The complex electrochemical actions taking place throughout the myocardium cause currents to flow within the body. These currents establish potential differences at the body surface which can be monitored by electrodes. The resultant surface ECG provides insight into the workings of the heart and often provides information as to the origin and extent of cardiac pathologies.

A typical surface ECG recording is shown in Figure 2.13.

Normal sequence of activation	Conduction velocity (meters/sec)	Time for impulse to traverse structure (sec)	Rate of pacemaker discharge (min^{-1})
SA node	—	~0.15	60–100
↓			
Atrial Myocardium	1.0–1.2		None
↓			
AV node	0.02–0.05	~0.08	None, except lower fibers: 40–55
↓			
AV bundle	1.2–2.0		
↓			
Bundle branches	2.0–4.0		25–40
↓			
Purkinje network			
↓			
Ventricular myocardium	0.3–1.0	~0.08	None

Figure 2.12: Normal Sequencing of Myocardial Activation

The normal sequencing of activation is shown in the column on the left. The remaining columns display the conduction velocity in various regions of the heart, the time for the activation to traverse regions of the heart, and the rate of pacemaker discharge in various regions of the heart. (From Katz, 1983)

Depolarization of the atria produce an electrical signal termed the P wave. The P wave develops slowly in time reflecting the slow cell to cell conduction in the atria. An isoelectric segment follows the P wave. During this isoelectric segment, conduction moves slowly through the AV node (producing the desired time lag between atrial and ventricular contraction) and along the proximal portion of the specialized ventricular conduction system. Figure 2.14 shows the time course of activation of different regions of the myocardium superimposed on the ECG. The next ECG deflection, the QRS complex, is the result of ventricular depolarization. The sharpness of this deflection reflects the activity of the ventricular conduction system. The QRS is larger in

A)

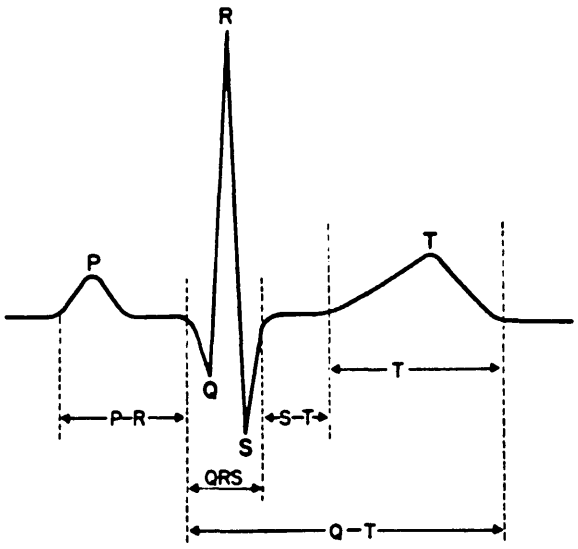

B)

	P-R Interval	QRS Interval	Rate	Q-T Interval	S-T,T Segment
Adults	0.18 To 0.20 Second	0.07 To 0.10	60	0.33 To o.43 Second	0.14 To 0.16 Second
Children	0.15 To 0.18 Second	Second	70	0.13 To 0.41 Second	0.13 To 0.15 Second
			80	0.29 To 0.38 Second	0.12 To 0.14 Second
			90	0.28 To 0.36 Second	0.11 To 0.13 Second
			100	0.27 To 0.35 Second	0.10 To 0.11 Second
			120	0.25 To 0.32 Second	0.06 To 0.07 Second

Figure 2.13: Typical Surface Electrocardiogram Recording

A) Shape of the electrocardiogram, illustrating the important deflections. (From Berne and Levy, 1981)
B) Normal values for the electrocardiogram. (Modified from HST090 Class Notes)

magnitude than the P wave due to the greater tissue mass of the ventricle. Another period of isoelectric activity, the S-T segment, follows the QRS complex. During the S-T segment, all regions of the ventricle are in a refractory state. The S-T segment leads into the T wave- the period of ventricular repolarization. The width of the T wave reflects the width of phase 3 of the action potential and the dispersion of action potential durations in the heart. Figure 2.15 shows the temporal relationships between the ECG and a representative cardiac action potential. Atrial repolarization is not observed on the surface ECG as it is small in magnitude and normally coincides with the large QRS complex.

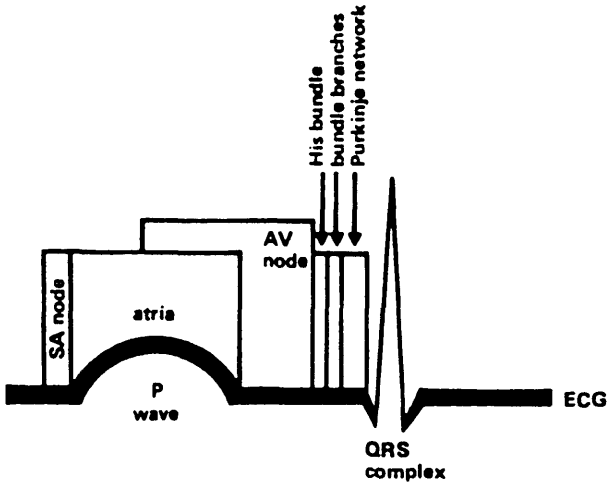

Figure 2.14: Time Course of Activation of Different Regions of the Heart Superimposed on the ECG

Tissues depolarized by a wave of activation commencing in the SA node are shown in a series of blocks superimposed on the initial deflection of the ECG. (From Katz, 1983)

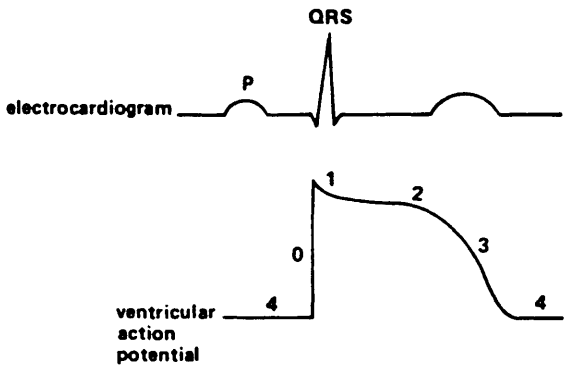

Figure 2.15: Temporal Relationships Between the ECG and a Representative Cardiac Action Potential

An ECG is shown on the top, and a representative action potential is shown on the bottom. The QRS complex is produced by the upstrokes (phase 0) of all of the action potentials throughout the ventricles; the S-T segment corresponds to the plateaus (phase 2), while the T wave is inscribed during repolarization (phase 3) of the ventricular mass. The isoelectric segment which comes after the T wave corresponds to ventricular diastole (phase 4). (From Katz, 1983)

2.3.5 The Dipole Model of Cardiac Electrical Activity

The surface ECG represents the composite activity of all cellular events occurring throughout the myocardium. The interpretation of the ECG is, therefore, based upon an understanding of these cellular events and their individual contributions to the surface potentials. The cellular events have been presented previously. The contribution of individual cellular events to the surface ECG is known as the forward problem in electrocardiography. A complete solution to the forward problem would include all of the time-dependent complexities of the

electrical activity of the heart as well as the passive electrical properties of the torso. The dipole model presents a simple representation of the electrical activity of the heart which can provide a more lucid basis for understanding and interpreting the surface ECG.

The dipole model formulates the electrical activity of individual heart cells as well as the various tissues comprising the torso, and from these derives the surface ECG. The electrical activity of individual heart cells is modeled by assigning a unit current dipole per unit surface area of the interface between normal and depolarized tissue. This dipole is oriented orthogonal to the interface, as shown in Figure 2.16. Only those cells along the wavefront of depolarization (or repolarization) contribute to the ECG. Thus, regions of the heart which are either wholly repolarized or depolarized do not contribute to the ECG. The heart is then situated at the center of a spherical torso. The torso is assumed to be comprised of a linear, homogeneous, anisotropic, conductive medium. If the radius of the torso is assumed large with respect to the heart, then all of the individual current dipoles may be assumed to originate from the sphere's center. The total electrical activity of the heart can then be expressed as a single equivalent dipole, termed the total cardiac dipole, which is the vector sum of all the individual dipoles.

Mathematically, the potential at any point along the surface of the torso is expressed as;

$$V(\theta) = \frac{3\ M_o}{4\ \pi\ \sigma\ R^2} \cos(\theta) \qquad (2.5)$$

where

M_o = magnitude of the total cardiac dipole,

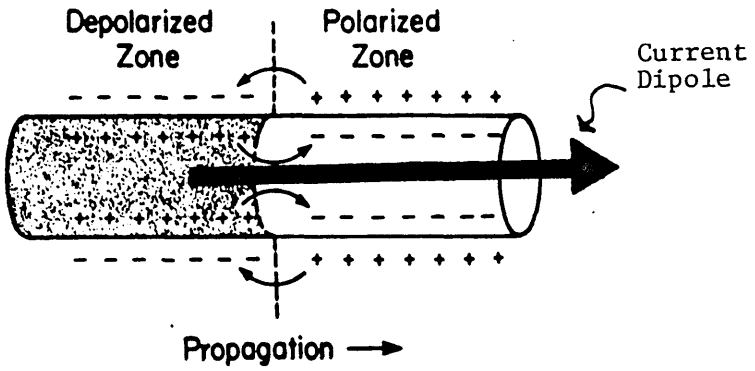

Figure 2.16: Flow of Current at the Advancing Front of Depolarization

The current dipole which represents the electro-chemical activity at this interface is assigned orthogonal to the interface. (Modified from Berne and Levy, 1981)

R = radius of the torso,

θ = angle between the point of observation and the total cardiac dipole,

σ = conductivity of the torso medium.

Alternately, the potential at a point A on the surface can be expressed as the scalor product;

$$V_A = \bar{M} \cdot \overline{OA} \qquad (2.6)$$

where

$\bar{M}$ = total cardiac dipole,

$\overline{OA}$ = vector from the torso center to the point A on the surface.

The magnitude of the vector $\overline{OA}$ is;

$$\text{magnitude } (\overline{OA}) = \frac{3}{4 \pi \sigma R^2} \tag{2.7}$$

A second point on the torso surface would be represented as;

$$V_B = \bar{M} \cdot \overline{OB} \tag{2.8}$$

and the potential difference between points A and B is;

$$\begin{aligned} V_{AB} &= V_A - V_B \\ &= \bar{M} \cdot \overline{OA} - \bar{M} \cdot \overline{OB} \\ &= \bar{M} \cdot (\overline{OA} - \overline{OB}) \\ V_{AB} &= \bar{M} \cdot \bar{L}_{AB} \end{aligned} \tag{2.9}$$

The vector $\bar{L}_{AB}$ is called a lead vector. Figure 2.17 illustrates the total cardiac dipole, $\bar{M}$, residing at the center of the spherical torso and also geometrically depicts the method of determining the potential difference between two points on the body surface. Thus, the potential measured between points A and B on the torso surface at any instant is the projection of the total cardiac dipole onto the lead vector. Note that if three orthogonal lead vectors are monitored simultaneously, the heart vector can be completely reconstructed.

Although the dipole model is a simplification of the complex processes that interact to form the ECG, the model provides an effective means in which to analyze the ECG. Clinically, such a model is often referred to for interpretation of abnormal electrical activity.

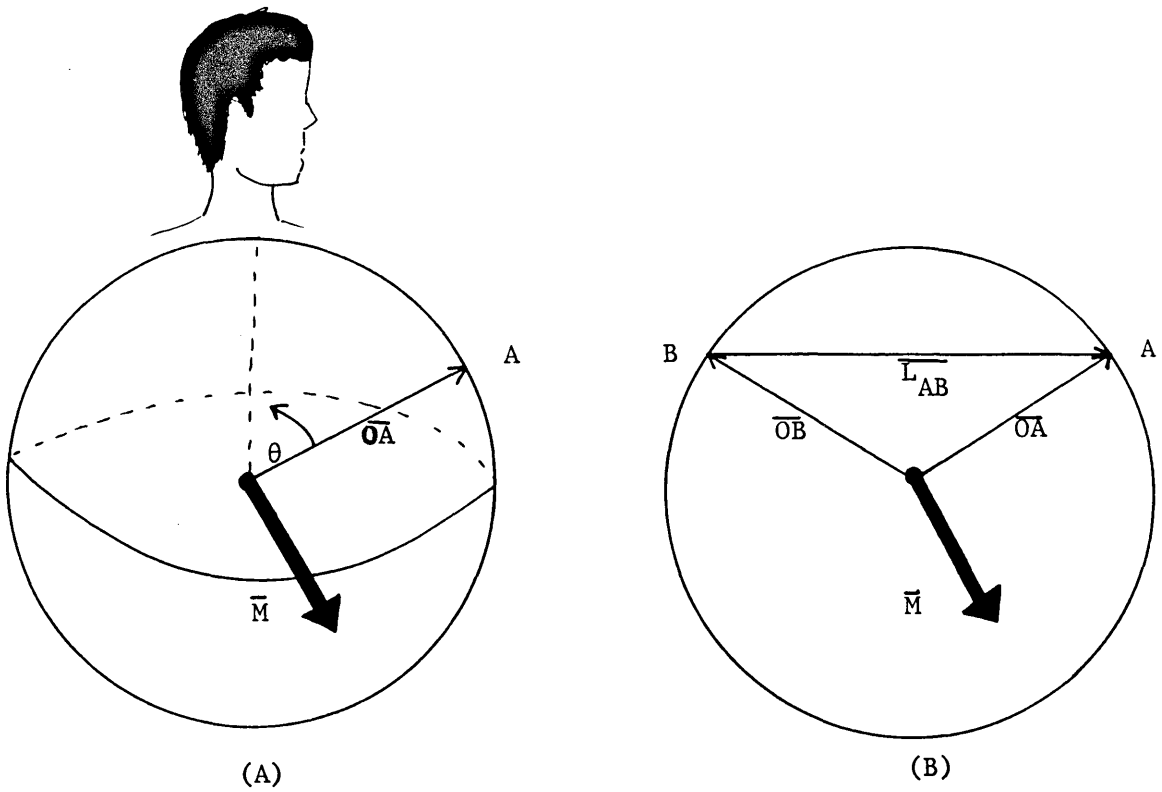

Figure 2.17: Vector Geometry of the Dipole Model

A) The total cardiac dipole, $\vec{M}$, resides at the center of a spherical torso. The potential at surface point A is equal to the projection of the total cardiac dipole onto the vector **OA**. B) Geometric method of determining the potential difference between two points on the body surface. A single plane view of the spherical torso shows the geometry used to form the lead vector L_{AB} as the potential measured between the points A and B on the body surface.

2.4 Regulation of the Heart

The heart responds to both intrinsic and extrinsic factors in the regulation of its electrical-mechanical performance. The rate of pacemaker discharge, the blood volume ejected during a beat, the strength of contraction and the sequencing of electrical activation are all regulated in the intact organism. Although the actions of the intrinsic and extrinsic regulatory mechanisms work in an interdependent fashion, they have been studied independently. The basics of these regulatory mechanisms are reviewed below.

2.4.1 Intrinsic Regulation of the Heart

Experiments with isolated heart preparations (preparations void of the extrinsic regulatory mechanisms) have been used to investigate the intrinsic regulation of the heart. In 1914, Starling (see Patterson and Starling, 1914) pioneered the isolated canine heart-lung preparation shown in Figure 2.18. With this preparation, preload (denoted here as the venous return) and afterload were independently controlled. The response of the isolated heart to step changes in venous return is shown in Figure 2.19. Starling found that as venous return (and thus right atrial pressure) was increased, end-diastolic volume (EDV) increased and stroke volume (SV) increased. (Note that SV = EDV - End Systolic Volume.) The relationship between SV and EDV was not linear, and in some cases of high atrial pressure the SV actually diminished. Starling also studied the response of the heart to changes in afterload. Results from one experiment are shown in Figure 2.20. An increase in afterload

led to an increase in EDV and right atrial pressure. Note that after a transient period, the SV returned to its original value.

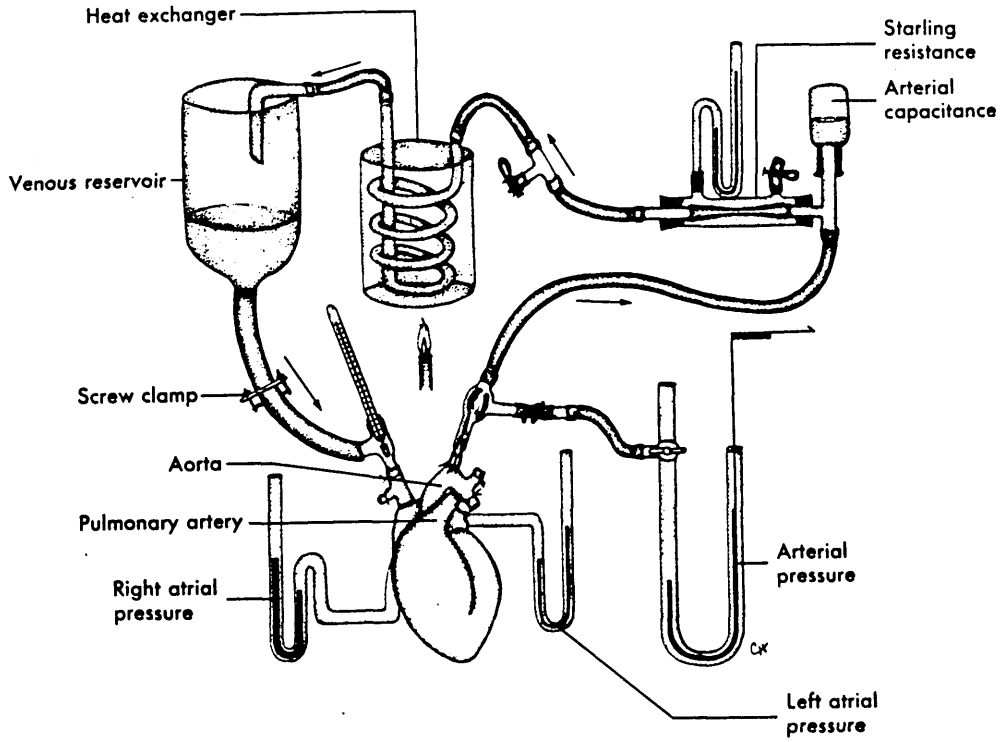

Figure 2.18: Heart-Lung Preparation of Patterson and Starling

(Redrawn from Patterson and Starling, 1914)

Starling's experiments demonstrated the relationship between EDV and the work performed by the heart. The EDV is, in turn, a measure of the end diastolic muscle fiber length. (Because of the complicated geometry of the ventricle, ventricular volume might more correctly be a statistical representation of the average fiber length.) Thus, Starling's Law of the Heart, as the above relationships have become

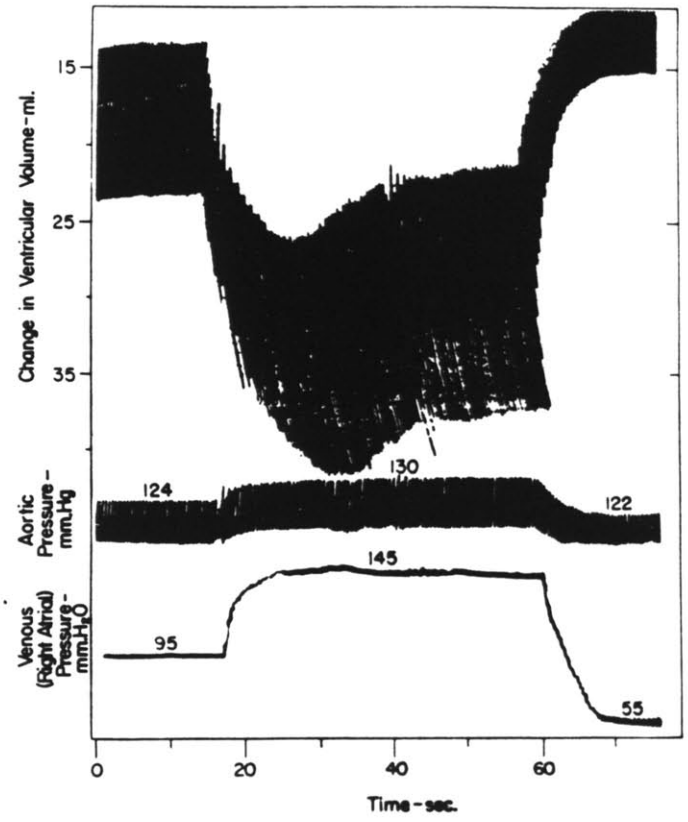

Figure 2.19: Intrinsic Regulation of the Heart to Changes in Preload

Figure shows changes in ventricular volume in a heart-lung preparation when the venous reservoir was suddenly raised (right atrial pressure increased from 95 to 145 mm H_2O) and subsequently lowered (right atrial pressure decreased from 145 to 55 mm H_2O). An increase in ventricular volume is registered as a downward shift in the tracing. (From Patterson et al., 1914)

known, must be derived from the length-tension relationships presented in section 2.3.2 (see also Figure 2.9). Figure 2.21 shows this dual relationship between myocardial length-tension and ventricular volume-pressure.

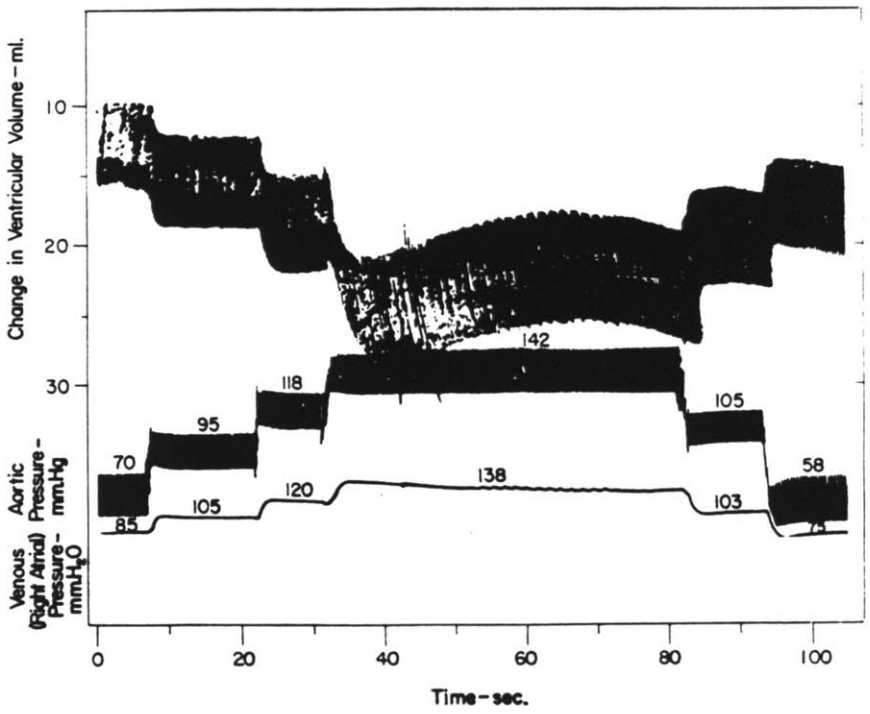

Figure 2.20: Intrinsic Regulation of the Heart to Changes in Afterload

Figure shows changes in ventricular volume, aortic pressure, and right atrial pressure in a heart-lung preparation when peripheral resistance was raised and subsequently lowered in several steps. An increase in ventricular volume is registered as a downward shift in the tracing. (From Patterson et al., 1914)

Starling's heart-lung preparations also demonstrated the conservation of mass principle, as applied to the heart. Under normal steady state conditions, the volume of blood ejected from the left ventricle during a given cycle is equal to the volume of blood entering the right atrium during that cycle. This relationship must be true else all the blood would be displaced into the body, the pulmonary

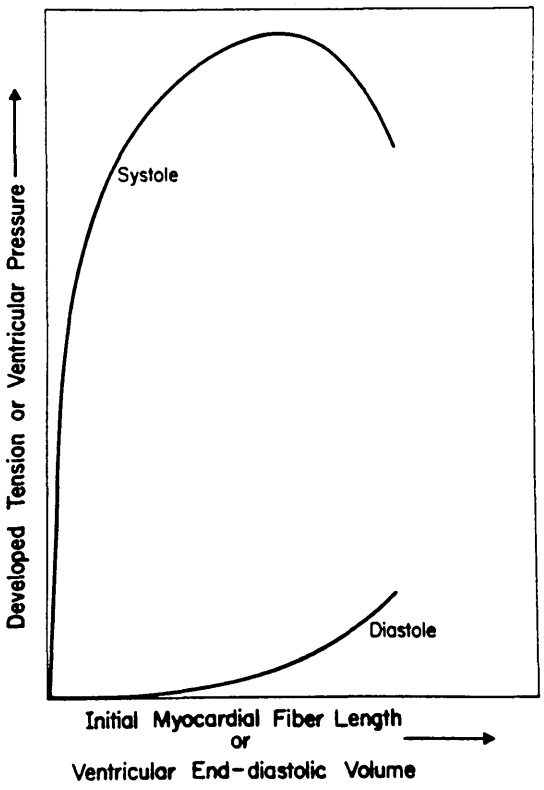

Figure 2.21: Dual Relationship Between Myocardial Length-Tension and Ventricular Volume-Pressure

Length-Tension and Ventricular Volume-Pressure data acquired during ventricular contraction of the intact dog heart. (From Berne and Levy, 1981)

circulation, or the heart itself.

The heart also has an intrinsic ability to alter its pacemaker rate. Stretch receptors located within the right atrium respond to distension within that chamber. As the chamber is increasingly stretched, the pacemaker rate increases.

2.4.2 Extrinsic Regulation of the Heart

The autonomic nervous system (ANS) is the dominant extrinsic regulatory mechanism of the heart. The ANS has both efferent and afferent limbs which communicate through the central nervous system to form a closed-loop control system. The basics of this control system is discussed below.

The ANS has two efferent pathways; the sympathetic nervous system (SNS) and the parasympathetic nervous system (PSNS). SNS stimulation exerts upon the heart the facilitatory influences of increased heart rate, increased conduction velocity, shortening of action potential duration, increased contractility, and decreased duration of mechanical systole with respect to the duration of diastole. Constriction of the peripheral vasculature is also induced. PSNS stimulation exerts upon the heart the diminutive influences of decreased heart rate, decreased conduction velocity through the AV node, and some decrease in the strength of contraction. Under most conditions the heart is governed by the tonic influences of both the SNS and the PSNS. An increase in heart rate, for example, is typically accomplished through the reciprocal action of increased sympathetic tone and decreased parasympathetic tone.

Sympathetic fibers leave the spinal cord through the thoracic and lumbar spinal nerves. These fibers synapse primarily in the vertebral and prevertebral ganglia. The postganglionic fibers innervate the heart as an extensive plexus, or "nerve net". Transmission at the junction between all cells is chemical. In the ganglia the neurotransmitter is acetylcholine. Norepinephrine is the transmitter at the majority of the postganglionic endings. The left and right sympathetic fibers tend to

innervate the heart with a differential distribution. Fibers on the left side are predominantly found in the ventricle and, thus, have a more pronounced effect on contractility than on heart rate. Conversely, fibers on the right side are predominantly found in the atria and have a more pronounce effect on heart rate than on contractility.

The parasympathetic fibers outflow from the brain stem (as the vagus nerves) and the sacral area of the spinal cord. These fibers synapse with postganglionic cells located within the heart itself. The cardiac ganglion cells are principally located near the SA node and AV junction. The neurotransmitter at the ganglia and the postganglionic endings is acetylcholine. As is the case with the sympathetic fibers, there tends to be a differential distribution of left and right fibers. Left fibers are found predominantly in the AV junction and have a more pronounced effect on AV conduction than on heart rate. Right fibers are found predominantly in the SA node and have a more pronounced effect on heart rate than on AV conduction.

There are three major afferent ANS pathways concerned with the regulation of the circulation. The aortic nerve runs from the aortic arch into the central nervous system via the vagus. Its sensory endings respond to stretch (or distension) of the aorta. The carotid sinus nerves, whose sensory ending also respond to stretch, run from the bifurcation of the common carotid arteries to the central nervous system via the glossopharyngeal nerves. And, afferents from the great veins, also responding to stretch, run from the roots of both venae cavae and the pulmonary veins via the vagi to the brain stem.

Extrinsic regulation of the heart can also be accomplished through hormonal influences. Some of the major influences are discussed below.

The adrenal medulla secretes the catecholamines norepinephrine and epinephrine. These catecholamines have the identical direct cardiac effects of increased heart rate, increased conduction velocity, shortening of action potential duration, increased contractility, and a relative decrease in the duration of mechanical systole. (Since norepinephrine is the SNS postganglionic neurotransmitter, the above effects parallel the direct cardiac effects of SNS stimulation.) Peripherally, norepinephrine causes constriction of both arterial and venous vessels while epinephrine can cause either constriction or dilation of arterial vessels.

The administration of acetylcholine to the heart will, in general, cause the opposite effects of norepinephrine and epinephrine. The direct cardiac effects are decreased heart rate, decreased conduction velocity through the AV node, and some decrease in the strength of contraction. (These direct cardiac effects parallel PSNS stimulation.) Peripherally, acetylcholine causes both the arterial and venous to vessels relax.

In the in situ heart, hormonal influences are tempered by the action of the ANS. For example, the infusion of norepinephrine leads to constriction of the peripheral vasculature, which leads to an increase in arterial pressure, which is responded to by the ANS by a decrease in heart rate. Thus, the response of the ANS can distort the direct effects of the hormonal influences. (Berne and Levy, 1981; HST090 Class Notes, 1985)

Chapter III

Sudden Cardiac Death

3.1 The Problem of Sudden Cardiac Death

Sudden death, as defined by the World Health Organization, is death which ensues within twenty four hours after onset of symptoms. Sudden cardiac death (SCD), sudden death of a primary cardiac nature, claims approximately 500,000 lives in the U.S. annually (Horowitz and Morganroth, 1982) and represents the majority of all sudden deaths. Although SCD has been associated with coronary heart disease (CHD), approximately fifty percent of those who die suddenly have shown no prior clinical evidence of overt CHD (Horowitz and Morganroth, 1982). The majority of SCD's occur outside the hospital (Kannel and Thomas, 1982) and are attributed to the malignant cardiac electrical rhythm disturbance of ventricular fibrillation (VF). In VF, the normally synchronous activity of the ventricles degenerates into a chaotic activity such that no effective pumping action results. Blood flow ceases and death ensues within minutes.

3.2 Ventricular Fibrillation and Ventricular Tachycardia

VF is an electrical rhythm disturbance. The ventricles cease to beat in a coordinated, synchronous pattern, but rather beat in a chaotic pattern. Cells throughout the ventricle are excited independent of any central rhythmic pacemaker. At any given instant in time, cells throughout the ventricle can be found in different phases of their action potential. Excitation no longer spreads via the normal cardiac conduction system, instead, excitation spreads chaotically on a cell to cell basis to those cells which are non-refractory.

Figures 1.1 and 1.2 (recall from Chapter I) schematically depict normal depolarization and repolarization, respectively, in an area of ventricular myocardium. Each square box is a heart element. Each element represents the activity of the heart over a local region in which cellular refractory times are correlated. A white box represents a repolarized region. A black box represents a recently depolarized region. A gray box represents a refractory region not recently depolarized. The wavefront of excitation can be observed by following the location of the black colored cells. These figures illustrate normal excitation - a fluent progression of the wavefront is observed. Figure 3.1 depicts VF using the same coding scheme. Note the randomness and tortuosity of the wavefront. Often in VF a true wavefront is difficult to identify.

Once VF has been initiated it rarely reverts spontaneously to a normal rhythm. The fractionated wavefront sustains itself by continuously following a pathway mapped out by non-refractory elements. This pathway is time dependent, thus there is no single consistent loop

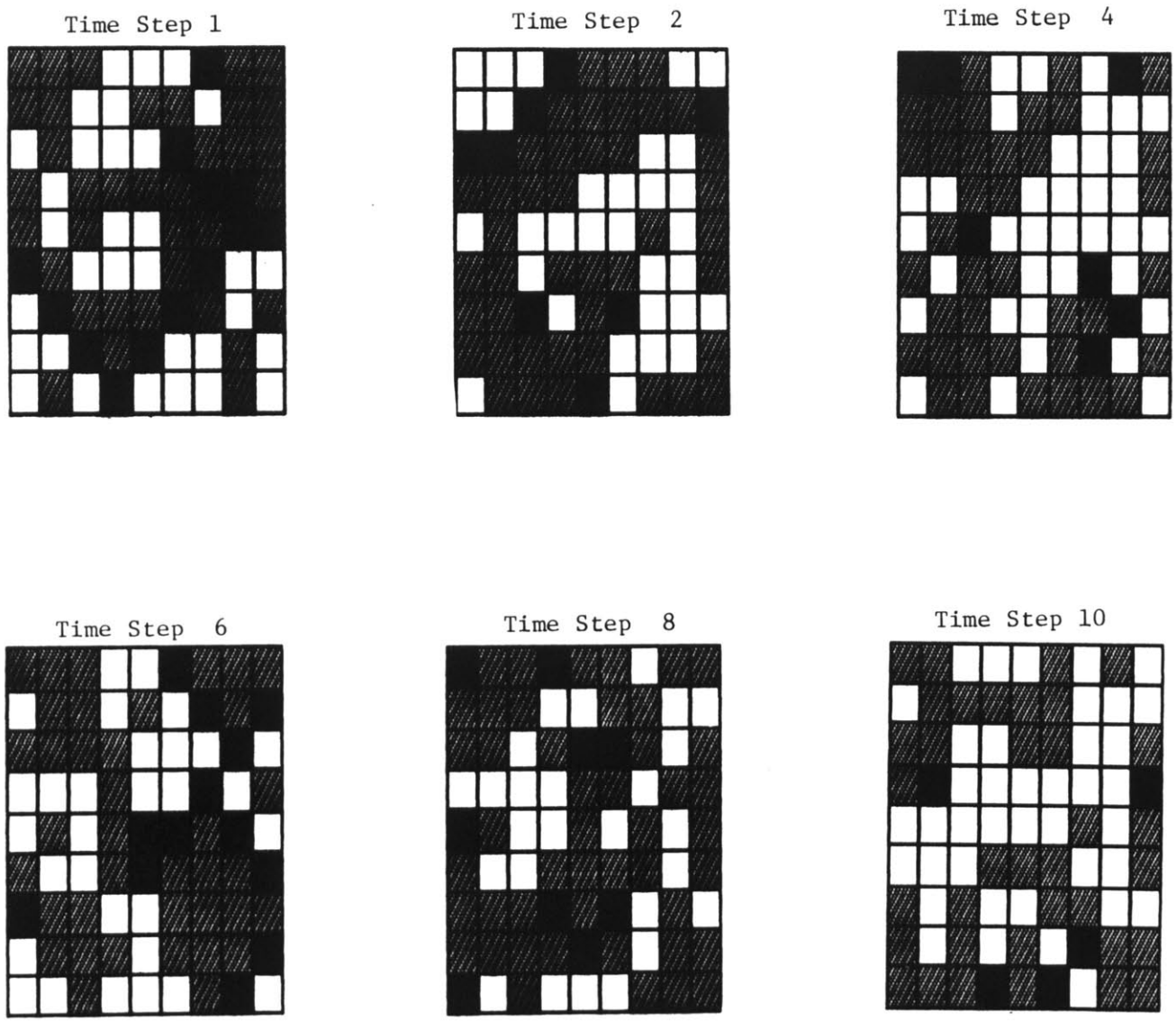

Figure 3.1: Schematic of Ventricular Fibrillation

Figure depicts the chaotic nature of VF in a region of the heart. A white box represents a repolarized area. A gray box represents a depolarized area. A black box represents a recently depolarized area.

of excitation. Re-excitation of a given element will occur once that element is non-refractory and any wavefront pathway reaches that element. The dipole model predicts that the chaotic excitation in VF will lead to a chaotic looking surface ECG. Figure 3.2 shows that such is the case. VF produces no identifyable QRS complex or T wave.

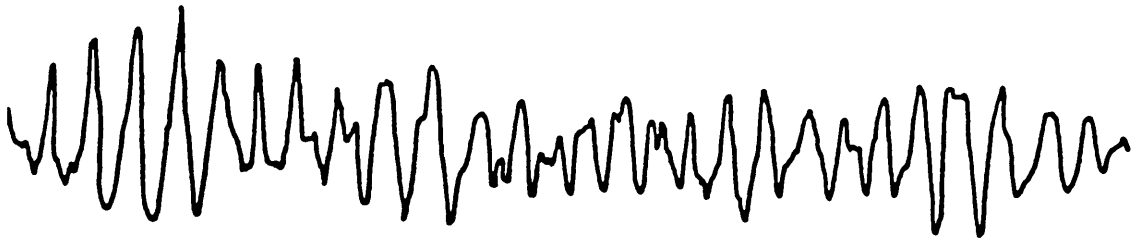

Figure 3.2: Surface ECG During Ventricular Fibrillation

(From Smith, 1985)

A second clinically significant rhythm disturbance is ventricular tachycardia (VT). In many cases, VT is thought to be a stable loop of excitation which continually cycles along the same pathway through the ventricle. Tissue along the pathway repolarizes shortly before encroachment of the excitation wavefront. In this manner, a single pathway is continuously traversed. Smith and Cohen (1984) depict the pathway of VT as in Figure 3.3. They note that for a reentrant path to be self-sustaining, the tissue at a given location along the path must no longer be refractory when the reentrant wave of excitation returns. Quantitatively, this leads to a rough criterion for reentry as;

$$l > v \tau \qquad (3.1)$$

where

l = loop circumference,

v = characteristic conduction velocity,

τ = characteristic refractory period.

Decreased conduction velocity, decreased refractory period, and increased loop circumference all facilitate reentry. Figure 3.4 shows the surface ECG during an episode of VT. VT rates range from 100 to 300 beats per minute. Hemodynamically, individuals experiencing VT can exhibit anything from normal cardiac function to severely compromised cardiac function. The study of VT is particularly important in that the stable excitation loop often degenerates into the chaotic excitation of VF.

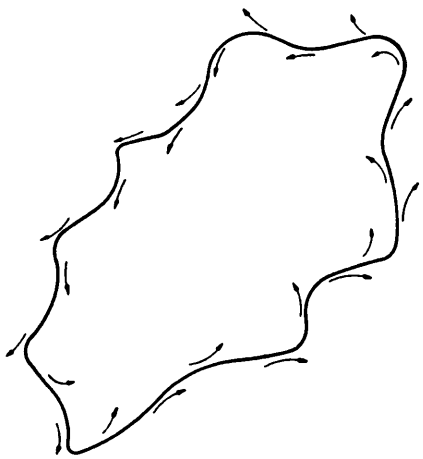

Figure 3.3: Pathway of Ventricular Tachycardia

For self-sustained reentry, the loop circumference must be greater than the product of the characteristic conduction velocity and the characteristic refractory period. (From Smith and Cohen, 1984)

Figure 3.4: Surface ECG During Ventricular Tachycardia

(From Smith, 1985)

3.3 Initiation of Ventricular Fibrillation

VF is thought to be a chaotic pattern which, once initiated, seldom spontaneously reverts to a normal rhythm. Two principal mechanisms are theorized as initiators of VF: reentry and multiple ectopic foci. Both theories are discussed below.

The concept of reentry, used above in the explanation of VF, is the most generally accepted mechanism of VF. Reentry occurs when a previously excited pathway repolarizes and is then depolarized a second time by the original excitation wavefront. Figure 3.5 depicts in a dynamic fashion the method by which reentry can occur. The excitation wavefront encounters a refractory region of tissue and thus propagates around the tissue. Later in time, when the wavefront reaches the rear of the tissue, a channel of tissue has become non-refractory. This recovered tissue is excited and propagates the action potential back up towards the front of the tissue. If the channel of tissue forms a complete loop, reentry has occurred. A stable continuous loop will manifest itself as VT. A non-stable, sustained loop can trigger the global asynchrony of VF.

The multiple ectopic foci theory postulates that there are multiple locations throughout the ventricle from which an ectopic focus originates. An ectopic focus is a spontaneously developed action potential originating from a location other than the sinus node. If multiple foci exist, with each focus having its own periodic or non-periodic pacemaker rate, then the resultant excitation would be the chaotic activity of VF.

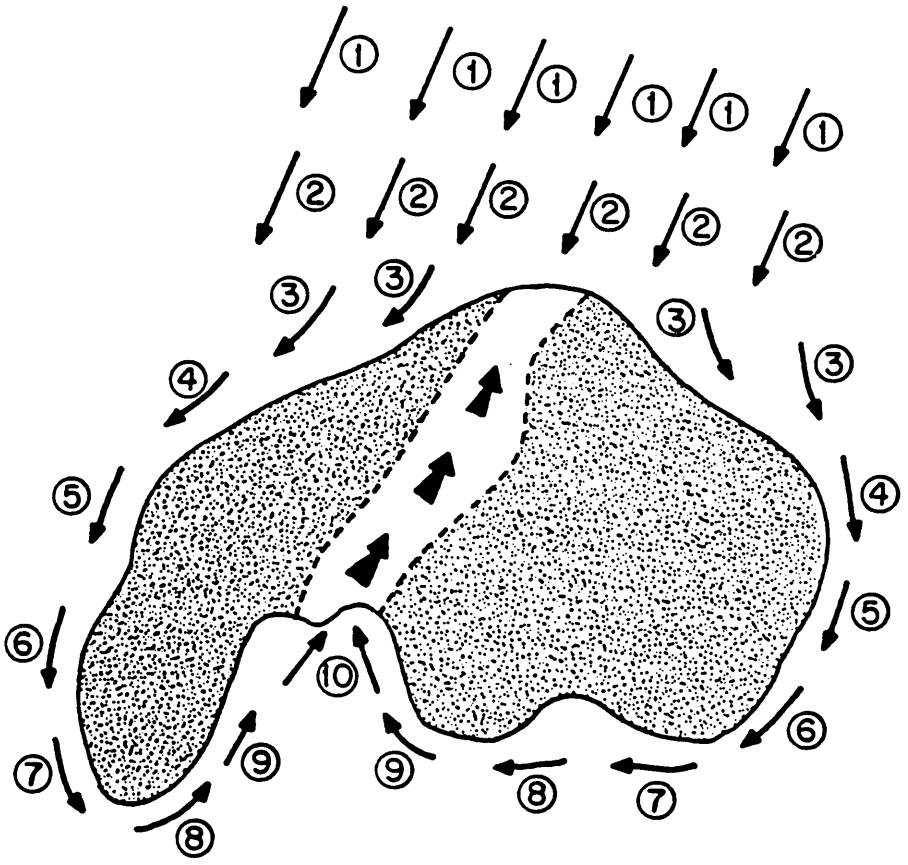

Figure 3.5: Spread of Activation Around a Refractory Island

The wavefront of activation first impinges upon the refractory island at time 2. By time 10, a channel through the island has recovered, resulting in a reentrant wavefront. Sustained reentry is possible if the wavefront successfully emerges to repeat the activation sequence 2 through 10. (From Smith, 1985)

3.4 Treatment of Ventricular Fibrillation

In that VF causes immediate circulatory and respiratory collapse, the most immediate treatment is that which will return these functions - namely cardiopulmonary resuscitation (CPR). In CPR, chest compressions (which compress the heart between the sternum and backbone) and mouth to mouth breathing replace the function of the heart and diaphragm, respectively.

CPR treatment has several drawbacks, however. First, CPR is not a definitive therapy. More advanced treatment is required to revert the fibrillation. Second, CPR is not always effective. A physiologically acceptable blood flow can not always be established even with proper administration of CPR. Third, CPR is not readily available outside of the hospital setting. Only a small subset of the general population has been trained in CPR and this subset poorly represents those most likely to witness a cardiac emergency. Lastly, the administration of CPR can cause damage to the victim, i.e. broken ribs during chest compressions. (This last point, in practice, is quickly dismissed as inaction during cardiac arrest will surely result in death.) Even with all of the above detracting factors, if CPR is administered immediately after a victim collapses, the chances of survival are doubled. (Eisenberg et al., 1986)

The definitive therapy for VF is defibrillation. A large electric charge is delivered to the heart which simultaneously depolarizes all cells in the heart. This breaks the asynchrony and allows the ensuing sinus beat to propagate normally. A drug regiment and/or surgery may be required to maintain the normal cardiac rhythm.

3.5 Predictors of Sudden Cardiac Death

3.5.1 Predictors of Sudden Cardiac Death in Humans

Presently, there exists no screening technique available to the general public for confident identification of the individual specifically at risk for SCD. A number of risk factors have been simultaneously associated with SCD and CHD (i.e. high blood pressure, ECG patterns of left ventricular enlargement, obesity and heavy cigarette use). These factors, however, fail to confidently distinguish the individual at risk of SCD from those at risk of CHD (Kannel et al., 1975; Kannel and Thomas, 1982).

In the clinical setting, individuals experiencing hemodynamically significant rhythm disturbances can be referred for invasive electrophysiologic study. Electrical stimulating catheters are advanced to the heart from a peripheral vein and provocative electrical stimulation of the heart initiated. The stability of the heart is based upon its ability to withstand the stimulation and maintain a normal rhythm. (Hamer et al., 1982) This technique has proven useful in monitoring the effectiveness of therapy for the individual already diagnosed as having a high risk of sudden death. But, due to its highly invasive character and the associated morbidity and mortality, the method can not be used on the general population.

3.5.2 Predictors of Sudden Cardiac Death in the Experimental Animal

In the experimental animal, VFT testing has been used successfully to access the stability of the ventricles. Electrical current is passed through the ventricles in an attempt to initiate VF. The level of current passed through the ventricle is progressively increased until fibrillation occurs. The current level which initiates VF, termed the VFT, provides a graded measure of ventricular stability.

In 1940 Wiggers and Wegria found that a single electrical pulse of sufficient amplitude delivered to the ventricle during late systole could initiate VF. More recently, using single pulse stimulation, Verrier and Lown (1982) have demonstrated the existence of both a vulnerable period (VP) and a protective zone (PZ) during ventricular repolarization. Figure 3.6 shows the temporal relationship of these zones with respect to the surface ECG. A single pulse delivered during the VP can initiate VF. The nadir of the VP curve identifies the time at which the ventricle is most susceptible to stimulation. If, however, a second stimulus is delivered during the PZ, VF can be avoided.

VFT determinations via the single pulse technique are accomplished by stepping throughout the course of ventricular repolarization a fixed current stimulus applied to the ventricle. A rest period is provided between stimuli. If VF occurs, this current level is the VFT. If VF does not occur, the current level is increased and the process repeated until VF is initiated. The current level which induces VF is the VFT. Han (1969) introduced an alternate, less time consuming method for measuring the VFT. He applied a train of current to the ventricle with

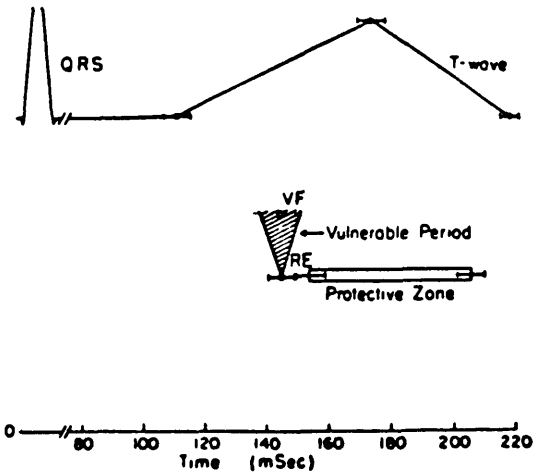

Figure 3.6: Temporal Relationships Between the Vulnerable Period, Protective Zone and Surface ECG

The VP curve has a characteristic V shape, the nadir of which coincides temporally with that for provoking VF. The PZ is a relatively broad zone which occurs 10 to 20 msec after the VP nadir and is approximately 50 msec in duration. (Modified from Verrier et al., 1978)

a fixed current intensity which spanned both the VP and the PZ. After a rest period, trains of stimuli with a progressively higher current intensity were applied. The current intensity which initiated VF was the VFT. A number of references in the literature (Verrier and Lown, 1982; Verrier et al., 1978; Spear et al., 1973; Moore and Spear, 1975) have shown both techniques to be a reproducible measure of ventricular susceptibility to fibrillation in the experimental animal.

3.5.3 Dispersion of Refractoriness and Reentry

The spatial dispersion in cellular refractory periods has been theorized to provide the substrate for reentrant rhythm disturbances.

According to this theory, islands of refractory tissue develop within the heart (see Figure 3.7). An incoming wave of activation is forced to travel around the refractory islands, thus fractionating the wavefront. Reentry may then occur via the mechanism explained in Section 3.3.

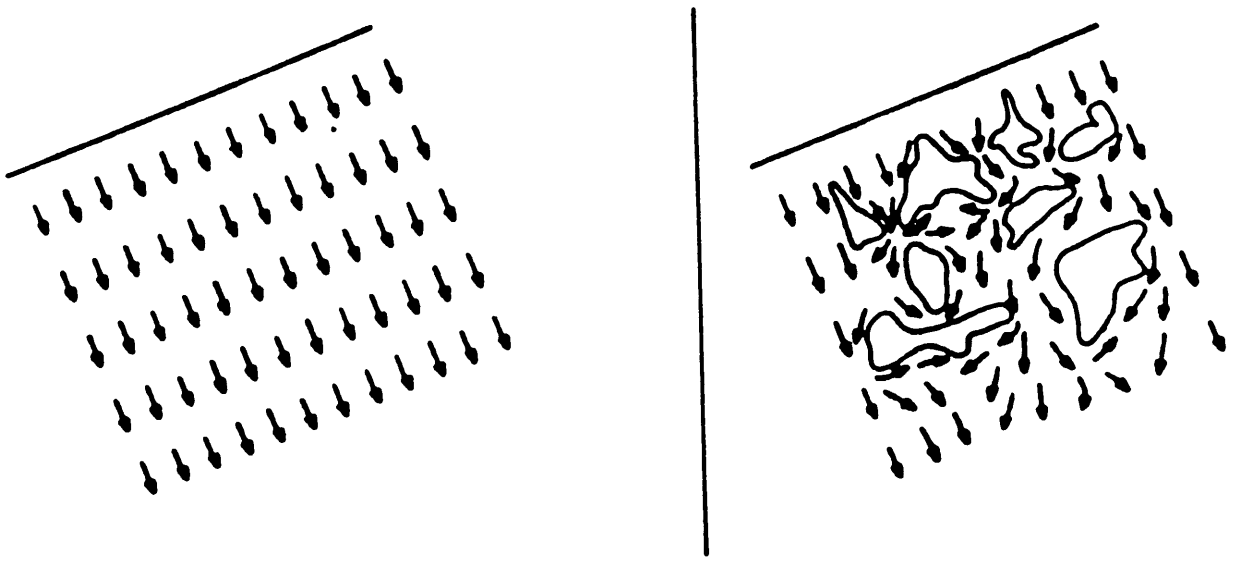

Figure 3.7: Refractory Tissue Leading to Wavefront Fractionation

Spatial homogeneity in refractory times (Left) results in even spreading of the depolarization wave. Spatial inhomogeneity in refractory times (Right) leads to wavefront fractionation and reentry. Unshaded regions represent islands of refractory tissue. (From Smith and Cohen, 1984)

Han et al. (1964) asserted a direct relation between dispersion and VF by stating:

> ...those agencies known to favor the development of ventricular fibrillation were found to increase the temporal dispersion of recovery of excitability, whether the average refractory period was reduced (sympathetic nerve stimulation, ouabain intoxication, ischemia) or increased (chloroform, quinidine in high dosage, or hypothermia).

Spear et al. (1973) depict this relation with respect to VFT testing as shown in Figure 3.8. (Spear et al. showed that myocardial ischemia increases dispersion while lidocaine injection decreases dispersion.) They further showed that the delivery of current during VFT testing directly increases the temporal dispersion of refractoriness in relation to the intensity of current delivered.

The dispersion of refractoriness theory also predicts the existence of the VP during ventricular repolarization. Throughout the time course of ventricular repolarization a dispersion of refractoriness exists across the ventricles. Islands of refractory tissue thus develop. A wave of activation initiated during this time would fractionate and could initiate VF.

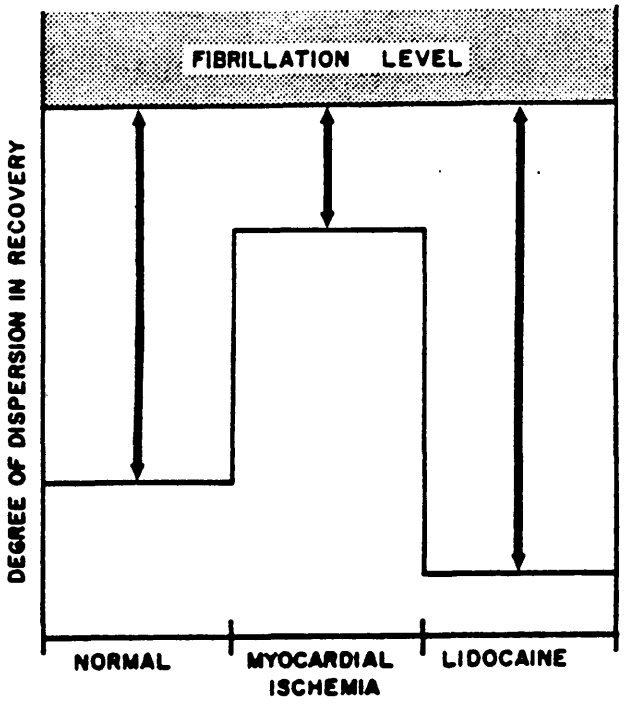

Figure 3.8: Effect of Delivering Current During the Vulnerable Period of the Cardiac Cycle

The figure is a schematic diagram describing the effect of delivering current during the vulnerable period of the cardiac cycle under normal conditions, myocardial ischemia and lidocaine administration. The ordinate is the degree of dispersion in recovery of excitability. The shaded area above indicates the degree of dispersion in recovery which must be induced by a fibrillating train of pulses to bring the heart to a fibrillation level under the three conditions plotted on the abscissa. (From Spear et al., 1973)

Chapter IV

Dispersion of Refractoriness and Alternation of the Heart

4.1 A Mathematical Representation of Dispersion

Smith and Cohen (1984), Smith et al. (1984a, 1984b), and Smith (1985) represent the dispersion of refractoriness concept mathematically in Figure 4.1 as a distribution of cellular refractory periods. The distribution has a mean value ($\bar{\tau}$) and a standard deviation (σ). The symbol T represents the interstimulus interval (inverse of the heart rate r). Of particular importance in the distribution is the population which lies outside (i.e. to the right) of the interstimulus interval. This population is denoted by the symbol F. These cells cannot be stimulated at the rate r. Thus, fractionation of activation wavefronts will occur about these cells. Note that dispersion is not the only important feature in this representation. Rather, the interaction between dispersion, mean refractory period and heart rate is emphasized.

Smith and Cohen (1984) explicitly incorporated this mathematical representation of dispersion of refractoriness into a simple finite-element model of the conduction processes of the left ventricle. The model sought to determine if a dispersion in cellular refractory periods was, by itself, a sufficient condition to generate a variety of reentrant rhythm disturbances. Thus, the complex geometry of the ventricle, the specialized electrical conduction system, the detailed excitation processes of myocardial cells, automaticity, etc. were not modeled. The model develops insight into the relationships between dispersion of refractoriness and the cardiac rhythm. A review of the model is presented in the following sections.

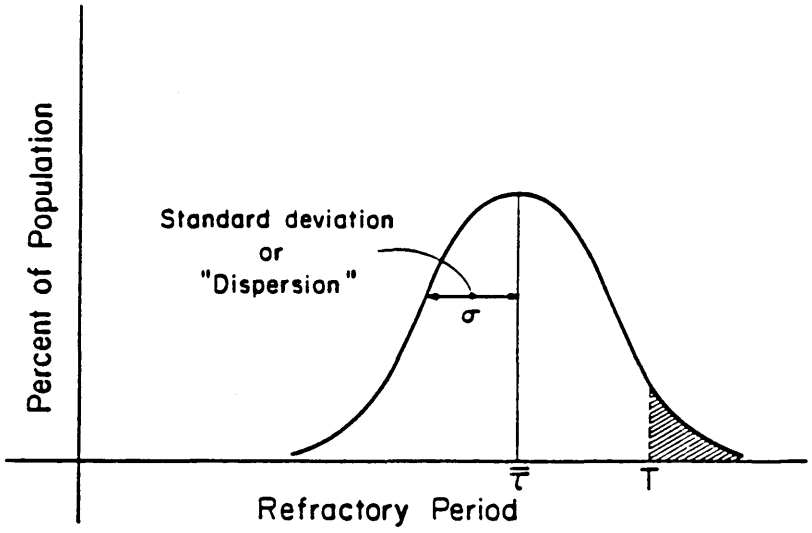

Figure 4.1: Distribution of Cellular Refractory Periods

The distribution has a mean value $\bar{\tau}$ and a standard deviation σ. T is the interstimulus interval. The shaded area, denoted the F population, indicates refractory times which exceed the interstimulus interval. (From Smith and Cohen, 1984)

4.2 A Model of the Heart Incorporating Dispersion

4.2.1 Topology of the Heart Model

Smith and Cohen (1984) approximated the ventricle as a thin walled cylindrical shell, shown in Figure 4.2. The shell was comprised of a series of L rings, each ring stacked one on top of the other. Each ring was subdivided into a string of D elements. Each element was square with linear dimension ξ. ξ physically represented the spatial length over which refractory periods are correlated. ξ was typically of the order of 1 mm. The total number of elements, N, was the product of L and D.

4.2.2 Element Electrical Activity

Figure 4.3 shows the electrical activity of an element. This activity is a simplified representation of the action potential of a cardiac cell. Each element could be in one of two electrical states: depolarized and repolarized. Once an element depolarized, it was refractory to stimulation for the duration of its preassigned refractory period. At the conclusion of the refractory period, the element state reverted back to that of repolarized. Refractory periods were randomly assigned to the elements according to a truncated Gaussian distribution with mean ($\bar{\tau}$) and standard deviation (σ). This assignment of refractory periods emulates the spatial dispersion in cellular recovery from

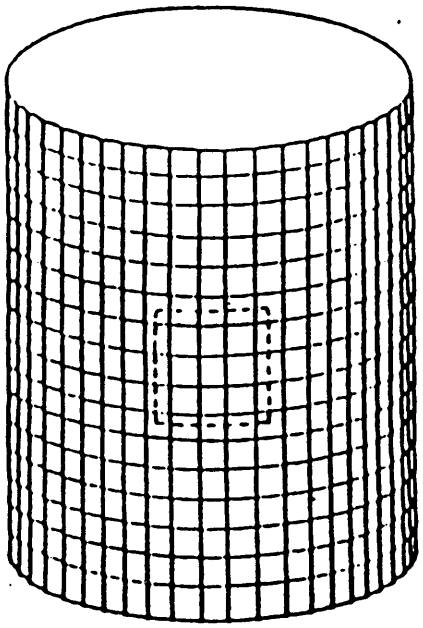

Figure 4.2: Topology of the Finite-Element Heart Model

The heart model shell is comprised of a series of L rings, each ring stacked one on top of the other. Each ring is subdivided into a string of D elements. (From Smith and Cohen, 1984)

excitation within the myocardium.

4.2.3 Electrical Conduction

The model contained one pacemaker element capable of spontaneous depolarization. This element spontaneously depolarized at a fixed interval r = 1/T. The remaining elements exhibited a stable repolarization state. Spread of electrical activation proceeded on an element to element basis via edge-triggered activation. A given element was depolarized if two conditions were met: 1) the element was non-

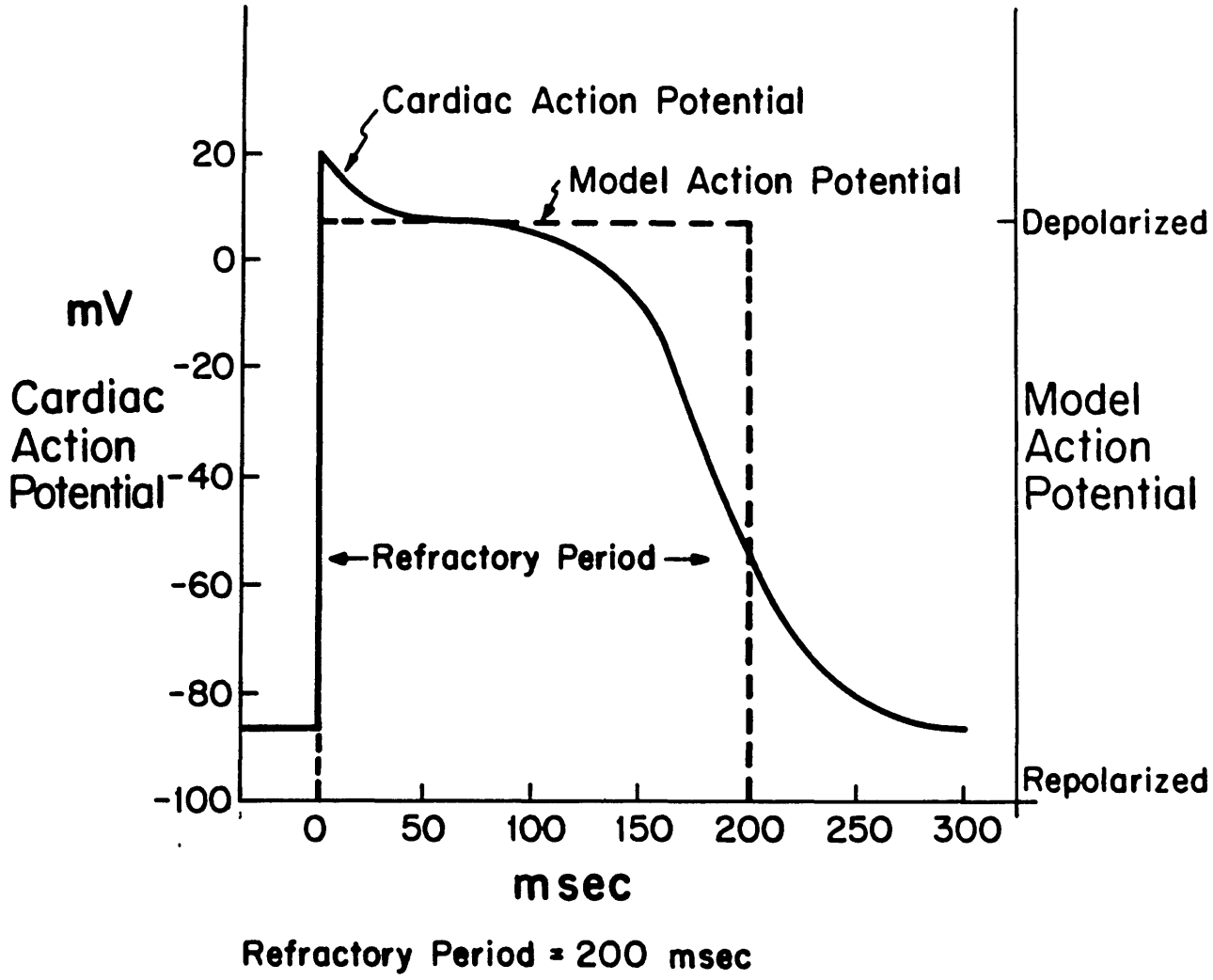

Figure 4.3: Element Electrical Activity

refractory, and 2) a neighboring element was depolarized during the previous time iteration. A neighboring element, shown in Figure 4.4

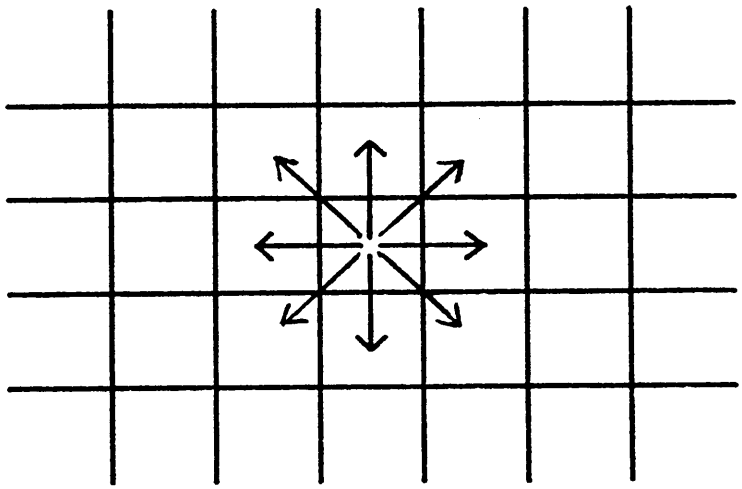

Figure 4.4: Assignment of Eight Nearest Neighbors

(Redrawn from Smith and Cohen, 1984)

was defined as one of the eight adjacent elements. Figure 4.5 shows the normal spread of electrical excitation. In the figure, a white box represents a repolarized element, a black box represents a recently depolarized element, and a gray box represents a refractory element not recently depolarized. Conduction velocity, v, was controlled by appropriate scaling of the iteration time t. One iteration per t seconds corresponded to a conduction velocity of ξ/v.

4.2.4 Generation of Simulated ECG's

The generation of simulated ECG's was based upon the dipole model

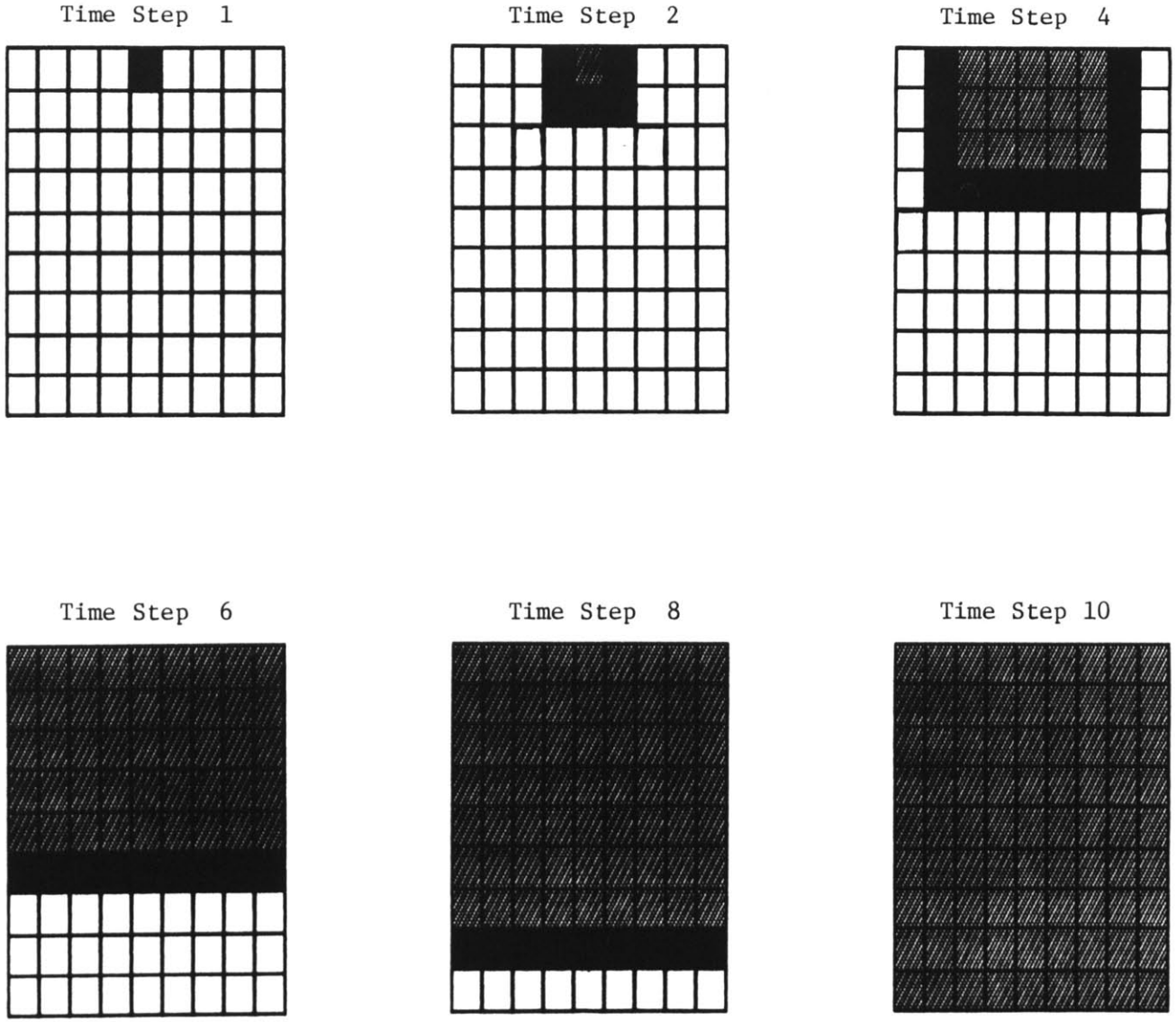

Figure 4.5: Schematic of Normal Depolarization in the Model of Smith and Cohen (1984)

A normal depolarizing wave spreads through a region of the heart. A white box represents a repolarized element. A gray box represents a depolarized element. A black box represents a recently depolarized element.

of cardiac electrical activity. A unit vector current dipole was assigned to each unit interface between all repolarized and depolarized elements, and oriented orthogonal to that interface. The cylindrical ventricle was situated at the center of a large spherical torso. The torso was assumed to be comprised of a linear, homogeneous, anisotropic, conductive medium. The total cardiac dipole could then be found as the vector sum of all the individual element interface dipoles. This summation could be made irrespective of the individual element interface dipoles. The total cardiac dipole was then projected onto the body surface in the form of a standard lead vector (scaling the conductivity and geometric considerations of the torso to unity).

4.3 Results of the Heart Model

By varying the parameters of the model, a number of reentrant rhythm disturbances were simulated. Figure 4.6

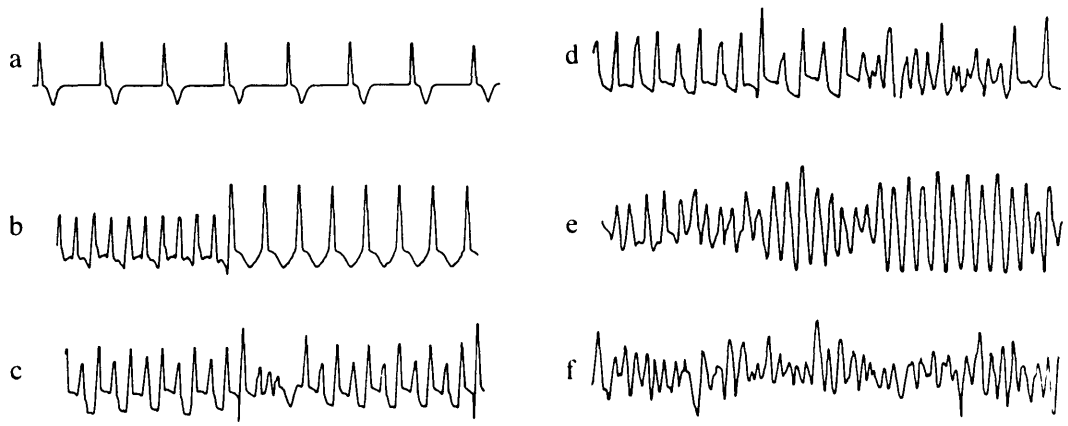

Figure 4.6: Simulated ECG's

(a) Normal rhythm. (b) Development of 2:1 conduction block (type i disturbance). (c) Three-beat reentrant excitation (type ii disturbance). (d) Multi-beat self-terminated reentrant activity (type ii disturbance). (e) Sustained reentrant rhythm that resembles VT (type iii disturbance). (f) Disorganized self-sustained rhythm that resembles VF (type iii disturbance). (From Smith and Cohen, 1984)

shows several of the simulated ECG's. The disturbances were of three main types: (i) simple 2:1 or 3:1 conduction blocks (non-reentrant) in which only every second or third pacemaker excitation resulted in

depolarization of the bulk of the array (see Figure 4.6b); (ii) short self-terminating reentrant disturbances (see Figures 4.6 c and d); and (iii) self-sustaining reentrant rhythms (see Figures 4.6 e and f). Note that Figure 4.6e resembles clinical tracings of VT, while Figure 4.6f resembles clinical tracings of VF.

The electrical stability of the model was systematically examined as a function of r, σ, v and $\bar{\tau}$ by first fixing σ, v and $\bar{\tau}$ and choosing r such that a normal rhythm resulted. A critical rate, r_c, was then found by decreasing r until a type i, ii or iii disturbance evolved. Figure 4.7 shows r_c versus σ, v and $\bar{\tau}$.

In Figure 4.7a (r_c versus σ), 2:1 conduction block was the most common disturbance for $\sigma < 100$ msec. For $\sigma > 100$ msec, type ii and iii disturbances occurred. As σ increased in this region, reentry occurred more easily (at lower r_c).

Figure 4.7b (r_c versus v) shows a monotonic rise in r_c with increasing v (up to v = 100 cm/sec). The disturbances noted in this region were of type iii. This result is consistent with the rough criterion for reentry of $l > v\,\tau$ (recall equation 3 .1). As conduction velocity increases, the opportunity for reentry increases. Above v = 100 cm/sec the disturbances were either type i or ii.

Figure 4.7c (r_c versus $\bar{\tau}$) shows that for a given σ there is a $\bar{\tau}$ value for which the critical rate is maximized. This is a result of the interplay between the development of wavefront fractionation and reentrant loops of excitation. Figure 4.1 shows that the F population (which facilitates wavefront fractionation) is increased by increasing $\bar{\tau}$. Yet, equation 3.1 shows that reentrant loops are facilitated by small τ. Figure 4.7c shows that the interaction of these two divergent

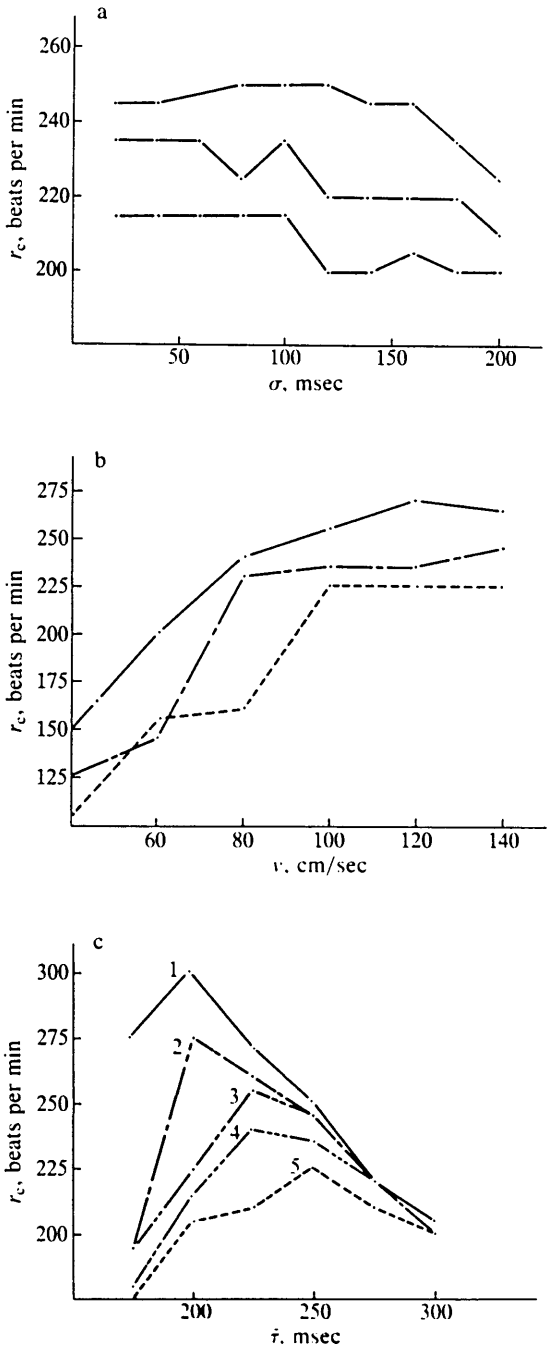

Figure 4.7: Critical Rates in the Model of Smith and Cohen (1984)

See test for discussion. (From Smith and Cohen, 1984)

criteria predict a region of maximum r_c.

4.4 Discussion of the Heart Model

The simple finite-element model allowed Smith and Cohen (1984) to examine the dependence of electrical stability on the four parameters r, σ, v and $\bar{\tau}$. Conceptually, they found two important factors which determined stability: 1) the size of the F population (as represented by Figure 4.1) and 2) the reentry criterion $l > v \tau$ (equation 3.1). In these two factors v is a free parameter, l is influenced by the size of the F population, and, as stated in the previous section, mean refractory period has a divergent effect. (That is, as mean refractory period decreases the F population <u>increases</u>, yet, the reentry criterion is <u>less</u> likely to be satisfied.)

The work of Han et al. (1964) and Spear et al. (1973) seems to support the results of Smith and Cohen (1984). Recall that both Han et al. (1964) and Spear et al. (1973) found electrical stability to decrease with increased dispersion. Han et al. (1964) further noted that this inverse relation existed whether the average refractory period was increased or decreased. Since the F population, v and l were not explicitly controlled, Han et al. (1964) seemed to be observing the interplay between the two stability factors noted by Smith and Cohen (1984).

4.5 Alternation as a Precursor to Rhythm Disturbances

Smith and Cohen (1984) were able to adjust the model parameters in order to study the behavior of the model as it approached states of reentrant activity. Prior to any frank rhythm disturbance, they found a distinct and regular pattern of electrical alternation (electrical alternans) in the morphology of the simulated ECG's. Figures 4.6c and d display this alternation. The ECG alternated between two distinct morphological patterns. Thus, beat 1 was similar to beats 3,5,7,... and beat 2 was similar to beats 4,6,8, ..., yet the odd and even beats were dissimilar. The source of the alternation was a population of model elements (the F population) which had a refractory period greater than the interstimulus interval. These elements could not respond to every heart beat. The wavefront of activation followed an alternating route as it circumvented these refractory barriers. Thus, a spatial-temporal alternation in the contour of the heart beat resulted. Smith and Cohen (1984) further suggested that there existed a sub-population of elements which were activated every second beat. Note that genesis of the alternation was based upon a populational effect - the action potentials of individual cells, when activated, were invariant.

Experimental evidence of electrical alternans has been provided by Adam et al. (1984), Smith (1985) and Smith et al. (1985). These authors investigated the relationship between electrical alternans of the ventricle and susceptibility to VF. Changes in dispersion, mean refractory period and interstimulus interval were accomplished in an animal preparation by altering heart rate, inducing systemic hypothermia and ligating coronary artery blood flow. They were able to inversely

correlate the degree of alternation present in the ventricular surface ECG with the VFT.

The above evidence supports a regime of electrical alternation as the transition stage between normal rhythms and chaotic reentrant rhythms. Feigenbaum (1980) has recently shown that some experimental systems have a common path to chaotic activity through a series of period-doubling bifurcations. If we note that electrical alternans represents a period doubling of the excitation frequency r, then the transition to VF may follow a trajectory similar to the systems described by Feigenbaum. (Smith, 1985; Smith and Cohen, 1984)

4.6 The Study of Electrical and Mechanical Alternation of the Heart

The dipole model accounts for the surface ECG as a vector sum of the individual activities of the various heart elements. A current vector is assigned at the interface between all depolarized and repolarized tissue. The contribution to the surface ECG from two vectors equal in magnitude but opposite in direction is null. The two vectors cancel. Thus, in the detection of surface ECG alternans, certain portions of the alternating component of the ECG may cancel. The vector summation may mask identification of a portion of those elements which are only activated every other beat.

The finite-element computer model predicts another form of alternation which does not suffer from the vector degeneracy. If the spatial-temporal contour of the heart beat alternates, then the mechanical activity of the heart should alternate as well as the electrical activity. An illustrative model of the composite mechanical activity of the heart (reflected in myocardial contractility or developed ventricular pressure) derived from the contribution of individual elements would provide a more integral sum of element activity. Individual element contractions sum in a linear fashion to produce the composite chamber contraction. (Caro et al., 1978) Thus, the analysis of mechanical alternation (mechanical alternans) of the heart might provide additional insight into the stability of the cardiac rhythm. A combination of electrical and mechanical alternans would be expected to provide the most information.

This thesis will investigate the role of an F population in the formation of electrical and mechanical alternans, and in the

determination of ventricular susceptibility to malignant reentrant rhythm disturbances (i.e. VF). A finite element computer model of the heart, in which the size of the F population (used as an approximation of the size of the alternating sub-population) can be controlled, will be constructed. The model will be exercised and the relationship between the F population and alternation will be investigated. An experimental animal model of the heart will also be investigated. Conditions which alter the stability of the heart will be compared to the electrical and mechanical alternans produced.

Chapter V

Mechanisms of Electrical and Mechanical Alternans

5.1 Introduction

Prior to delving into the models of the heart studied within this thesis, a review of the mechanisms of electrical and mechanical alternans will be presented. Electrical alternans occurs when the ECG alternates between two distinct morphological patterns. Similarly, mechanical alternans occurs when the mechanical activity of the heart (i.e. as measured via ventricular chamber pressure, ventricular contractility,...) alternates between two distinct morphological patterns. Mechanical alternans is most often detected in the systemic blood pressure of humans as this pressure can be monitored non-invasively (palpation at the body surface). Different theories variously hold that electrical and mechanical alternans are or are not related phenomenon. The review which follows will first present the mechanisms of electrical alternans, then the mechanisms of mechanical alternans and, lastly, the mechanisms of electrical-mechanical alternans.

5.2 Mechanisms of Electrical Alternans

Electrical alternans has been observed clinically during Prinzmetal's angina (Rozanski et al., 1978; Rozanski and Kleinfeld, 1982), in the long QT syndrome (Schwartz and Malliani, 1975; Sharma et al., 1981), during myocardial infarction (Puletti et al., 1980), in pericardial effusion (Colvin, 1958; McGregor and Baskind, 1955) and during exercise (Ring and Fenster, 1986; Wayne et al., 1983). The phenomenon can be isolated to the QRS complex (Colvin, 1958) or to the T wave (Navarro-Lopez et al., 1978) or found in both (McGregor and Baskind, 1955; Smith et al., 1985). In the experimental animal, electrical alternans has been seen during coronary artery occlusion (Adam et al., 1984; Hashimoto et al., 1983; Hellerstein and Liebow, 1950; Smith et al., 1985), rapid atrial pacing (Smith et al., 1985) and systemic hypothermia (Adam et al., 1984; Smith et al., 1985). In excised heart tissue, electrical alternans have been induced by rapid pacing (Lu et al., 1968; Spear and Moore, 1971), a reduction in tissue temperature (Lu et al., 1968) and changes in the content of the perfusion bath (Lu et al.,1968). Electrical alternans has been associated with an increased tendency for the heart to fibrillate (Adam et al., 1984; Navarro-Lopez et al., 1978; Rozanski et al., 1978; Rozanski and Kleinfeld, 1982; Smith et al., 1985). Three principle theories are advanced as the mechanism for electrical alternans: 1) populational changes in electrical conduction, 2) alternation of the cellular action potential waveform, and 3) global movement of the heart within the chest. Each of the three mechanisms is discussed below.

5.2.1 Populational Changes in Electrical Conduction

Alternation of electrical conduction is theorized to occur when the sequencing of myocardial activation alternates between two different pathways. Chapter four showed that such a process might occur if certain cells within the myocardium display a refractory period longer than the interstimulus interval. Two patterns of the depolarization/repolarization wavefront develop. Excitation progresses via the first pattern, then the second, then back to the first, etc. The genesis of the alternation is derived from the populational effect of the activation wavefront circumventing the refractory barriers - the action potentials of individual cells are invariant. Brody and Rossman (1937) have postulated that such an alternation might occur either in the specialized electrical conduction system of the heart or in the cell to cell conduction.

In either case, the development of surface ECG alternans can be understood by applying the dipole model of the heart. During any given time within the cardiac cycle the electrical state of individual cardiac cells will differ on alternate beats. The dipole model would then predict an alternation in the magnitude and/or direction of the total cardiac dipole, and thus the surface ECG. Smith and Cohen (1984) have shown that the application of the dipole model to a finite element computer model of a heart which exhibits alternation in element to element conduction does produce a surface ECG which contains alternans. In the model, the individual electrical activity of a given element was identical each time the element was excited. The surface alternation was formed from a spatial-temporal alternation in the contour of the

heart beat. Smith and Cohen (1984) also found that a sub-population of elements participated only in every second heart beat. Note, however, that a spatial-temporal alternation of the heart beat can occur even if all cells within the heart participate in every beat.

5.2.2 Alternation of the Cellular Action Potential Waveform

A number of investigators (Boyett and Jewell, 1980; Hogancamp et al., 1959; Kleinfeld and Stein, 1968; Lu et al., 1968; Nakashima, 1978; Spear and Moore, 1971) have shown the cellular action potential of a given cell to alternate on an every other beat basis. An example of this alternation is provided in Figure 5.1.

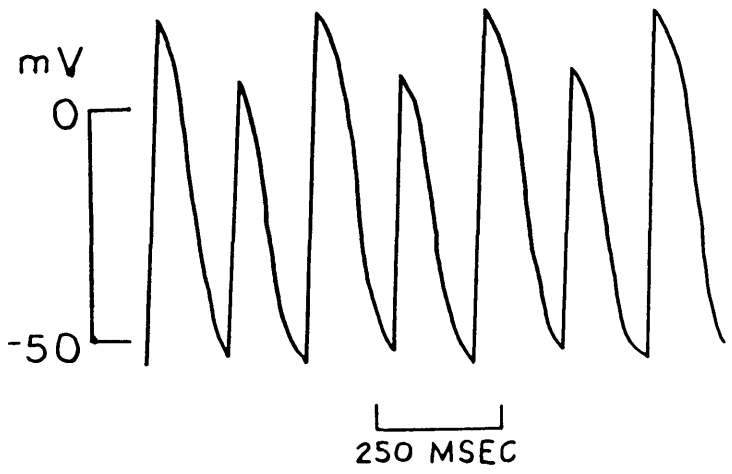

Figure 5.1: Electrical Alternation in a Single Ventricular Fiber

(Modified from Hogancamp et al., 1959)

Kleinfeld and Stein (1968) specifically identified four modes of action potential alternation in the: 1) rate of depolarization, 2) rate of

repolarization, 3) magnitude of the action potential, and 4) magnitude of hyperpolarization. They correlated alternation in the rate of depolarization and of repolarization of the action potential with electrical alternans of the QRS complex and T wave, respectively.

It has has also been suggested that alternation of the cellular action potential waveform can be induced secondary to an alternation in the contraction processes of the cell (Adler et al., 1985a; Spear and Moore, 1971). Spear and Moore (1971) have found that alternation in the isometric force appears to have its basis in alternate incomplete relaxation causing an alternate decrease in the inotropic state of the muscle. The actual failure is mechanical, but the failure effects the formation of the transmembrane potential. Both the calcium and potassium ions have been implicated in this process.

The development of surface ECG alternans can again be understood by applying the dipole model of the heart. The alternating cellular action potential waveforms cause the magnitude and/or direction of the total cardiac dipole to alternate. Surface ECG alternans result.

Note that populational changes in electrical conduction and alternation of the cellular action potential waveform both result in an alternation in the magnitude and/or direction of the total cardiac dipole. Analysis of surface ECG can not distinguish between the two mechanisms at this time. In fact, detailed extracellular electrical recordings taken directly from the heart would have difficulty in distinguishing between these two mechanisms of alternation. This is because the population changes in electrical conduction can cause the orientation of the propagating wavefront to alternate as it passes through regions of the myocardium. Figure 5.2 shows this concept. The

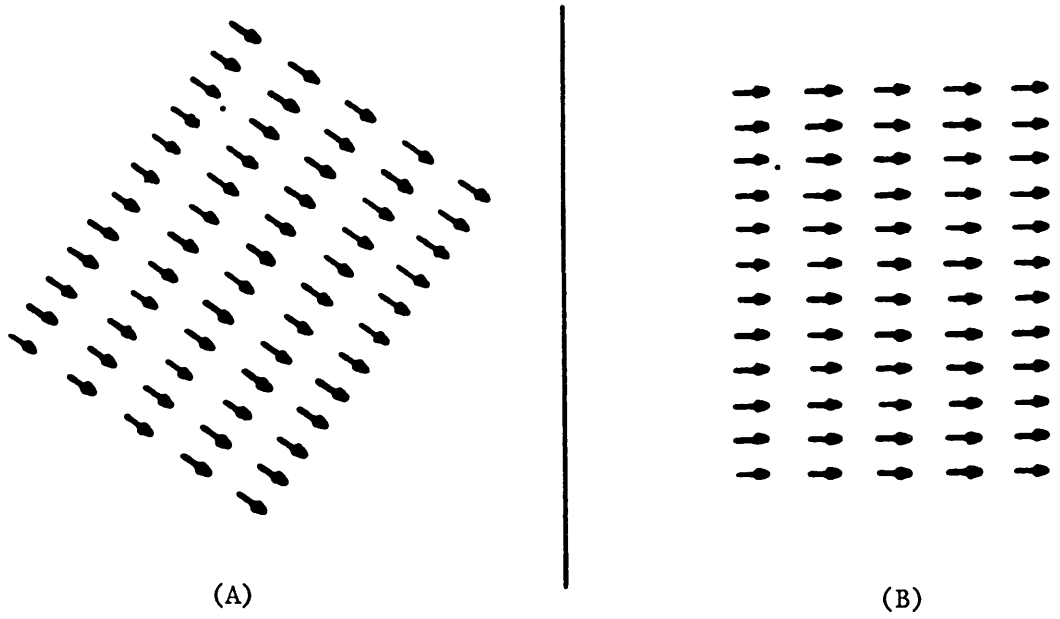

Figure 5.2: Alternating Orientation of the Propagating Wavefront

A propagating wavefront traverses a region of the myocardium traveling in the direction shown in A. On the ensuing beat, the wavefront traverses the region traveling in the direction shown in B. ECG recorded from this area would alternate.

propagating wavefront first traverses a region of the myocardium traveling in the direction shown in Figure 5.2A. On the ensuing beat, the wavefront traverses the region traveling in the direction shown in Figure 5.2B. This pattern repeats. An electrocardiogram taken from this area will show alternation. There is, however, no failure in the response of individual cells. Yet, individual cellular action potentials will alternate as a consequence of the alternate orientation of the propagating wavefront. (Recall from Figure 2.16 that the

orientation of the propagating wavefront determines the orientation of the generated current dipole and, thus, the orientation of its contribution to the observed electrocardiogram.)

It is interesting to observe in Figure 5.1 that, on close observation, the intervals between successive action potentials alternate. Populational changes in electrical conduction may have contributed to this phenomenon. Conversely, an alternation in the action potential may cause a change in electrical conduction. (Recall that action potentials elicited prior to completion of the full recovery time tend to be altered in form and have a slower conduction velocity.) In either case, the above two forms of electrical alternans might often be found simultaneously.

5.2.3 Global Movement of the Heart Within the Chest

Alternation of the electrical activity of the heart has been observed clinically in association with pericardial effusion (Colvin, 1958; McGregor and Baskind, 1955). In pericardial effusion, the pericardial sac which encases the heart becomes fluid filled. The heart floats within the sac and is free to rotate. It is theorized that a periodic rotation develops at a frequency of half the heart rate. The total cardiac dipole, which is constant in magnitude for all beats, rotates in orientation on alternate beats. Consequently, the surface ECG alternates.

Although Colvin (1958) suggested that this mechanism may not be restricted to cases of pericardial effusion, it is generally accepted to be restricted as such. Additionally, two non-invasive diagnostic means

exist by which this mechanism can be differentiated from the others. First, the global movement of the heart causes alternation in the P wave, QRS complex and the T wave. The previously mentioned mechanisms have only been shown to cause alternation in the QRS complex and the T wave. Second, global movement of the heart within the chest can be detected by echocardiography.

5.3 Mechanisms of Mechanical Alternans

Mechanical alternans is typically diagnosed as an alternation in pulse pressure - a condition clinically termed pulsus alternans. In a broader sense, however, mechanical alternans can be found in myocardial pressure, volume, flow or contractility. Clinically, in the experimental animal, and in excised heart tissue mechanical alternans has been associated with a rapid heart rate (Gilbert et al., 1965; Lewis, 1910; Mitchell et al., 1963; Spear and Moore, 1971), hypothermia (Lu et al., 1968), coronary artery occlusion (Hashimoto et al., 1983), premature ventricular contractions (Carlson and Rapaport, 1984; Nayler and Robertson, 1965), aortic stenosis (Cohn et al., 1967), various drugs (Badeer, 1967; Lu et al., 1968), cardiac tamponade (Gaffney et al., 1984), systemic hypertension (Hada et al., 1982), and the markedly degenerate heart (Hada et al., 1982; Lewis, 1910). Two fundamental mechanisms have been proposed to explain mechanical alternation: 1) modulation of the heart via intrinsic regulatory mechanisms, and 2) an alternation in the contractile state of the heart. These mechanisms, and their various extensions, are discussed subsequently.

5.3.1 Modulation of the Heart via Intrinsic Regulatory Mechanisms

Figure 5.3 illustrates how modulation of the heart via intrinsic regulatory mechanisms (recall Section 2.4.1) can explain mechanical alternation. In a fixed contractile state, the heart alternates between two pressure - volume contours. Carlson and Rapaport (1984) claimed that the duration of systole was longer during the strong beat. Since

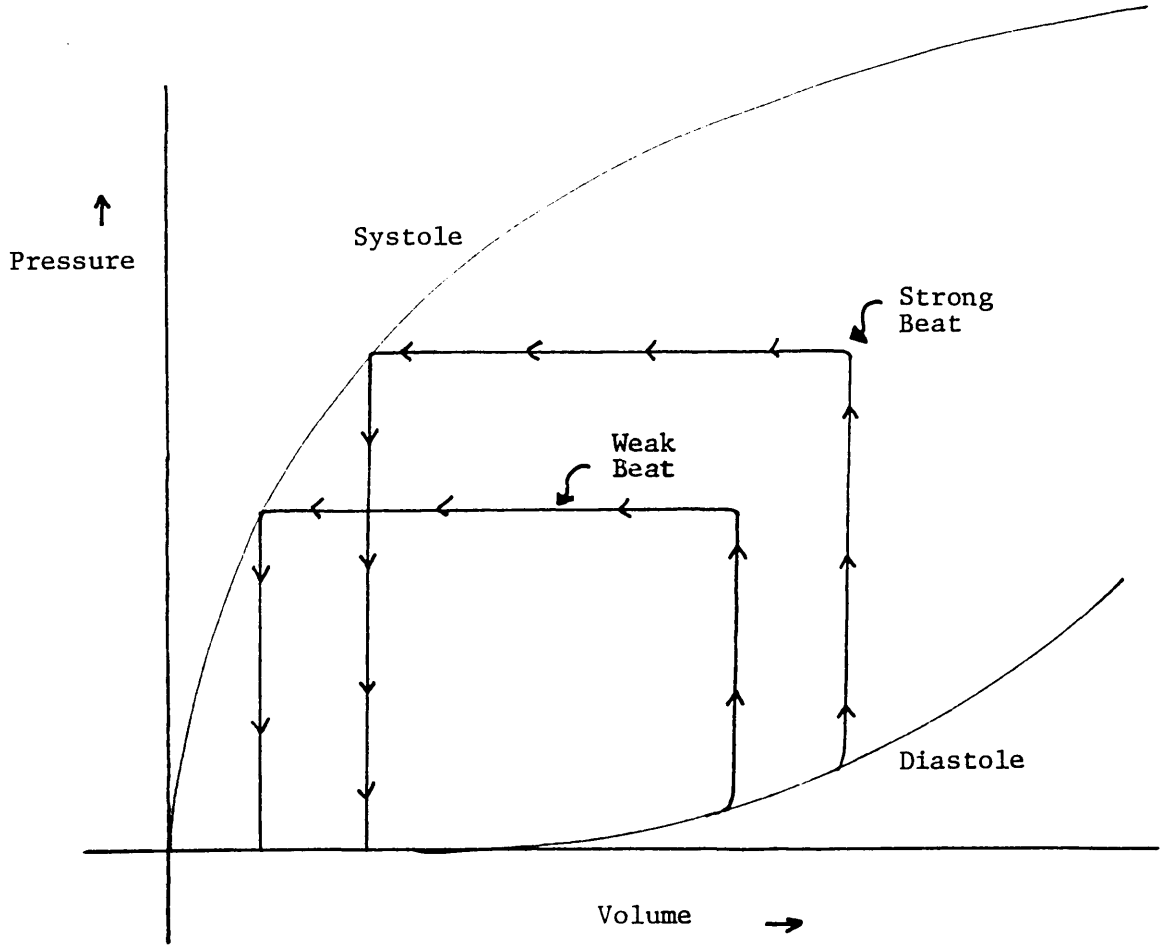

Figure 5.3: Pressure-Volume Loop Showing Mechanical Alternans Due to Intrinsic Modulation

the interval between beats is fixed, the ensuing beat has less diastolic filling time. The end diastolic volume is reduced and a weak beat results. The weak beat has a shortened systole allowing a prolonged filling time for the ensuing strong beat. Thus, the interstimulus interval remains fixed, but the relative durations of systole and diastole alternate. End diastolic volume alternates causing the developed pressure to alternate via intrinsic regulatory mechanisms of the heart.

Mitchel et al. (1963) affirmed that an inadequate diastolic period might hinder ventricular filling, but added that it might foster incomplete ventricular relaxation as well. In this case, the relationship between diastolic fiber length and myocardial contractility is stressed. The weak beats are initiated from short diastolic fiber lengths and the strong beats from long diastolic fiber lengths. Time is not the true variable, but end diastolic fiber length. Since end diastolic fiber length is a direct function of end diastolic volume, an alternation in end diastolic volume will always accompany this form of mechanical alternans.

5.3.2 Alternation in the Contractile State of the Heart

Alternation in the contractile state of the heart (also termed the myocardial theory) holds that alternation in the mechanical performance of the heart is a direct result of alternation in myocardial contractility. Figure 5.4 illustrates a pair of pressure - volume loops which display a beat to beat alternation in contractile state. The activity of the heart alternates between the two pressure - volume curves and, thus, the two contractile states. Note that although Figure 5.4 does not display an alternation in diastolic performance - such may also be the case. McGaughey et al. (1985) have provided evidence that intrinsic regulation of the heart may potentiate this alternation in contractile state.

Two cellular phenomenon are advanced to explain the changes in contractility; 1) an alternation in the number of cells involved in systole (Sideris et al., 1981; Wiggers, 1952) and 2) an alternation in

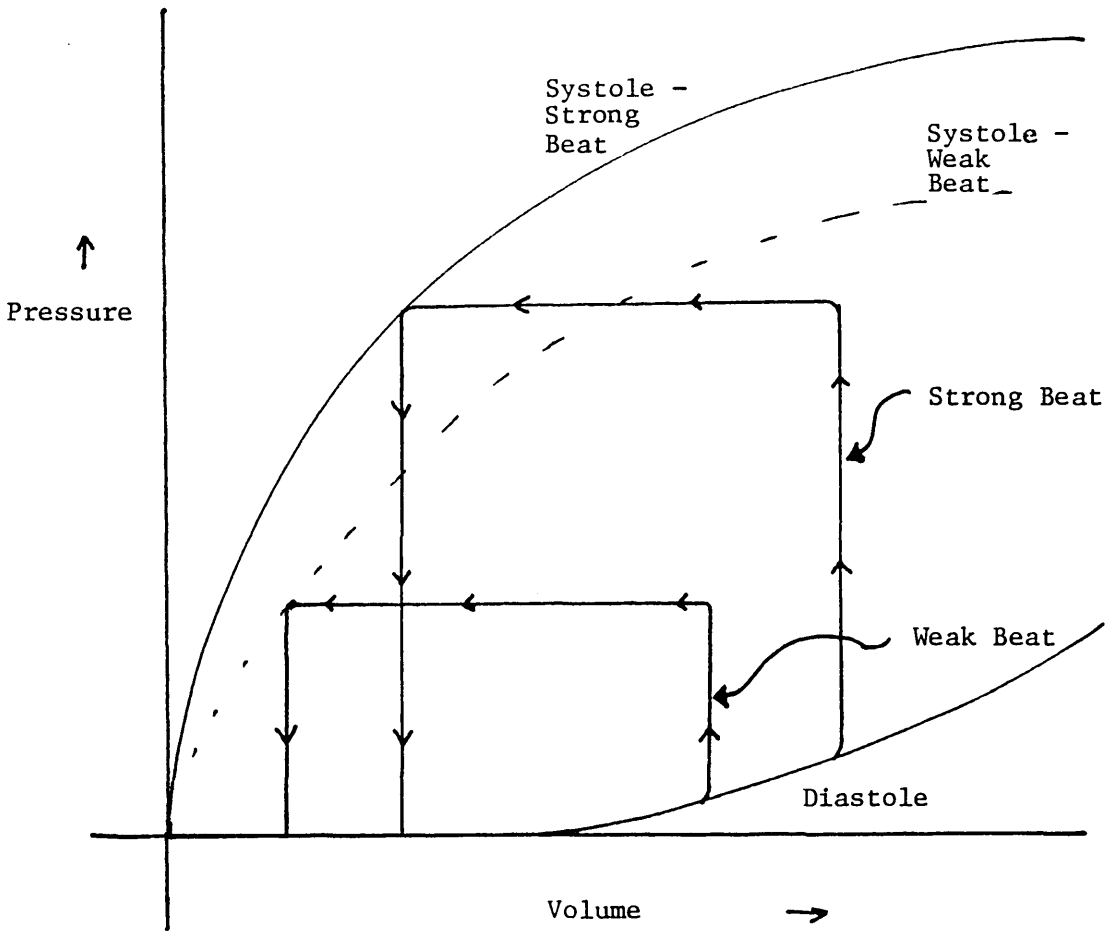

Figure 5.4: Pressure-Volume Loop Showing Mechanical Alternans Due to Myocardial Contractility

the contractile strength of each cell (Adler et al., 1985a; Badeer et al., 1967; Gilbert et al., 1965; Guntheroth et al., 1969; Nayler and Robertson, 1965). These two explanations are entirely analogous to the cases of 1) populational changes in electrical conduction and 2) alternation of the action potential waveform, for the case of electrical alternans. Although these two alternans mechanisms were reported separately for the case of electrical alternans, they have been combined into one general mechanism in the case of mechanical alternans. This

classification parallels the manner in which each alternans form is classically described in the literature.

5.4 Mechanisms of Electrical - Mechanical Alternans

The incidence of combined electrical-mechanical alternans is somewhat rare in the literature, being associated with a rapid heart rate (Kleinfeld et al., 1963; Lu et al., 1968; Spear and Moore, 1971), coronary artery occlusion (Hashimoto et al., 1983), a decrease in temperature (Braveny, 1964), and various drugs (Ellis, 1960; Lu et al., 1968). The mechanisms of combined electrical-mechanical alternans are derived from the mechanisms of either electrical or mechanical alternans. This can be understood by compressing the various mechanisms of alternation into three general categories: 1) a populational change in electrical conduction, 2) alternation in the response to activation of individual cells and, 3) global mechanical actions of the heart.

The first mechanism category is comprised of populational changes in electrical conduction and mechanical alternation in the number of cells involved in systole. These two cases, in fact, may be reconciled as one. If a sub-population of cells are electrically activated in an alternating fashion, then they are equally mechanically activated in this alternating fashion. This results in a dual alternation.

The second mechanism category is comprised of alternation of the action potential waveform and alternation in the contractile strength of each cell. The basic failure for this category occurs within the cell. Since the electrical and mechanical activities of individual heart cells are tightly bound, any alternation derived from within the cell might be expected to elicit an alternation in both the electrical and mechanical activities of the cell.

The third mechanism category is comprised of global movement of the

heart within the chest and modulation of the heart via intrinsic regulatory mechanisms. Both of these mechanisms entail macroscopic movement of the heart. Electrical alternans, therefore, develops due to macroscopic movement in the orientation of the total cardiac dipole. In the case of global movement of the heart within the chest, mechanical alternans might be expected as a direct result of the movement of the heart. For the case of modulation of the heart via intrinsic regulation, the mechanism of mechanical alternation has been previously explained.

Chapter VI

A Finite-Element Electrical-Mechanical Model of the Heart

6.1 Introduction

Smith and Cohen (1984) have shown in a finite-element model of the ventricle that a region of electrical alternans was consistently encountered during the transition from a normal rhythm to a chaotic rhythm. Adam et al. (1984), Smith (1985), and Smith et al. (1985) further showed in an animal model an inverse correlation between the degree of alternation present in the ventricular surface ECG and the electrical stability of the heart (as measured by the VFT test). This thesis has developed the hypothesis that mechanical alternans could well accompany the electrical alternans. The electrical and mechanical alternans may serve as a measure of the size of the F population and the electrical stability of the heart. As well, the combined study of both alternans forms may define a clearer relationship between alternation of the heart and electrical stability.

In order to evaluate the relationship between electrical alternans, mechanical alternans and the size of the F population, a simple finite-element electrical-mechanical computer model of the heart was constructed. The electrical portion of the model was almost identical to the model of Smith and Cohen (1984) detailed in Chapter IV. The mechanical portion of the model will be described presently. Thus, features of electrical excitation as well as mechanical contraction were modeled. The surface ECG, blood pressures, left ventricular volume, and left ventricular pressure were simulated. Electrical and mechanical alternans were then quantified utilizing a method described by Smith (1985).

6.2 Construct of the Finite-Element Heart Model

6.2.1 Topology of the Finite-Element Heart Model

A single left ventricle was approximated as a thin-walled cylindrical shell, shown previously in Figure 4.2. The shell was comprised of a series of L rings, each ring being sub-divided into D square elements of linear dimension ξ. The total number of elements, N, was the product of L and D. This is precisely the topology of the model of Smith and Cohen (1984).

6.2.2 Electrical Activity of the Finite-Element Heart Model

The electrical activity of the finite-element heart model closely parallels the model of Smith and Cohen (1984) described in Section 4.2. Element electrical activity is exactly as described previously. An element has two electrical states: depolarized and repolarized. Refractory periods were assigned according to a truncated Gaussian distribution. Electrical conduction followed the same scheme as Smith and Cohen (1984) except that a neighboring element, shown in Figure 6.1, is defined as one of the four adjacent elements sharing a common face. Figure 6.2 illustrates the normal spread of electrical excitation. Simulated ECG's were derived in the same manner suggested by Smith and Cohen (1984). Three vectors were derived, each representing a projection onto orthogonal leads of a Cartesian coordinate system. The three vectors are termed ECG X, ECG Y and ECG Z.

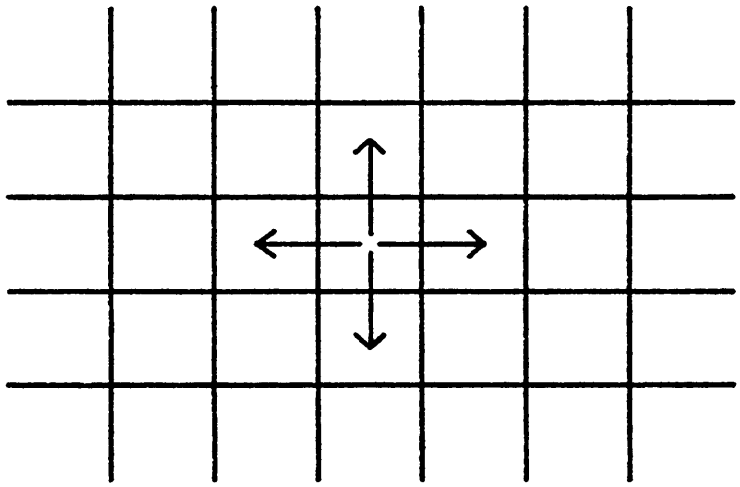

Figure 6.1: Neighboring Element Assignments

A neighboring element is defined as one of the four adjacent elements sharing a common face.

6.2.3 Mechanical Activity of the Finite-Element Heart Model

6.2.3.1 Element Mechanical Activity

Figure 6.3 shows the mechanical activity of an element. This activity has been based upon the previously explained excitation-contraction process of the cardiac cell. The mechanical activity of an element can be in one of two states: contracted or relaxed. Once an element contracts, it remains contracted for a period of time equal to its previously assigned element electrical refractory period. When the contraction period completes, the element reverts back to the relaxed state. Element excitation-contraction coupling, depicted previously in

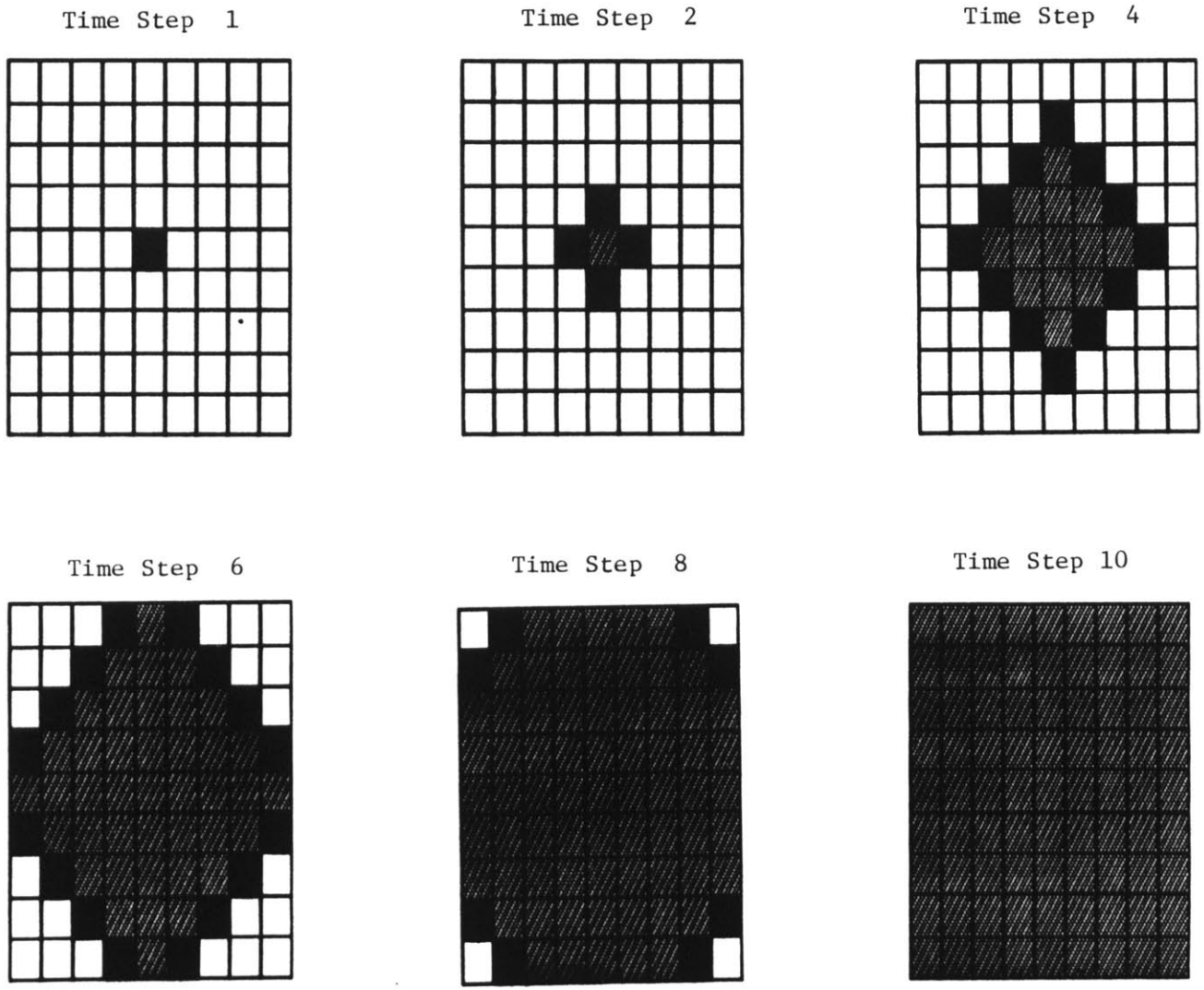

Figure 6.2: Schematic of Normal Spread of Electrical Excitation

Figure depicts the flow of a normal depolarizing wave. A white box represents a repolarized area. A gray box represents a depolarized area. A black box represents a recently depolarized area.

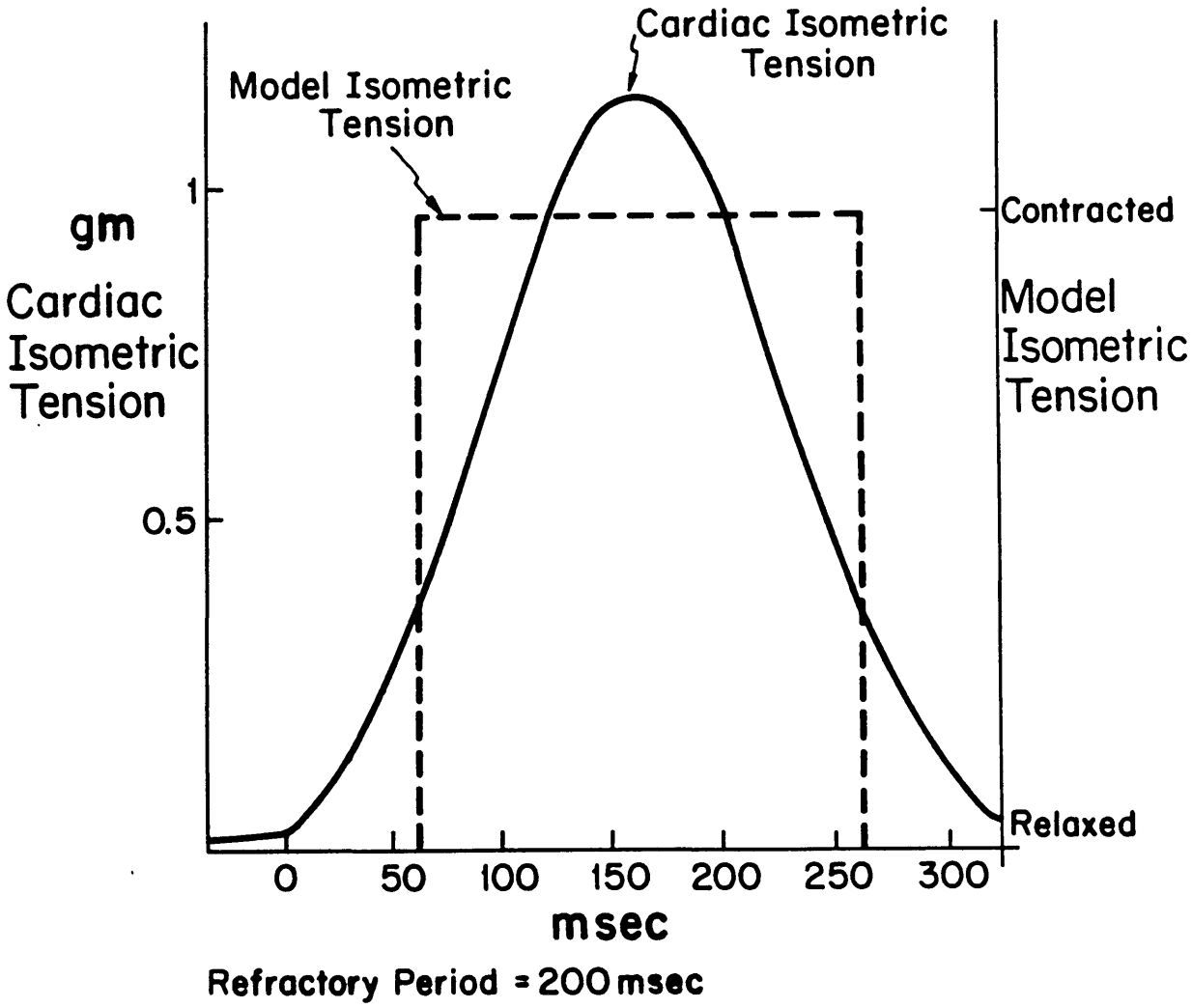

Figure 6.3: Element Mechanical Activity

Figure 2.7, is modeled as one-to-one. Contraction is initiated directly by and in synchrony with electrical depolarization. Thus, all depolarized elements are contracted and all repolarized elements are relaxed. This scheme departs from the timing of the actual excitation-contraction process. (Recall that contraction occurs a short time after electrical depolarization.) But, this modeling approximation is common to all elements. Thus, the derived blood pressures, left ventricular volume and left ventricular contractility will consequently experience a simple time shift in their entire waveform. This shift in time does not, however, alter the results of the alternans quantification process.

6.2.3.2 Mechanical Contraction

Rules have been assigned to govern the contraction pattern of the cylindrical shell. Each ring within the shell is constrained to concentric fixed-height contractions about the cylinder midline. Thus, the height and center of each ring remain fixed, while the radius is allowed to contract/ expand. Since there is no vertical contraction, adjacent rings do not interact directly. Each element within a ring is assigned a length-tension relationship for its contracted state and for its relaxed state. The radius of each ring can then be determined from the activation state of the elements which comprise the ring and the internal shell pressure.

Equations describing the above mode of contraction can now be written. The length-tension relationship for an element is;

$$t_{ij} = f(l_{ij}) \qquad (6.1)$$

where

t_{ij} = tension of the j^{th} element in the i^{th} ring,

l_{ij} = length of the j^{th} element in the i^{th} ring,

and the length-tension relationship is uniform for all elements. Next, a quasi-static approximation of element movement is made in which it is assumed that elements on a ring do not accelerate. All elements on the ring must assume a common tension. Thus, the length-tension relationship can be simplified to;

$$T_i = f(l_{ij}) \tag{6.2}$$

where

T_i = tension in the i^{th} ring.

Laplace's law relates ring tension to ring radius and internal shell pressure for a thin walled shell (assuming the external shell pressure is zero) as;

$$T_i = P\, r_i \tag{6.3}$$

where

P = internal shell pressure,

r_i = radius of the i^{th} ring.

The circumference of a given ring is;

$$CIRC_i = \sum_{j=1}^{D} l_{ij} = 2\, \pi\, r_i \tag{6.4}$$

where

$CIRC_i$ = circumference of the i^{th} ring,

D = number of elements in a ring.

The volume of blood surrounded by each ring is;

$$Q_i = h \pi r_i^2 \tag{6.5}$$

where

Q_i = volume of the i^{th} ring,

h = constant height of each element.

Finally, the expression for the total shell chamber volume is;

$$Q = \sum_{i=1}^{L} Q_i \tag{6.6}$$

where

Q = total shell chamber volume,

L = number of rings in the shell.

A definitive functional length-tension relationship must now be derived. To do so, recall that from empirical data Suga and Sagawa (1974), Suga et al. (1973), Sunagawa et al. (1982), and Sunagawa and Sagawa (1982) have mathematically described the ventricle via the volume-pressure ratio,

$$\frac{Q(t)}{P(t)} = C(t) \tag{6.7}$$

where

Q(t) = instantaneous ventricular volume,

P(t) = instantaneous ventricular pressure,

C(t) = instantaneous ventricular capacitance.

C(t) is a measure of the instantaneous contractile state of the ventricle, independent of ventricular volume or outflow impedance. It is desired that this empirical relationship be maintained in the finite-element model. Thus, a general power law tension-length relation

of the following form was selected;

$$(T_i)^{\alpha} = k_{ij}\, l_{ij} \tag{6.8}$$

where

α = a static constant,

k_{ij} = constant for the j^{th} element in the i^{th} ring.

Note that k_{ij} can take on only two values - the value K_c for contracted elements and the value K_r for relaxed elements. It was desired that an α be found to satisfy the empirical volume-pressure relation of equation 6.7. Substituting equation 6.8 into equations 6.3-6.6 yields;

$$Q = \frac{(2\pi)^{\frac{2\alpha}{\alpha-1}}}{4\pi}\, h\, p^{\frac{2\alpha}{1-\alpha}} \sum_{i=1}^{L} \left[\frac{N_{ci}}{K_c} + \frac{N_{ri}}{K_r}\right]^{\frac{-2}{\alpha-1}} \tag{6.9}$$

where

N_{ci} = number of contracted elements in the i^{th} ring,

N_{ri} = number of relaxed elements in the i^{th} ring.

Equation 6.9 reduces to the equation 6.7 ratio if;

$$\frac{2\alpha}{1-\alpha} = 1 \tag{6.10}$$

and

$$C = \frac{(2\pi)^{\frac{2\alpha}{\alpha-1}}}{4\pi}\, h \sum_{i=1}^{L} \left[\frac{N_{ci}}{K_c} + \frac{N_{ri}}{K_r}\right]^{\frac{-2}{\alpha-1}} \tag{6.11}$$

Thus, α is specified as;

$$\alpha = \frac{1}{3} \tag{6.12}$$

and the length-tension relationship has the form;

$$(T_i)^{\frac{1}{3}} = k_{ij}\, l_{ij} \qquad (6.13)$$

It is interesting to note that a cubic length-tension relationship resembles the simple static relationship between length and tension in human papillary muscle shown previously in Figure 2.9. The shell capacitance is expressed as;

$$C = \frac{h}{8\,\pi^2} \sum_{i=1}^{L} \left[\frac{N_{ci}}{K_c} + \frac{N_{ri}}{K_r} \right]^3 \qquad (6.14)$$

The value of C can be determined directly from the present state of the shell. Thus, the entire mechanical contraction process can be represented by a single measure - the contractile state of the shell. Note that if all elements in the shell are contracted, a "systolic" capacitance, C_s is defined as;

$$C_s = \frac{h\,H}{8\,\pi^2} \frac{D^3}{K_c^3} \qquad (6.15)$$

Likewise, if all elements in the shell are relaxed, a "diastolic" capacitance, C_d, is defined as;

$$C_d = \frac{h\,H}{8\,\pi^2} \frac{D^3}{K_r^3} \qquad (6.16)$$

6.2.3.3 Generation of Simulated Blood Pressure

Figure 6.4 shows an electrical circuit model of the mechanical properties of the left ventricle and the periphery. Electrical voltage represents mechanical pressure and the flow of electrical current represents the flow of blood. The ventricle is modeled as a time-varying capacitor. The value of this capacitance is derived from the state of the shell, as explained in the previous section. The mitral

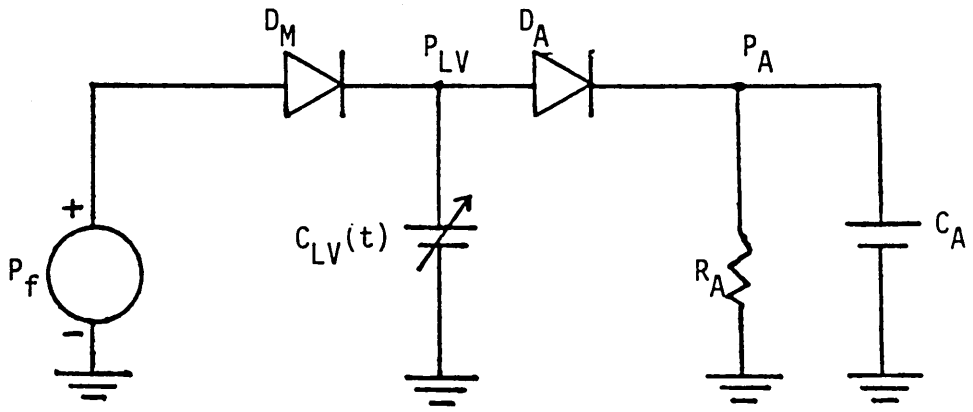

Figure 6.4: Electrical Circuit Model of the Mechanical Properties of the Left Ventricle and Periphery

The ventricle is modeled as the capacitor $C_{LV}(t)$. The mitral and aortic valves are modeled as the ideal diodes D_M and D_A, respectively. The pressure source P_f is the preload. The parallel resistor-capacitor R_A-C_A form the Windkessel afterload.

valve and the aortic valve are modeled as the ideal diodes D_M and D_A, respectively. Preload to the ventricle is assumed to be a constant filling pressure of value P_f. Ventricular afterload is that of the Windkessel approximation with a peripheral resistance, R_A, shunting a peripheral capacitance, C_A.

Figure 6.5 shows the four possible states which the mechanical properties model can assume. State 1 (D_M = ON, D_A = ON) does not correspond to a natural physiologic state, but is required during

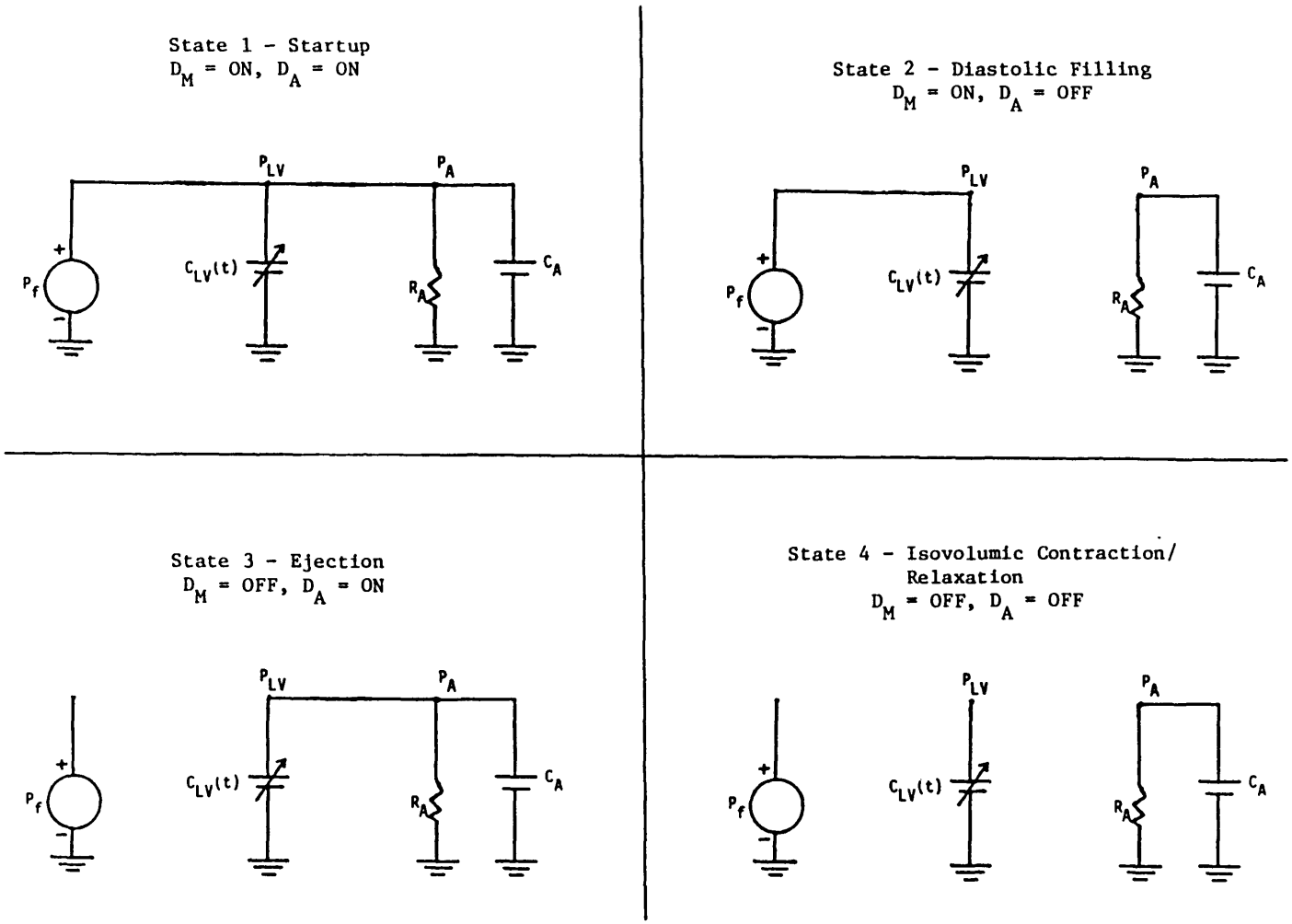

Figure 6.5: Four States of the Mechanical Properties Model

startup of the finite-element heart model. State 2 (D_M = ON, D_A = OFF) corresponds to the diastolic filling period. State 3 (D_M = OFF, D_A = ON) corresponds to the ejection phase. State 4 (D_M = OFF, D_A = OFF) represents both the isovolumic contraction phase and the isovolumic relaxation phase. The mathematical equations which govern ventricular pressure, ventricular volume and systemic pressure during each of the states are provided in Figure 6.6.

	Model State	Value of P_{LV}	Value of Q_{LV}	Value of P_A
1)	Startup	P_f	$C_{LV}(t)\ P_{LV}$	P_f
2)	Diastolic Filling	P_f	$C_{LV}(t)\ P_{LV}$	$P_{A_o} e^{\frac{-(t-t_o)}{R_A C_A}}$
3)	Ejection	$\frac{dP_{LV}(t)}{dt}\left[C_{LV}(t) + C_A\right] + P_{LV}(t)\left[\frac{dC_{LV}(t)}{dt} + \frac{1}{R_A}\right] = 0$	$C_{LV}(t)\ P_{LV}$	P_{LV}
4)	Isovolumic Contraction/ Relaxation	$\frac{Q_o}{C_{LV}(t)}$	Q_o	$P_{A_o} e^{\frac{-(t-t_o)}{R_A C_A}}$

Figure 6.6: Mechanical Properties Model Equations

Equations governing left ventricular pressure (P_{LV}), left ventricular volume (Q_{LV}) and arterial blood pressure (P_A) for the four model states. The subscript "o" denotes the value of the variable at the time the given state is entered.

6.3 Analysis Methods

6.3.1 General Scheme of Alternation Quantification

Smith (1985) and Smith et al. (1985) have found significant, yet extremely subtle, levels of alternation present in their ECG data. The alternation, often on the order of only a few millionths of the total waveform energy, is not easily identified through visual inspection. Thus, they developed a highly sensitive method of alternans quantification. They applied this method exclusively for the quantification of electrical alternans in physiologic models. The method will be applied herein for the study of electrical and mechanical alternans in both physiologic and finite-element models. A general review of the method is presented in this section. Ensuing sections provide the particulars employed in the analysis of the finite-element heart model data.

Figure 6.7 is a flowchart of the general method of alternation quantification. A single channel of data is appropriately sampled (see Figure 6.8A) and fiducial points (timing markers identifying a common location within each beat) are identified. A two pass process is used to locate the fiducial points. Beat detection is used in the first pass (see Figure 6.8B) to provide a crude estimate of the fiducial points (QRS detection for electrical data and peak systole for mechanical data). The results of the first pass are inspected to insure that all beats have been correctly identified. The second pass begins by computing a single template beat formed as the average of all beats identified during the first pass (see Figure 6.8C). This average is

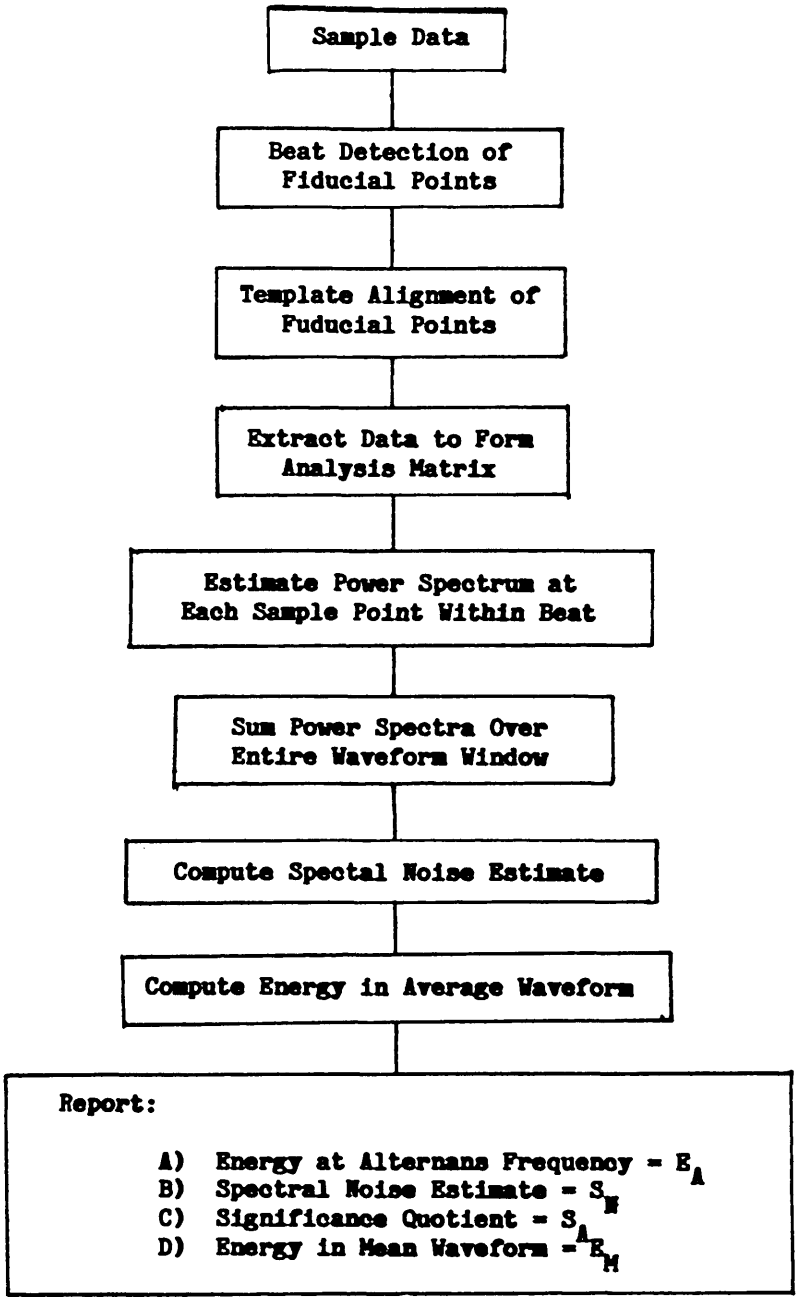

Figure 6.7: Flowchart of the Method of Alternation Quantification

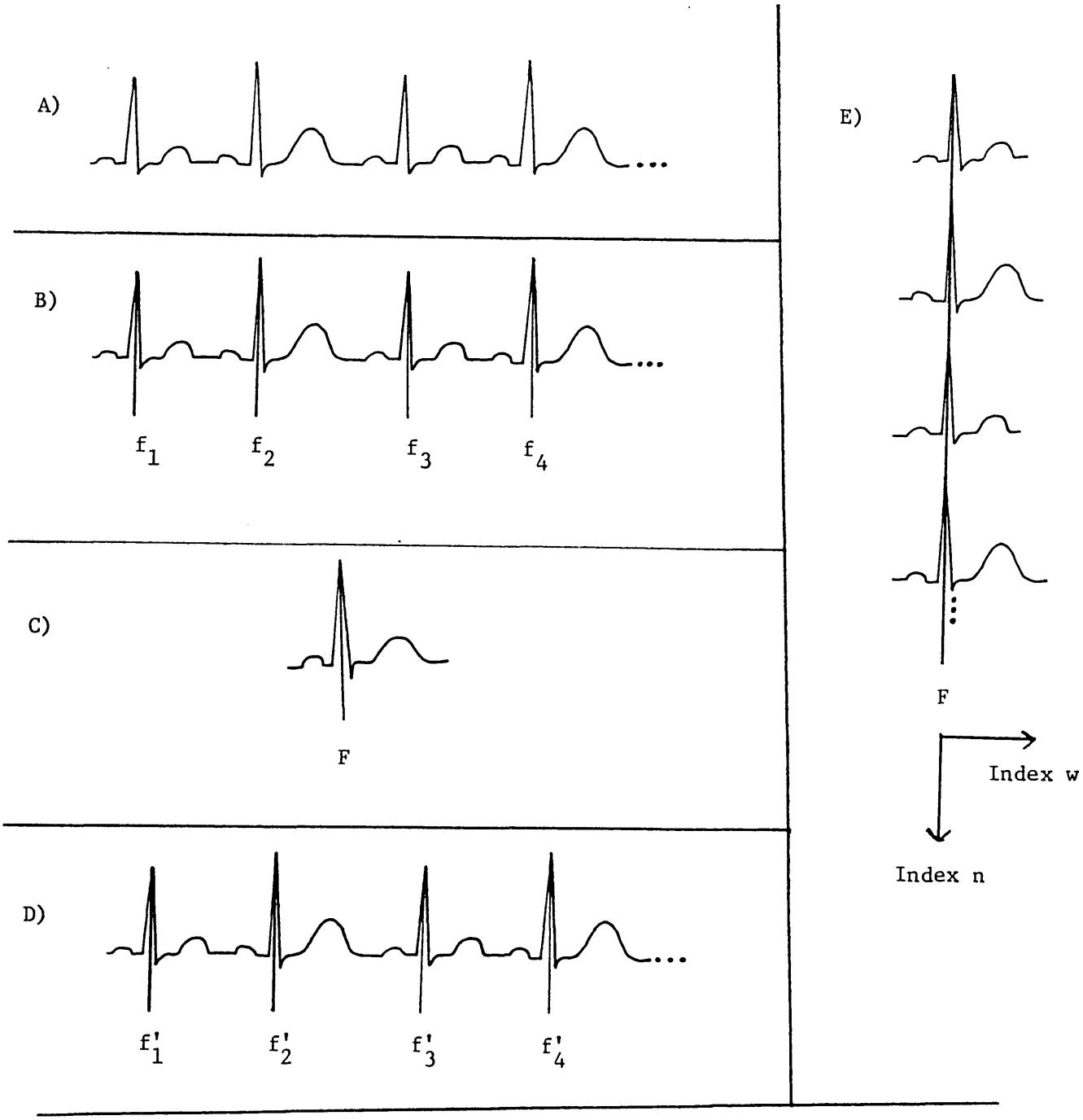

Figure 6.8: Illustration of ECG Beat Alignment

The waveform is sampled (A) and fiducial point estimates, denoted f_n are identified by QRS detection (B). A template beat is formed (C) and the fiducial point estimates are refined by comparison to the template beat (D). A data matrix M(n,w) is then formed (E). See text for details.

formed over a fixed, non-overlapping window of data centered about each fiducial point estimate. Each individual beat is then compared to the template beat and the fiducial point shifted to maximize the cross correlation between the beats (see Figure 6.8D).

A window of data, located about the fiducial point, is extracted from each of N beats. (A sequence of N=128 beats was used in all of the alternans analyses.) If the window width is denoted W, then a matrix of data has been formed. This matrix can be denoted M(n,w), where n is the beat index and w is the sample index (see Figure 6.8E). Thus, if w is held fixed, iterating down the column n allows the investigation of the activity at one distinct offset from the fiducial point in each successive wave. In particular, the next step in the method involves the computation of W power spectrum estimates, each estimate corresponding to a column of data formed when n is held fixed and w is sequenced. (The bias component of this power spectrum estimate is nulled by zero meaning the column prior to computing the spectrum.) A final composite power spectrum estimate is computed as the sum of the W individual spectra.

The composite power spectrum, shown in Figure 6.9, expresses the frequency domain activity of the entire signal as a function of the frequency domain activity at W offsets from the fiducial point. Three parameters are extracted from the composite power spectrum. First, the magnitude of the power spectrum at the location of the alternans frequency is extracted and denoted E_A. Note that since each of the individual power spectrum estimates was formed from a series of samples taken one sample per beat of the original waveform, the alternans frequency is precisely one half the sampling rate. As well, the

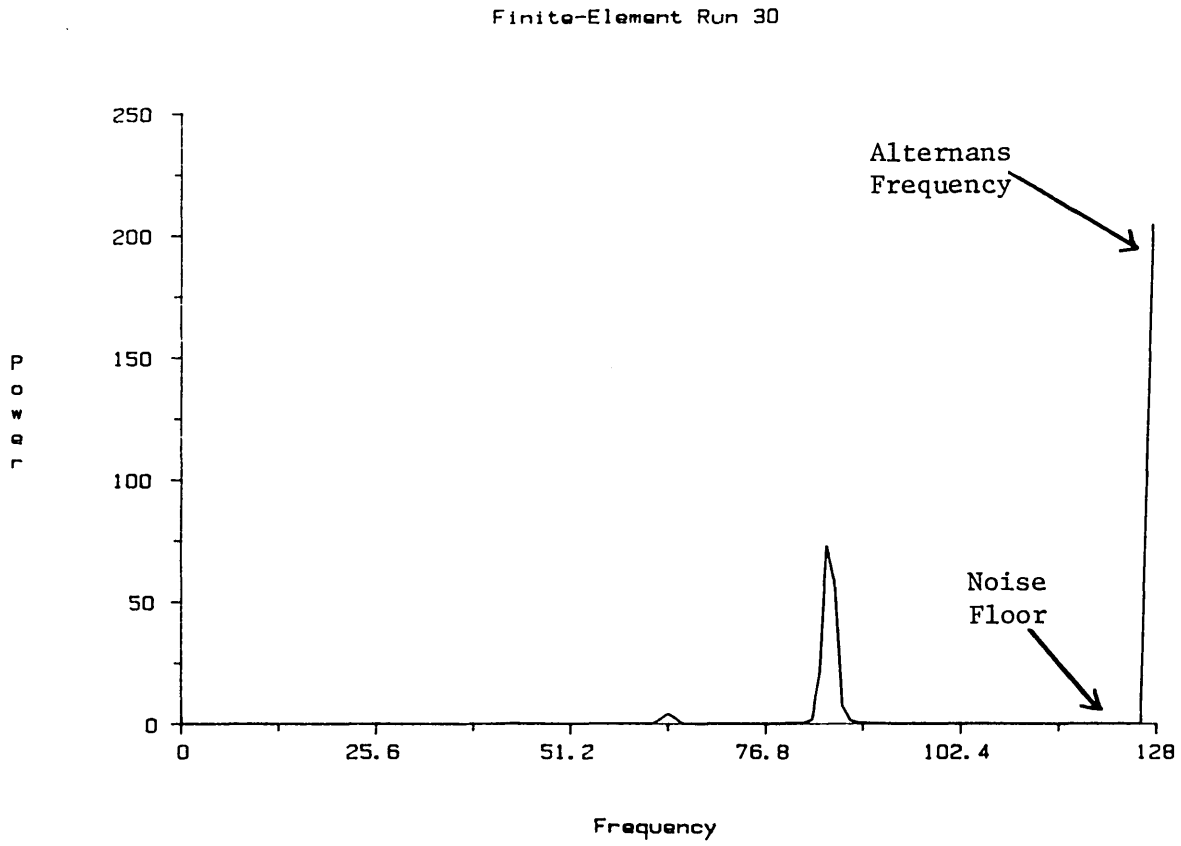

Figure 6.9: Composite Power Spectrum

alternans frequency is the maximum frequency reported in the composite power spectrum (and is found as the right-most frequency shown in Figure 6.9). A sample mean and standard deviation of eight spectrum estimates adjacent to the alternans frequency is then computed. The sample mean, denoted S_N, is considered the "noise floor" for this spectrum. Lastly, an alternans significance quotient, denoted S_A, is reported as;

$$S_A = \frac{E_A - S_N}{\text{noise sample standard deviation}} \qquad (6.17)$$

The remaining quantity reported in the general quantification

method is the energy of the mean (time-domain) waveform. The N waves from the matrix M(n,w) are averaged to form a single mean wave of length W. The energy of this mean wave is computed as the sum of the squares of the W wave values and reported as E_M.

An Alternating Morphology Index for a given parameter P is denoted by the symbol AMI(P). This dimensionless quantity is the magnitude of the energy at the alternans frequency minus the noise floor estimate, normalized by the energy in the mean waveform. All reported AMI values are considered significant only if the alternans energy is three and three tenths standard deviations above the noise floor estimate (i.e. alternans significance quotient greater than three and three tenths). All AMI values which do not meet the significance criterion are assigned a value of zero and subsequently plotted as the lowest value available on a given plot scale.

6.3.2 Scheme of Alternation Quantification for Electrical Data

The X, Y and Z ECG signals, although reported separately in the finite-element heart model, represent orthogonal projections of the total cardiac dipole onto a body surface. In consort they comprise a basis set of ECG data. Thus, the analysis of ECG data should produce a measure of alternans based upon the composite activity of all three ECG leads.

To achieve a composite measure, X, Y and Z ECG data are extracted from the model and the vector magnitude of these waves computed. The vector magnitude data is denoted V ECG. The four ECG leads constitute the sample data set. First pass beat detection is performed on a single

waveform (X ECG) by means of a QRS detector. Template alignment of fiducial points is performed on the V ECG data - this allows the detailed alignment to be based on information from the total cardiac dipole. A composite power spectrum is formed for each of the orthogonal leads. The alternans energy and spectral noise estimate are reported for each lead, the values being termed E_{A-X}, S_{N-X}, E_{A-Y}, S_{N-Y}, E_{A-Z}, and S_{N-Z}. A vector composite power spectrum is formed as the sum of the three composite power spectra. The alternans significance quotient, S_{A-XYZ}, is computed from the vector composite power spectrum. Finally, the energy in the mean waveform is computed from the lead V ECG and termed E_{M-XYZ}. The AMI is then found as;

$$AMI(ECG) = \frac{(E_{A-X} - S_{N-X}) + (E_{A-Y} - S_{N-Y}) + (E_{A-Z} - S_{N-Z})}{E_{M-XYZ}} \quad (6.18)$$

6.3.3 Scheme of Alternation Quantification for Mechanical Data

AMI's were computed for five mechanical parameters - left ventricular capacitance (LVC), left ventricular pressure (LVP), arterial blood pressure (ABP), derivative of left ventricular pressure (dLVP) and derivative of arterial blood pressure (dABP). The five AMI's are termed AMI(LVC), AMI(LVP), AMI(ABP), AMI(dLVP) and AMI(dABP), respectively. The sampled data sets for LVC, LVP and ABP were taken directly from the model output. Derivatives were computed using central differences. For example;

$$dLVP[i] = \frac{LVP[i+1] - LVP[i-1]}{2} \quad (6.19)$$

where i is the discrete iteration number. All waveforms were analyzed

according to the general technique described previously. First pass peak detection was not performed directly, rather the results from the electrical data were inserted. For a given parameter P, the AMI was computed as;

$$AMI(P) = \frac{E_{A-P} - S_{N-P}}{E_{M-P}} \qquad (6.20)$$

6.4 Execution of the Finite-Element Heart Model

Figure 6.10 shows the fixed parameters chosen for operation of the model. Model output was generated under the influence of perturbations in three model parameters - pacemaker rate, mean refractory period and standard deviation refractory period. For each of the three above parameters, three parameter values were selected roughly corresponding to a normal value, a moderate value and an extreme value. Normal, moderate and extreme values were based upon data in the literature acquired from dogs (Han and Moe, 1964; Han et al., 1966; Moore et al., 1965). Figure 6.11 shows the selected parameters as well as their corresponding values scaled to model time.

Parameter Symbol	Parameter Value	Parameter Description
D	35	Number of elements in a ring.
L	33	Number of rings in the shell.
C_A	2.0	Arterial capacitance (ml/mmHg).
ABP_o	85.0	Initial arterial blood pressure (mmHg).
R_A	1.0	Arterial resistance (mmHg/ml/sec).
h	$0.\overline{30}$	Height of each element.
P_f	10.0	Filling pressure (mmHg).
K_c	30.055789	Contracted length-tension relation ((mmHg**1/3) / (cm**2/3)).
C_s	0.2	Systolic capacitance (ml/mmHg).
K_r	8.158396	Relaxed length-tension relation ((mmHg**1/3) / (cm**2/3)).
C_d	10.0	Diastolic capacitance (ml/mmHg).
LVP_o	10.0	Initial LV blood pressure (mmHg).
LVV_o	100.0	Initial LV blood volume (ml).
t	0.005	Model iteration time step (sec).
rseed	338	Seed for random number generator.

Figure 6.10: Fixed Parameters of the Finite-Element Heart Model

Parameter	Normal Value		Moderate Value		Extreme Value	
	msecs	Iteration Steps	msecs	Iteration Steps	msecs	Iteration Steps
Inter-stimulus Interval (T)	500	100	335	67	250	50
Mean Refractory Period (τ)	180	36	210	42	240	48
Standard Deviation Refractory Period (σ)	10	2	35	7	60	12

Figure 6.11: Range of Parameters of the Finite-Element Heart Model

6.5 Results of the Finite-Element Heart Model

Figure 6.12 shows the electrical ECG data which is produced by the model. Note that the ECG contains no P waves because the model lacks atria. The magnitude ECG shown in the figure will be used, henceforth, to detail the time-domain electrical activity of the model.

The response of the model to the input parameters can be grouped into three stages: normal, alternation and fibrillation. The normal stage, of which a representative example is given in Figure 6.13, is characteristic of a healthy heart. Ventricular capacitance sweeps from its assigned maximum (relaxed) value to its assigned minimum (contracted) value. All elements within the model are excited each heart beat. Figure 6.14 is representative of the alternation stage. All parameters exhibit a characteristic alternation in beat shape. Ventricular capacitance never reaches the completely relaxed level (10 ml/mmHg). A certain number of elements can not be excited each heart beat. These elements form an alternating sub-population. Diminished ventricular performance results. The third model response stage is that of fibrillation. Figure 6.15 shows a fibrillatory response. The heart has failed as a pump. Ventricular capacitance remains near maximum contraction - there is a lack of any coordinated beat. As an element repolarizes, it is quickly depolarized. No single organized wavefront of excitation exists, rather activation spreads chaotically throughout the shell. Figures 6.13-6.15 provide a good representation of the typical waveforms produced from the 27 runs of the model.

Figure 6.16 is a chart of the AMI results of the finite-element heart model. The results of all runs with an interstimulus interval of

100 iteration steps were not listed. These model runs were not subjected to the AMI analysis. The window of data used in the AMI analysis was centered about peak systole (peak QRS for the electrical data) with a width of 62 time steps for data with an interstimulus interval of 67 time steps, and a width of 46 time steps for data with an interstimulus interval of 50 time steps. An AMI of "VF" denotes that the output waveforms were fibrillatory and could not be analyzed for an alternating morphology. The F population was determined as the total number of elements which had a refractory period greater than or equal to the interstimulus interval. Figure 6.16 also shows the rank correlation between each of the various AMI forms and the F population. The F population represented the population of elements whose long refractory periods provided a substrate for reentry.

From the results presented in Figure 6.16, three plots were created. Figure 6.17 shows the AMI's plotted versus the F population. The symbol V denotes that fibrillatory data was derived at the corresponding F population. Figure 6.18 shows the AMI for LV capacitance plotted versus standard deviation refractory period (with mean refractory period fixed). Figure 6.19 shows the AMI for LV capacitance plotted versus mean refractory period (with standard deviation refractory period fixed).

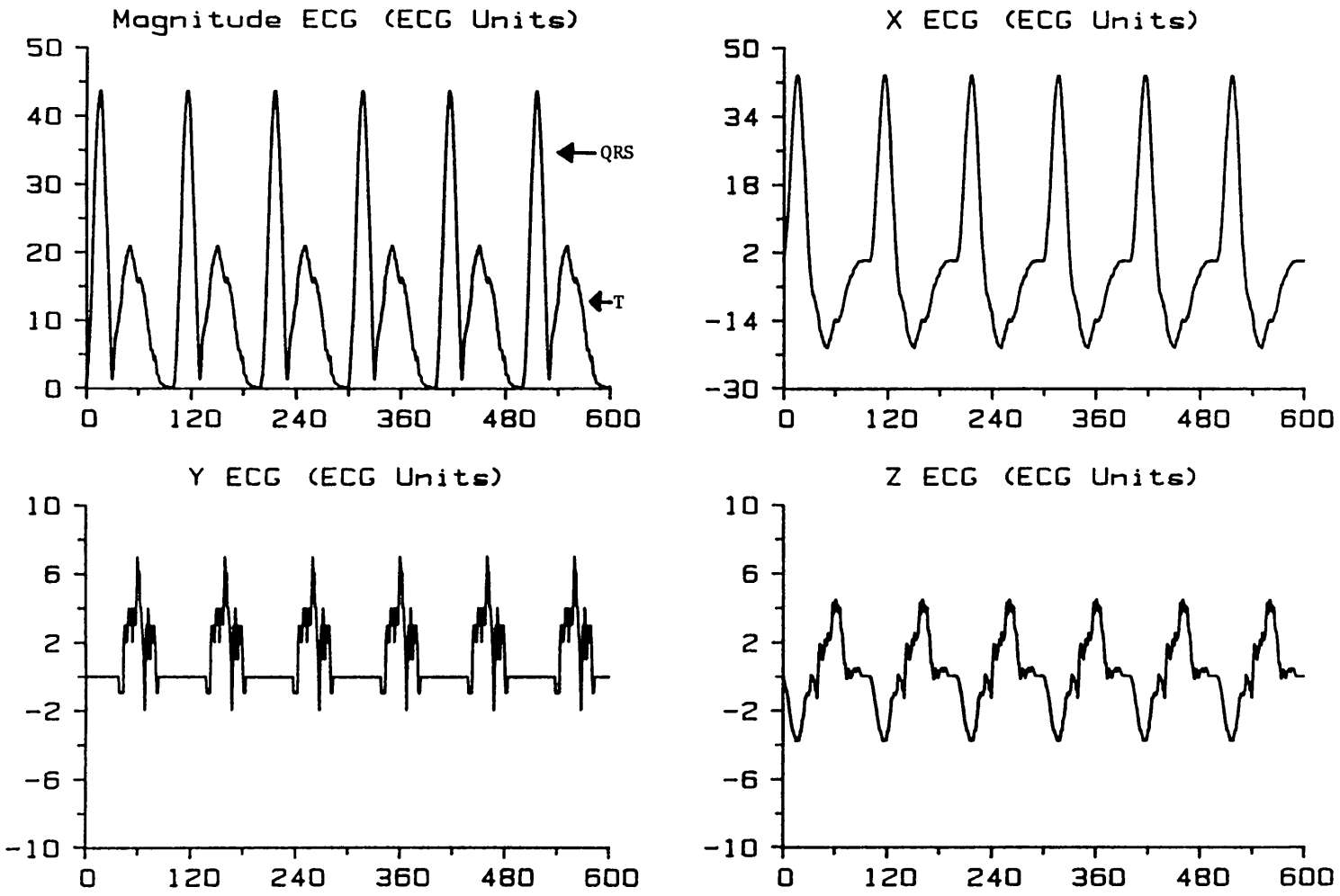

Figure 6.12: Computer Model ECG versus Iteration Steps

Run 12 X, Y, Z and Magnitude ECG (in ECG units) are plotted versus model iteration steps. Note that the abscissae of the plots are scaled differently.

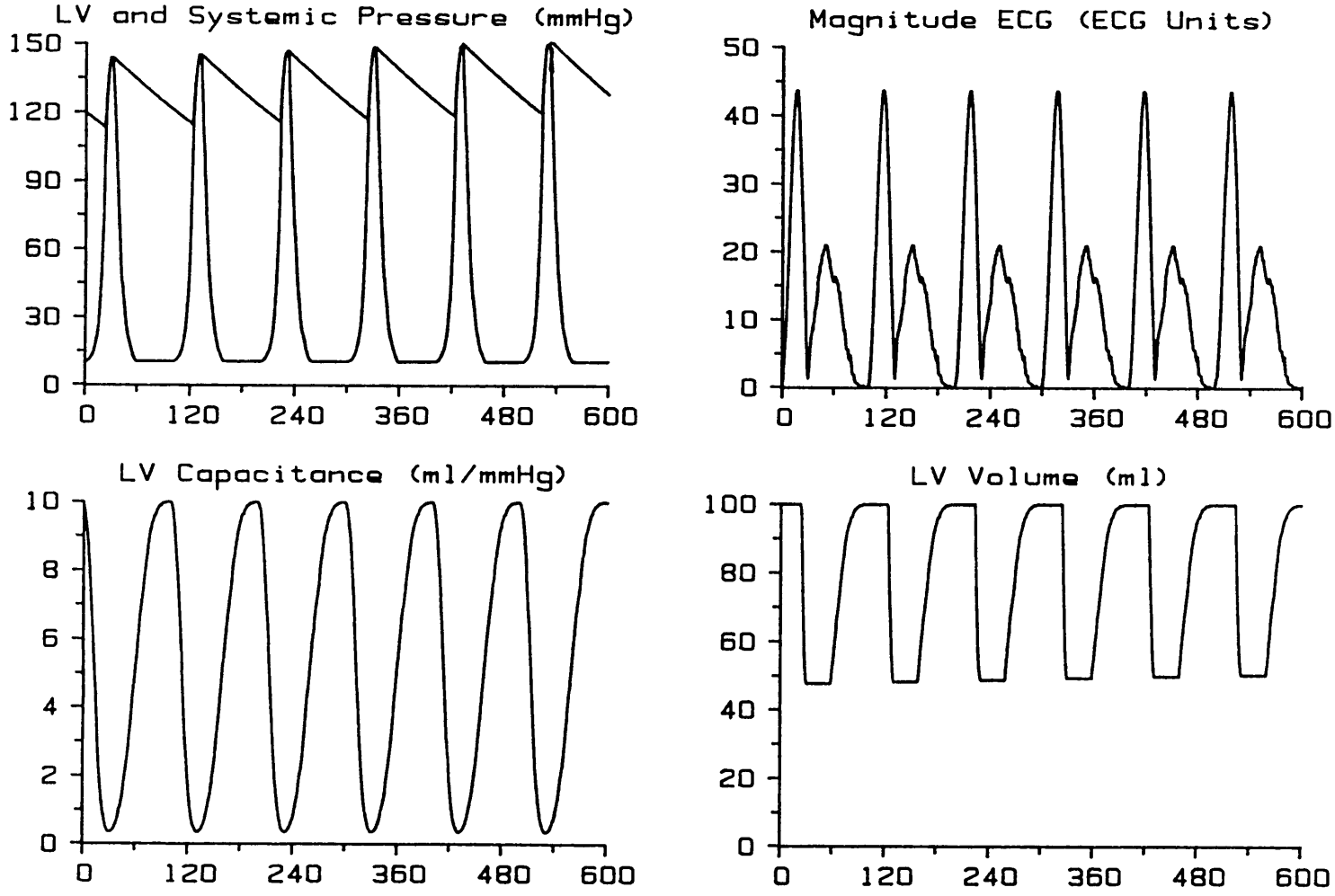

Figure 6.13: Computer Run 12 Output versus Iteration Steps

A normal heart rhythm.

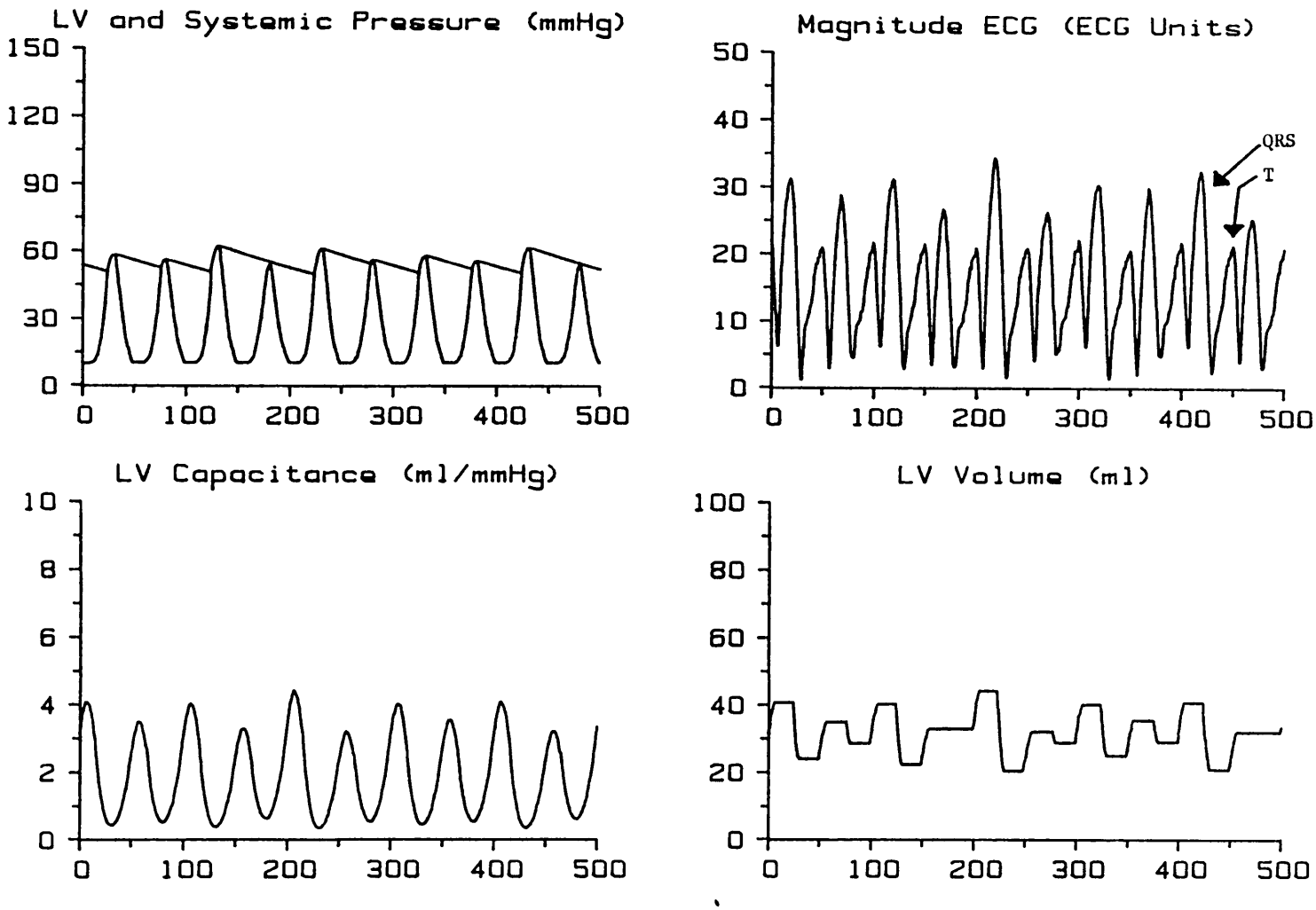

Figure 6.14: Computer Run 30 Output versus Iteration Steps

A heart rhythm displaying visable electrical and mechanical alternans.

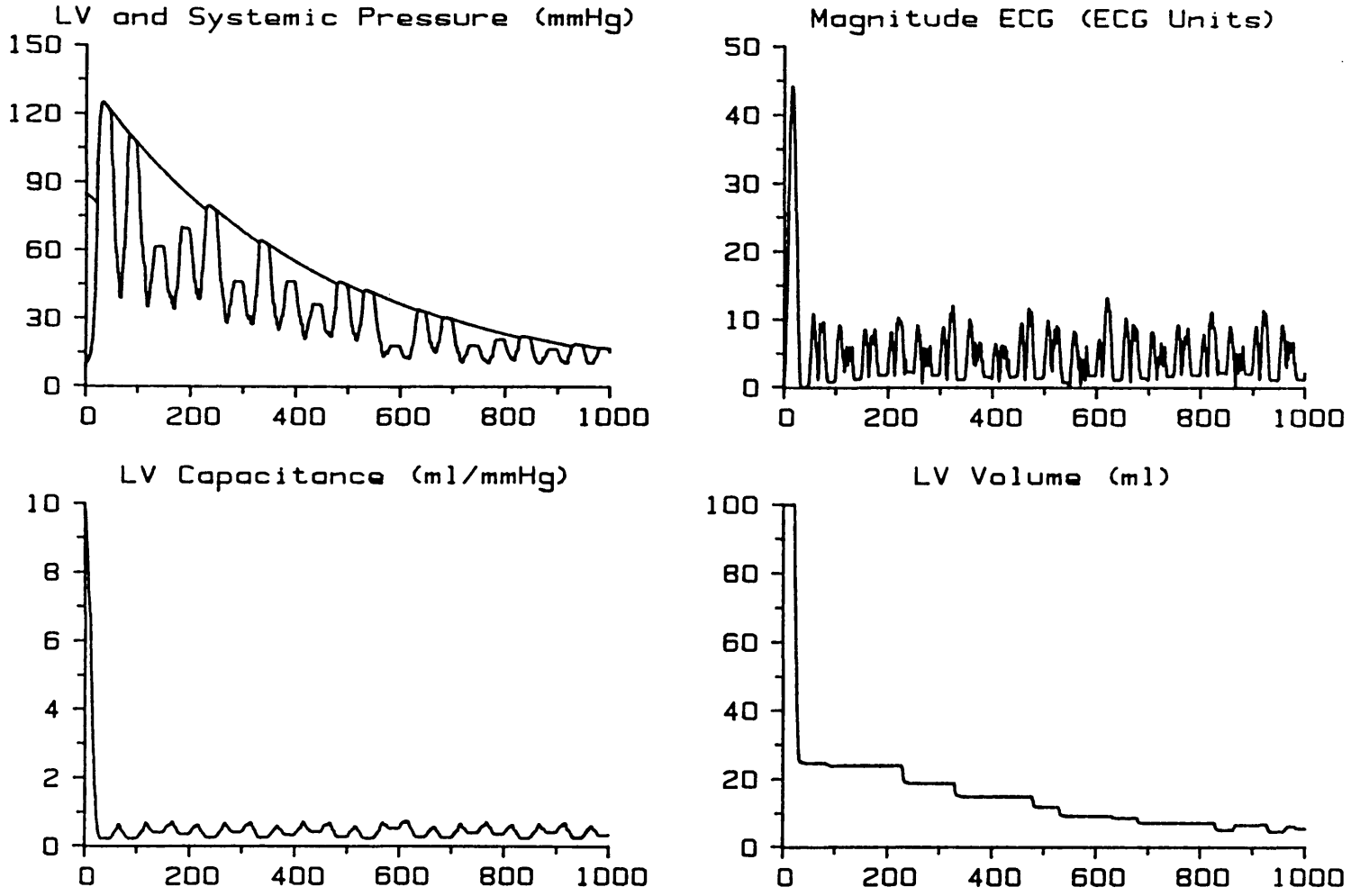

Figure 6.15: Computer Run 34 Output versus Iteration Steps

A heart rhythm which shows the rapid decay to a "fibrillatory" state.

Finite Element Model Results - Fixed Window

Run	T	σ	$\bar{\tau}$	F Pop	AMI's ECG	C	LVP	ABP	dLVP	dABP
19	67	36	2	0	0.0	0.0	0.0	0.0	0.0	0.0
20	67	36	7	0	0.0	0.0	0.0	0.0	0.0	0.0
21	67	36	12	7	0.002880	0.000975	0.000236	0.000117	0.008991	0.020250
22	67	42	2	0	0.0	0.0	0.0	0.0	0.0	0.0
23	67	42	7	1	0.0	0.0	0.0	0.0	0.0	0.0
24	67	42	12	25	0.000240	0.000209	0.000133	0.000012	0.003378	0.001527
25	67	48	2	0	0.0	0.0	0.0	0.0	0.0	0.0
26	67	48	7	6	0.000029	0.001192	0.0	0.000003	0.000102	0.000636
27	67	48	12	84	0.003127	0.003025	0.000725	0.000395	0.009704	0.066521
28	50	36	2	0	0.0	0.0	0.0	0.0	0.0	0.0
29	50	36	7	36	0.000489	0.000141	0.000106	0.000025	0.001723	0.010512
30	50	36	12	161	0.014245	0.011316	0.004086	0.001495	0.024129	0.485022
31	50	42	2	0	0.0	0.0	0.0	0.0	0.0	0.0
32	50	42	7	167	0.030271	0.007022	0.001523	0.000770	0.051338	0.304607
33	50	42	12	296	0.073793	0.012556	0.001153	0.000605	0.031610	0.226356
34	50	48	2	198	VF	VF	VF	VF	VF	VF
35	50	48	7	454	VF	VF	VF	VF	VF	VF
36	50	48	12	503	VF	VF	VF	VF	VF	VF
Rank Correlation of AMI to F Population (p<0.001 for all data)					0.968	0.937	0.920	0.953	0.960	0.953

Figure 6.16: AMI Results of the Computer Model

Results of the finite-element heart model for Runs 19-36. Interstimulus interval (T), mean refractory period $\bar{\tau}$ and standard deviation refractory period σ are expressed in iteration steps. F population is the total number of elements (out of 1155 total) which had a refractory period greater than or equal to the interstimulus interval. An AMI of "VF" denotes that the output waveforms were fibrillatory and could not be analyzed for an alternating morphology.

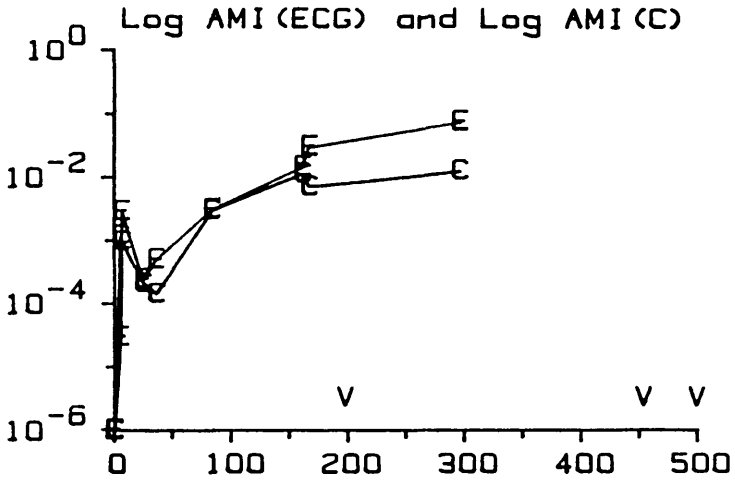

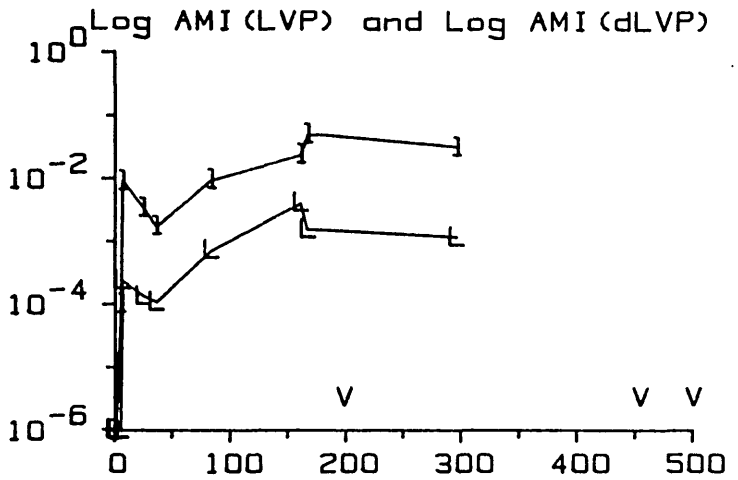

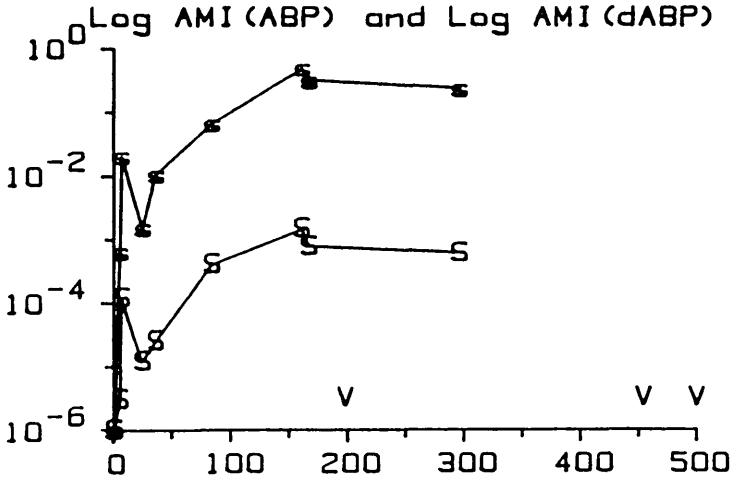

Figure 6.17: Log AMI's versus F Population

Symbols used in this figure are: E = AMI(ECG), C = AMI(C), L = AMI(LVP), l = AMI(dLVP), S = AMI(ABP), s = AMI(dABP), and V denotes fibrillation at this population. All AMI's are ploted on a logarithmic scale. Lines are an aid to the eye only.

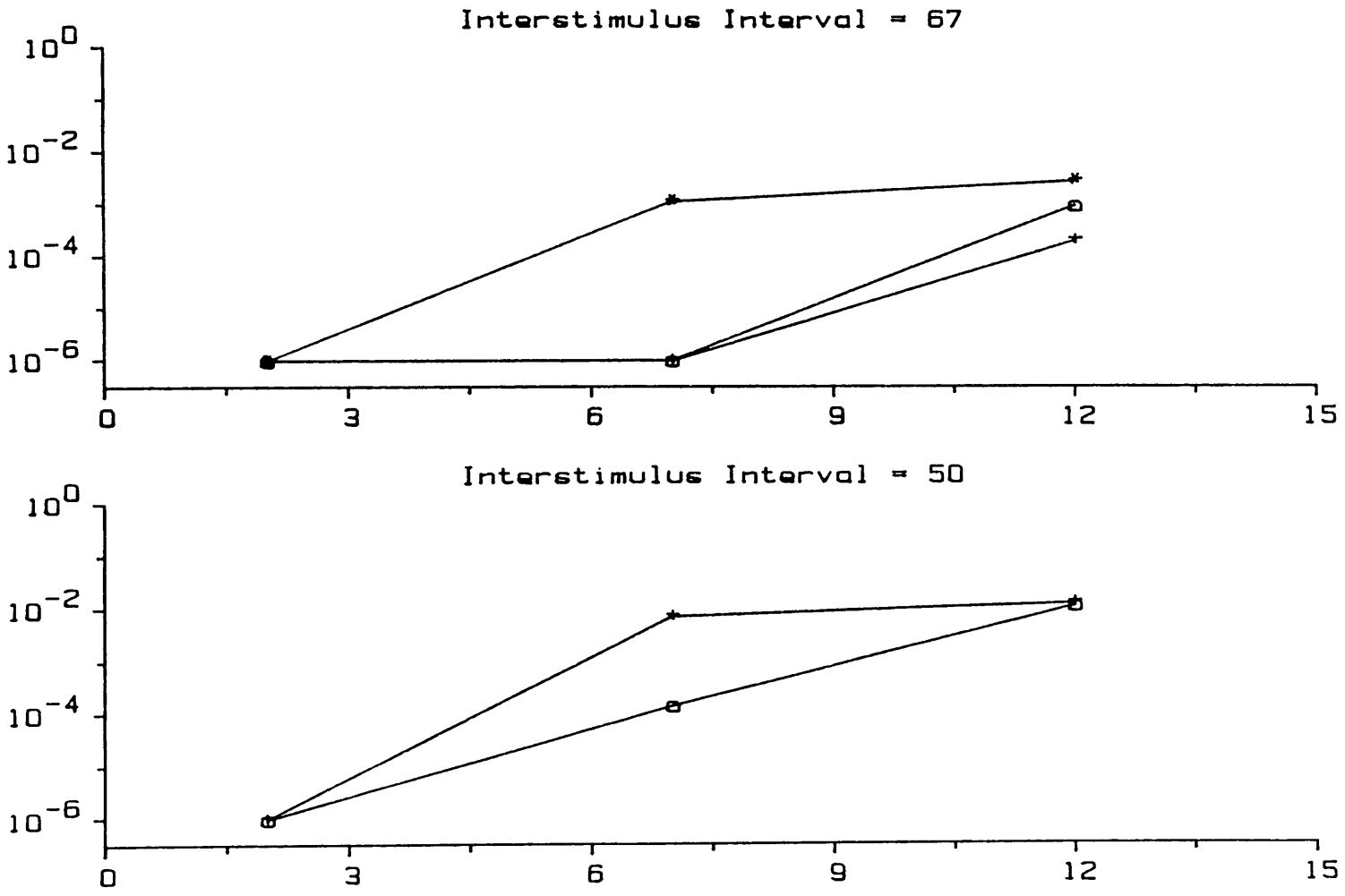

Figure 6.18: Log AMI(C) versus σ

The symbol "o" corresponds to $\bar{\tau}$ = 36, "+" corresponds to $\bar{\tau}$ = 42 and "*" corresponds to τ = 48. T, σ and τ expressed in iteration steps. On the bottom plot (T = 50), fibrillation resulted for all runs with τ = 48. Lines are an aid to the eye only.

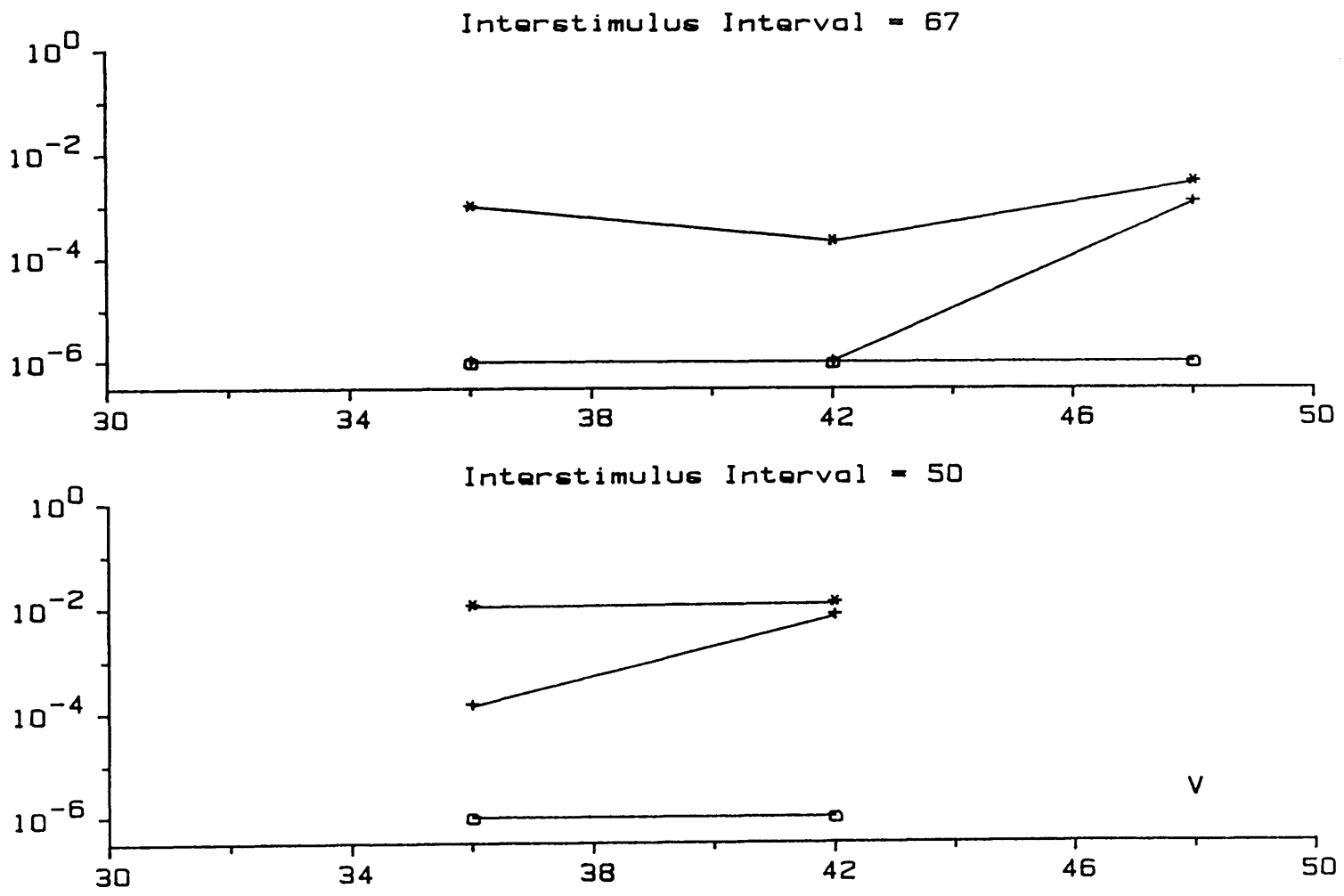

Figure 6.19: Log AMI(C) versus $\bar{\tau}$

The symbol "o" corresponds to σ = 2, "+" corresponds to σ = 7 and "*" corresponds to σ = 12. T, σ and τ expressed in iteration steps. On the bottom plot (T = 50), "V" denotes that fibrillation resulted for all runs with $\bar{\tau}$ = 48. Lines are an aid to the eye only.

6.6 Discussion of the Finite-Element Heart Model

6.6.1 The Transition From a Normal Rhythm to a Chaotic Rhythm

The finite-element heart model provided a simplified representation of the complex electrical and mechanical actions of the heart from which the relationships between electrical alternans, mechanical alternans and the size of the F population could be studied. The ECG, blood pressure and capacitance waveforms generated by the model were quantified as to the degree of alternating energy present. The alternans quantification allowed for a more detailed study of the transition from a normal rhythm to a chaotic (fibrillatory) rhythm. Three important concepts have been established by the model: 1) a regime of alternation was found in both the electrical and mechanical waveforms as the model progressed from a normal rhythm to a chaotic rhythm, 2) the magnitude of the alternation was positively correlated to the size of the F population, and 3) electrical and mechanical alternans seemed to identify an identical alternation in the spatial-temporal contour of the heart beat. These concepts are discussed below.

The three response stages of the model (normal, alternation, fibrillation) trace the transition from normal heart activity to fibrillation, i.e. as the model is increasingly perturbed, a stage of alternation always precedes the fibrillatory stage. This stage is observed as electrical alternans and mechanical alternans. Previous researchers (Smith and Cohen, 1984) had only investigated electrical alternans.

Alternation in the model was quantified and related to the F

population. (Recall that the F population represents the population of elements whose long refractory periods provide a substrate for wavefront fractionation.) The degree of alternation in both electrical and mechanical activity grew monotonically with the F population. This relationship is brought out in Figure 6.17. The normal stage of heart activity is lumped into a single point at an F population of zero. Alternation extends from an F population of zero to 296. As the F population grows, the degree of alternation grows (rank correlation coefficient = 0.937, $p<0.001$ for the LV capacitance waveform). The fibrillatory stage extends from an F population of 198 and beyond. In the case of this model, the alternation and fibrillatory stages overlap. Thus, the subtle quantification process shows that alternation may be a graded measure of the relative stability of the rhythm.

Figures 6.16 and 6.17 also show the close link between electrical and mechanical alternans displayed by the model. All six measures of activity (one electrical and five mechanical) follow an identical AMI contour with respect to the F population. Thus, the two alternans forms seem to identify an identical alternation in the spatial-temporal contour of the heart beat. Note that when alternation is detected in a pressure waveform, the magnitude of the alternans seems to be amplified in the pressure derivative. This may be due to the fact that the derivative mutes the mean value of a wave, thus providing a smaller mean wave energy by which the alternation is normalized.

Figures 6.18 and 6.19 show the changes in AMI(C) as σ and $\bar{\tau}$, respectively, are altered. These figures illustrate the concept discussed in Section 4.1 that dispersion (represented by σ) and mean refractory period alone do not provide all the information required to

assess the stability of the heart. Additional information is required. For example, observe in Figure 6.18 (Log AMI(C) versus σ) the plots corresponding to $\bar{\tau}$ = 48 iteration steps (graphing symbol "*"). At an interstimulus interval of 67 iteration steps, σ values of 2 and 7 iteration steps result in no significant alternation. Yet, at an interstimulus interval of 50 iteration steps, the same σ values result in VF. It was also noted in Section 3.5.3 that Han et al. (1964) were able to increase the susceptibility to VF whether the average refractory period was reduced or increased. Figure 6.19 (Log AMI(C) versus $\bar{\tau}$) presents data which agrees with their finding. An increase in AMI(C) can be accomplished by increasing or decreasing $\bar{\tau}$.

6.6.2 Alternation and the Susceptibility to Ventricular Fibrillation

This model clearly predicts that as perturbations in the model parameters of heart interval, mean refractory period and dispersion in refractory period are increased towards the fibrillatory stage, a stage of electrical-mechanical alternation will <u>always</u> precede the fibrillatory stage. As the degree of alternans increases, the model moves closer to the fibrillatory stage. Further, the model asserts that an alternation in the global activity of a population of elements is a sufficient condition for the formation of electrical-mechanical alternans. Finally, for this global mechanism of alternation and the given excitation-contraction properties assigned the elements, this model predicts that the degree of the observed electrical and mechanical alternans will be quite similar (i.e. they track each other well).

Chapter VII

A Physiologic Model of Electrical-Mechanical Alternans

7.1 Introduction

The finite-element model provided a simple representation of the electrical and mechanical activity of the heart. Quantifying both mechanical and electrical alternans showed that the model exhibited an orderly progression from a normal rhythm, through alternation, to a chaotic rhythm. The concept of a spatial-temporal alternation in the contour of the heart beat was used to explain the mechanism for the alternation. As well, all elements with a refractory period greater than the interstimulus interval (the F population) were shown to provide the substrate for reentry. The magnitude of the alternation and thus, the susceptibility to VF, was monotonically correlated to the size of the F population.

A physiologic model of the heart was next employed to determine if the theoretical concepts developed in the simple computer model could be applied to a complex model. An in-vitro physiologic model was constructed in the acute anesthetized dog. Physiologic signals of ECG and BP were monitored. The electrical stability of the model was perturbed through rapid atrial pacing and systemic hypothermia. Electrical and mechanical alternans were again quantified utilizing the method described by Smith (1985).

7.2 Protocol for Hypothermia Studies

Four dogs weighing between 20-30 kg were surgically prepared for hypothermia studies. Care of the animals was supervised by the Division of Comparative Medicine at the Massachusetts Institute of Technology. An acepromazine maleate (1 mg/kg) pre-anesthesia was administered subcutaneously. Anesthesia was induced by i.v. administration of sodium pentobarbital (initial dosage approximately 25 mg/kg) with supplements given as necessary to maintain deep anesthesia. Mechanical respiration was provided through an air-cuffed endotracheal tube by a Harvard Respirator. The chest was opened on the left side through the fifth intercostal space, the pericardium incised and the heart suspended in a pericardial cradle. Two copper wires (#26 gauge, insulated) were stripped at the tip and sewn onto the left atrial appendage for pacing. Two screw-type electrodes (Medtronic, Model 6917A-T) were screwed into the free wall of the left ventricle between the first and second diagonal branches of the left anterior descending coronary artery (2 cm inter-electrode spacing) for VFT measurements. Left ventricular pressure was monitored by advancing a catheter (Millar, Model SPC-350) through the left atrium into the ventricle. A second catheter (Millar, Model SPC-330) was placed in the left femoral artery to measure systemic blood pressure. (On experiment date 8-1-85 saline filled catheters were used to monitor the two blood pressures. The catheters were flushed with heparinized saline and connected to Statham P23a transducers.) A thermocouple was placed in the pericardial sac and sutured in place. This portion of the preparation is diagramed in Figure 7.1. The pericardium was then loosely approximated and all catheters and

electrodes exteriorized through the chest incision. The chest was closed in three layers and evacuated via a suction drainage tube. A counter-current heat exchanger (Travenol, Model 5MO343) was connected between the right femoral artery and the left femoral vein. Three pairs of transcutaneous needle electrodes were applied along three orthogonal orientations. These leads were termed ECG X (right arm to left arm, frontal plane), ECG Y (rostral to caudal, frontal plane), and ECG Z (dorsal to ventral, sagital plane). The data were bandpass filtered from 0.04-500 Hz (Electronics for Medicine ECG Amplifier, Model V1205B). Physiologic signals of ECG X, ECG Y, ECG Z, left ventricular pressure and systemic blood pressure were recorded on a Hewlett-Packard 3968A 8-track instrumentation tape recorder at a tape speed of three and three fourths inches per second (corresponding to a bandpass filter ranging from 0-1250 Hz).

Following a surgical recovery period of thirty minutes, the physiologic variables were recorded and VFT determinations made over a range of pacing rates. The minimum pacing rate was approximately 150 bpm and the maximum pacing rate was 190 bpm. VFT determinations were typically made at the minimum rate, maximum rate and a median rate. The animal was defibrillated extracorporally after each episode of VF (Hewlett-Packard 78671A Defibrillator-Monitor at 6-9 Joules/kg). The post-surgical temperature of the animal, typically 35-37 degrees C, was termed the normothermic temperature. A bolus of sodium heparin (100 ug/kg, i.v.) was administered and the counter-current heat exchanger opened. Pericardial temperature was initially reduced to 33 degrees C, and then to 29 degrees C. At each temperature, physiologic variables were recorded and VFT determinations made over a range of pacing rates.

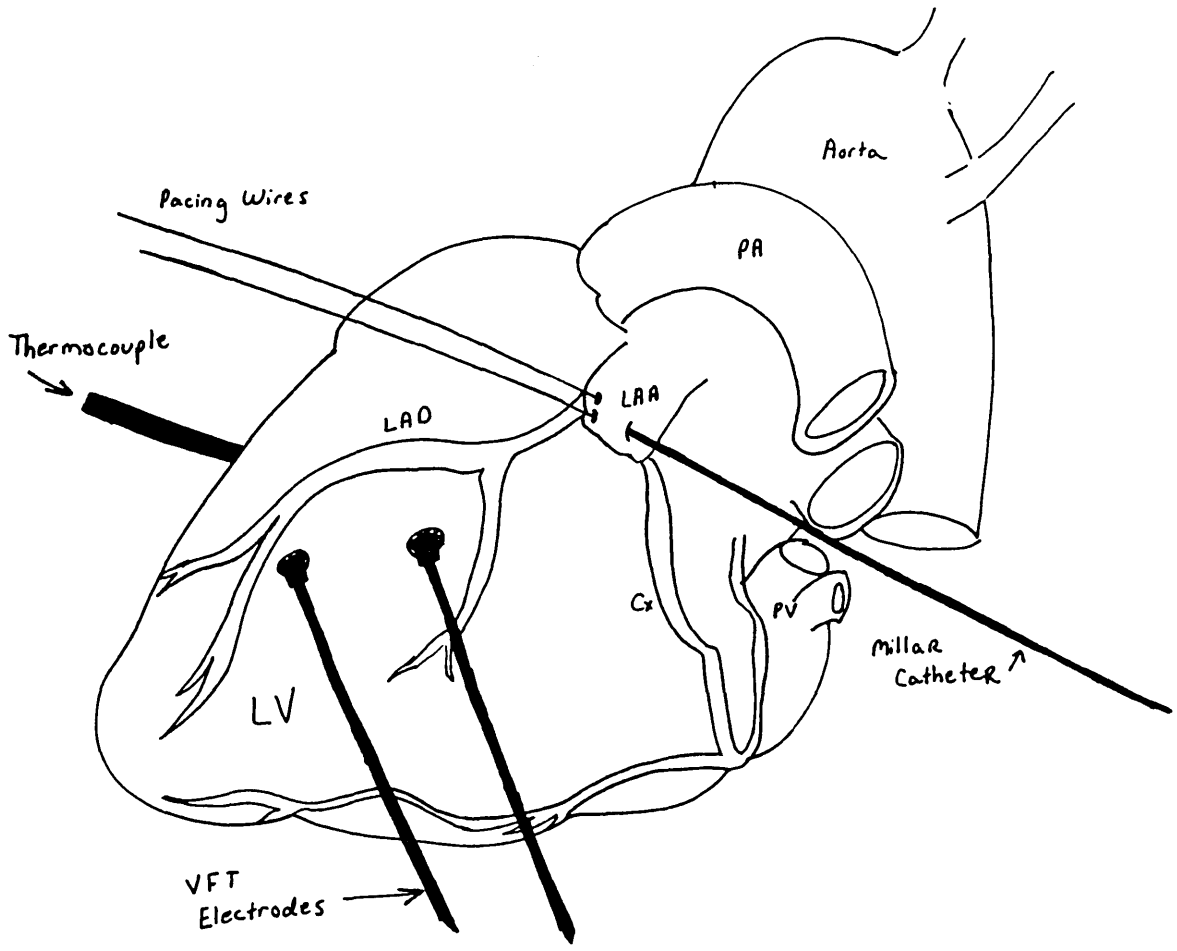

Figure 7.1: Schematic of the Heart Preparation in the Physiologic Model

Schematic shows two pacing wires, two VFT electrodes, a Millar catheter (for monitoring left ventricular pressure) and a thermocouple. PA=pulmonary artery, LAA=left atrial appendage, LAD=left anterior descending coronary artery, LV=left ventricle, Cx=circumflex coronary artery, PV=pulmonary vein.

Whenever possible, the pacing rates used were identical to those of the normothermic case. The animal was then rewarmed to the normothermic temperature and the protocol repeated. At the completion of the experiment the animal was euthanized by not defibrillating after the final VFT determination.

VFT determinations were made by passing square wave current through the two implanted screw-type electrodes. The square waves had a duty cycle of 50%, a period of 10 msecs and an initial amplitude of 2 mA. The stimulation was timed to span the period of ventricular repolarization. If the initial current amplitude did not induce VF, then after a rest period of approximately ten heart beats, the current was successively increased by 2 mA and the stimulation repeated until VF ensued. The current level at which VF was induced is defined as the VFT. A rest period of fifteen minutes was provided between successive VFT determinations.

7.3 Analysis Methods for the Physiologic Model

The general method for quantifying alternation was presented in Section 6.3.1 (recall Figures 6.7 and 6.8). The following sections will detail the particular scheme used to quantify electrical and mechanical alternans in the physiologic model.

7.3.1 Scheme of Alternation Quantification for Electrical Data

ECG X, Y and Z were replayed in real time on a Hewlett-Packard 3968A 8-track FM instrumentation tape recorder and filtered with a low-pass analog 6-pole Butterworth filter at a bandpass of 360 Hz. The data were sampled onto a digital computer by a 12-bit analog-to-digital converter. The sampling rate was 1000 samples per second (per channel). The vector magnitude of the ECG data was computed and termed the V ECG. The four ECG's constituted the sampled data set. First pass beat detection was performed on a single waveform (typically ECG Y) by identifying the QRS complex. Template alignment of fiducial points was performed on the vector magnitude data (V ECG).

Prior to extracting a matrix of data for composite power spectrum calculation, the ECG data was passed through a respiratory filter. This filter seeks to reduce the influence of respiratory modulation of the ECG on the alternation quantification process. The filter independently normalizes (to a value of zero) the bias level of each beat as a function of an isoelectric segment identified for each beat. The normalizing value was taken as the mean of a window of sixteen samples located eighty msecs in time prior to the fiducial point. The matrix of

data, M(n,w), was extracted from the respiratory filtered data.

A composite power spectrum was formed for each of the three orthogonal leads. The alternans energy and spectral noise estimate are reported for each lead. The alternans significance quotient was computed from the vector composite power spectrum. The AMI is then given as specified previously in equation 6.18.

Three separate windows were analyzed for the physiologic data. A 100 msec window centered about the fiducial point represents the activity of the QRS complex. The ensuing 200 msec represents the ST-T wave segment. Lastly, a 300 msec window comprised of the above two windows was formed. The results of these analyses are termed AMI(QRS), AMI(ST-T) and AMI(Q+T), respectively.

7.3.2 Scheme of Alternation Quantification for Mechanical Data

In a fashion similar to the ECG data, left ventricular pressure and arterial blood pressure were replayed and sampled onto a digital computer. The pre-sampling 6-pole Butterworth analog low-pass filter had a bandwidth of 20 Hz. The sampling rate was 200 samples per second (per channel). The derivatives of the above signals were again computed via the central difference formula (equation 6.19). No direct physiologic equivalent to ventricular capacitance was evaluated.

The above four signals were analyzed for alternation according to the general technique for alternation quantification. The window of data used in the analysis was centered about peak systole and had a width equal to;

$$\text{Width} = \frac{RR}{4} - (5 \text{ msecs}) \qquad (7.1)$$

where

RR = RR interval of the paced data in msecs.

First pass peak detection was based on results from the electrical data. The four categories of AMI results are termed AMI(LVP), AMI(ABP), AMI(dLVP) and AMI(dABP).

7.4 Results of the Physiologic Model

The combined effects of hypothermia and rapid atrial pacing consistently produced electrical and mechanical alternation. Figure 7.2 shows typical waveforms observed during the post-operative normothermic state and the hypothermic state. It is interesting to note that the mechanical alternation can become so advanced that the contraction of the weak beat is unable to eject blood from the ventricle. This condition is shown in Figure 7.3. From the body surface, this condition might be interpreted as 2:1 electrical:mechanical disassociation.

From the four experiment days, the AMI's of all the observed data as well as the measured VFT's were plotted over the time course of cooling and rewarming. Three of these plots are shown as Figure 7.4 (Experiment 1-28-86, Heart Rate = 140 bpm), Figure 7.5 (Experiment 1-28-86, Heart Rate = 160 bpm), and Figure 7.6 (Experiment 1-30-86, Heart Rate = 160 bpm). In plotting the AMI data, the following plotting symbols were used;

Q corresponds to AMI(QRS),
T corresponds to AMI(ST-T),
E corresponds to AMI(Q+T),

L corresponds to AMI(LVP),
l corresponds to AMI(dLVP),

S corresponds to AMI(ABP),
s corresponds to AMI(dABP), and

V corresponds to a VFT determination.

The rank correlation between the various AMI's and temperature were computed for the data of the three figures mentioned above. This information is given in Figure 7.7.

The effect of cooling on the AMI was plotted in Figure 7.8 for

AMI(dLVP). The open circles represent AMI(dLVP) at the normothermic temperature and the plus signs represent AMI(dLVP) at the hypothermic temperature. The lines connect AMI pairs corresponding to a given heart rate in a given animal. Figure 7.9 shows a similar plot for rewarming. Figure 7.10 is a two-by-two contingency table of changes in AMI(dLVP) versus cooling and rewarming (a quantity which did not change was discarded). The change in AMI(dLVP) was clearly related to the temperature intervention ($p<0.0006$, chi-square statistic).

Changes in VFT as a function of the interventions of cooling and rewarming are displayed in the two-by-two contingency table of Figure 7.11. The change in VFT depended on the intervention only at a $p<0.134$ level of significance (chi-square statistic).

The combined effects of core temperature and increase in heart rate on the AMI were also studied. Figure 7.12 plots one electrical AMI and two mechanical AMI's (plot symbols have been defined previously) versus heart rate for the four experiments, all data being recorded at a baseline temperature of 35+ degrees C. Figures 7.13 and 7.14 show similar data for temperatures of 33 and 29 degrees C, respectively. To evaluate this data, a two-by-two contingency table of increase in heart rate at a given temperature versus the change in AMI(dLVP) was constructed. This table is shown in Figure 7.15. The change in AMI(dLVP) was dependent upon the increase in heart rate at a given temperature at the $p<0.051$ significance level (chi-square statistic).

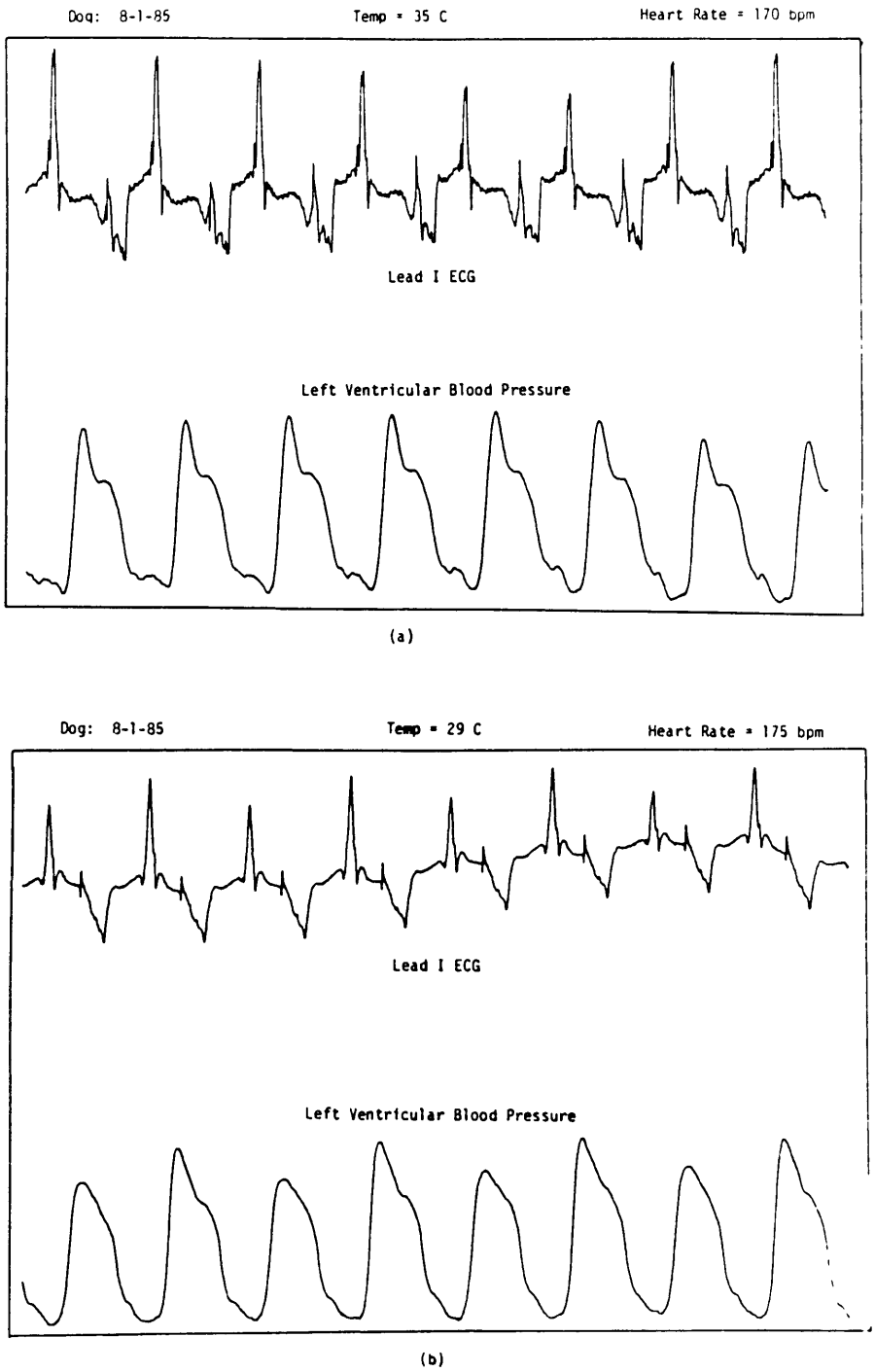

Figure 7.2: ECG and BP Waveforms at Normothermic and Hypothermic Temperatures

Normothermic in figure a, hypothermic in figure b.

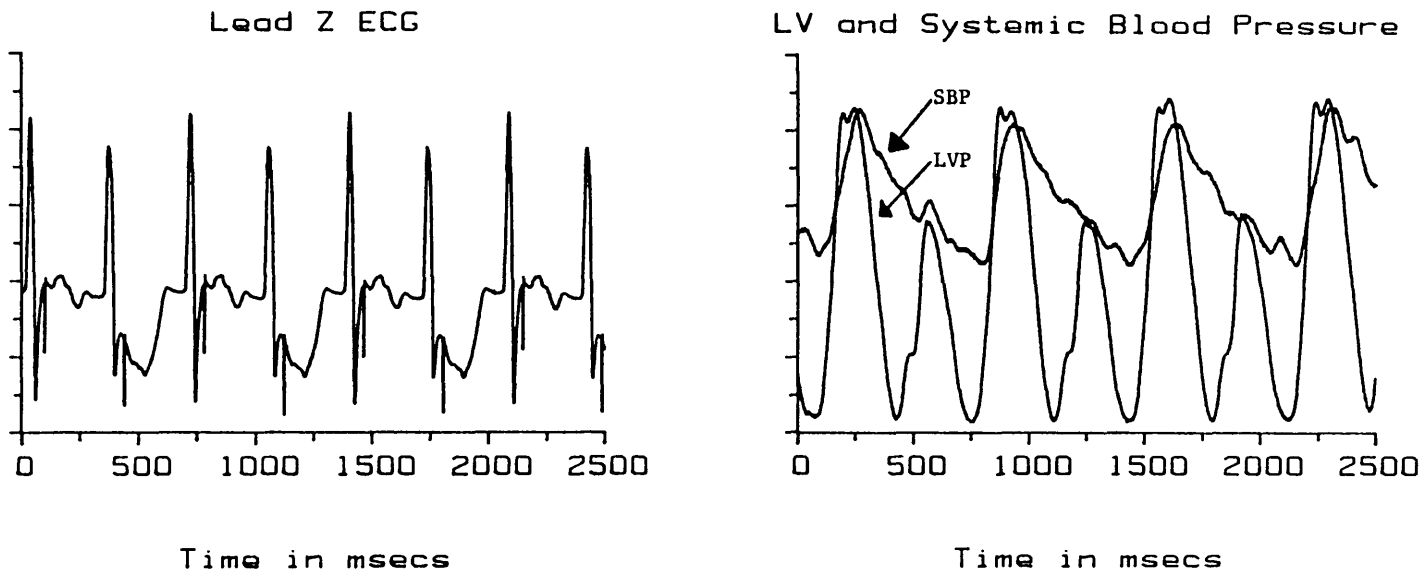

Figure 7.3: Apparent 2:1 Electrical:Mechanical Disassociation

Data from Experiment 1-23-86. Heart Rate=175 bpm. LVP=left ventricular pressure, SBP=systemic blood pressure.

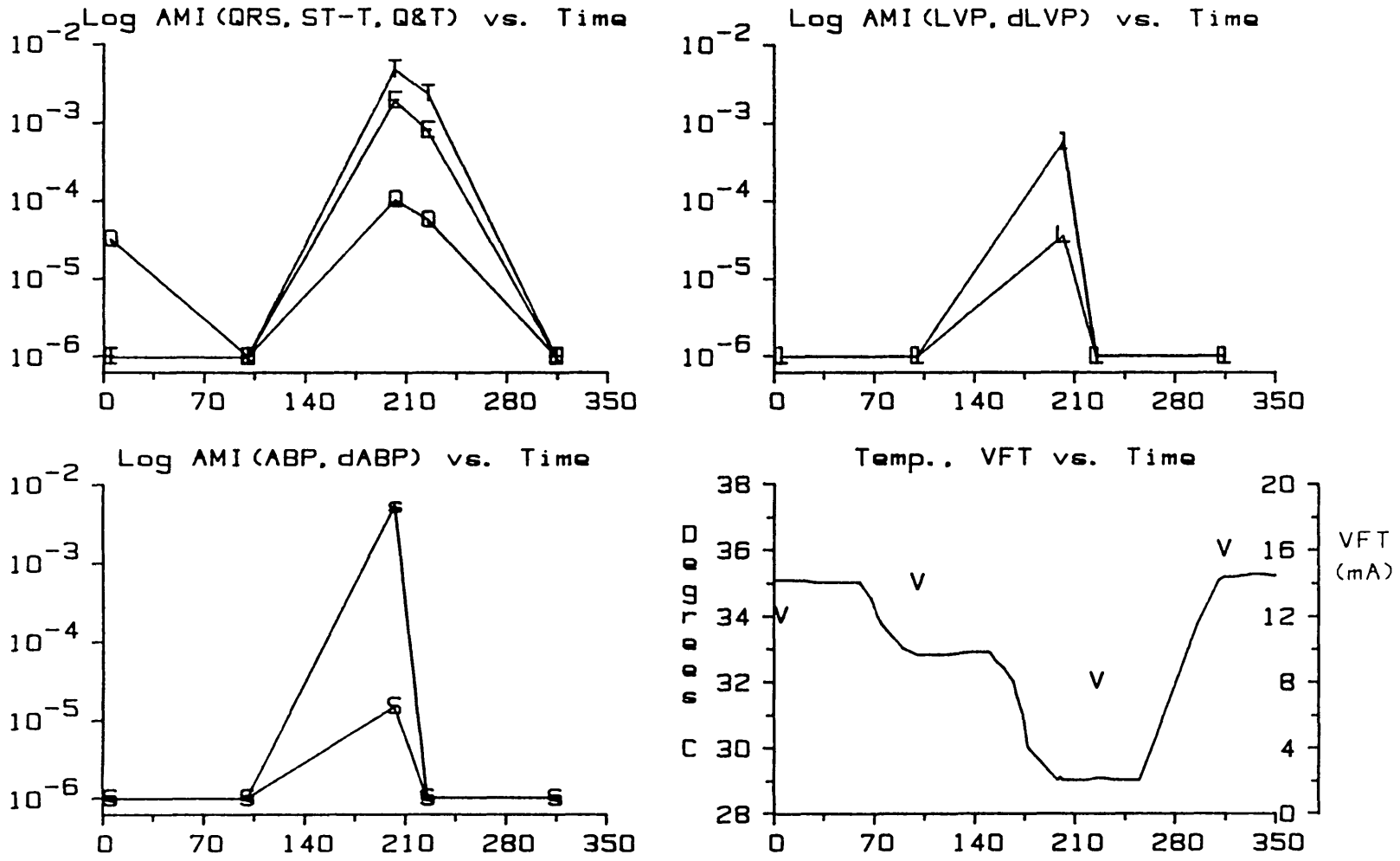

Figure 7.4: AMI, Temperature and VFT Results, 1-28-86, HR=140 bpm

The two upper plots and the lower left plot show log AMI's versus elapsed time in minutes into the experiment. Plotting symbols are defined in the text. Lines are an aid to the eye only. The lower right plot shows temperature (solid line) and VFT determinations versus time.

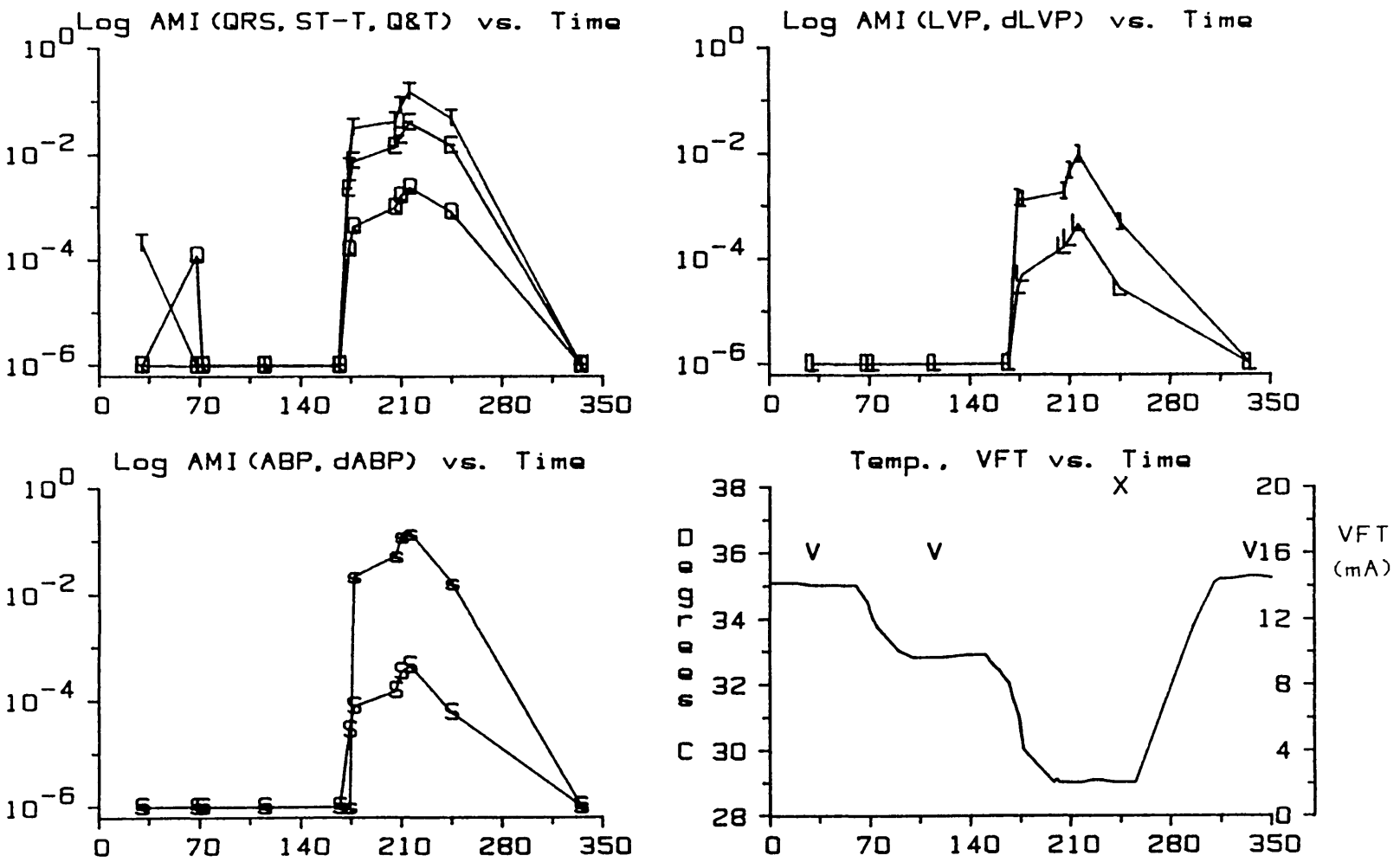

Figure 7.5: AMI, Temperature and VFT Results, 1-28-86, HR=160 bpm

The two upper plots and the lower left plot show log AMI's versus elapsed time in minutes into the experiment. Plotting symbols are defined in the text. Lines are an aid to the eye only. The lower right plot shows temperature (solid line) and VFT determinations versus time. The VFT determination denoted "X" had an out of scale value of 46+ mA.

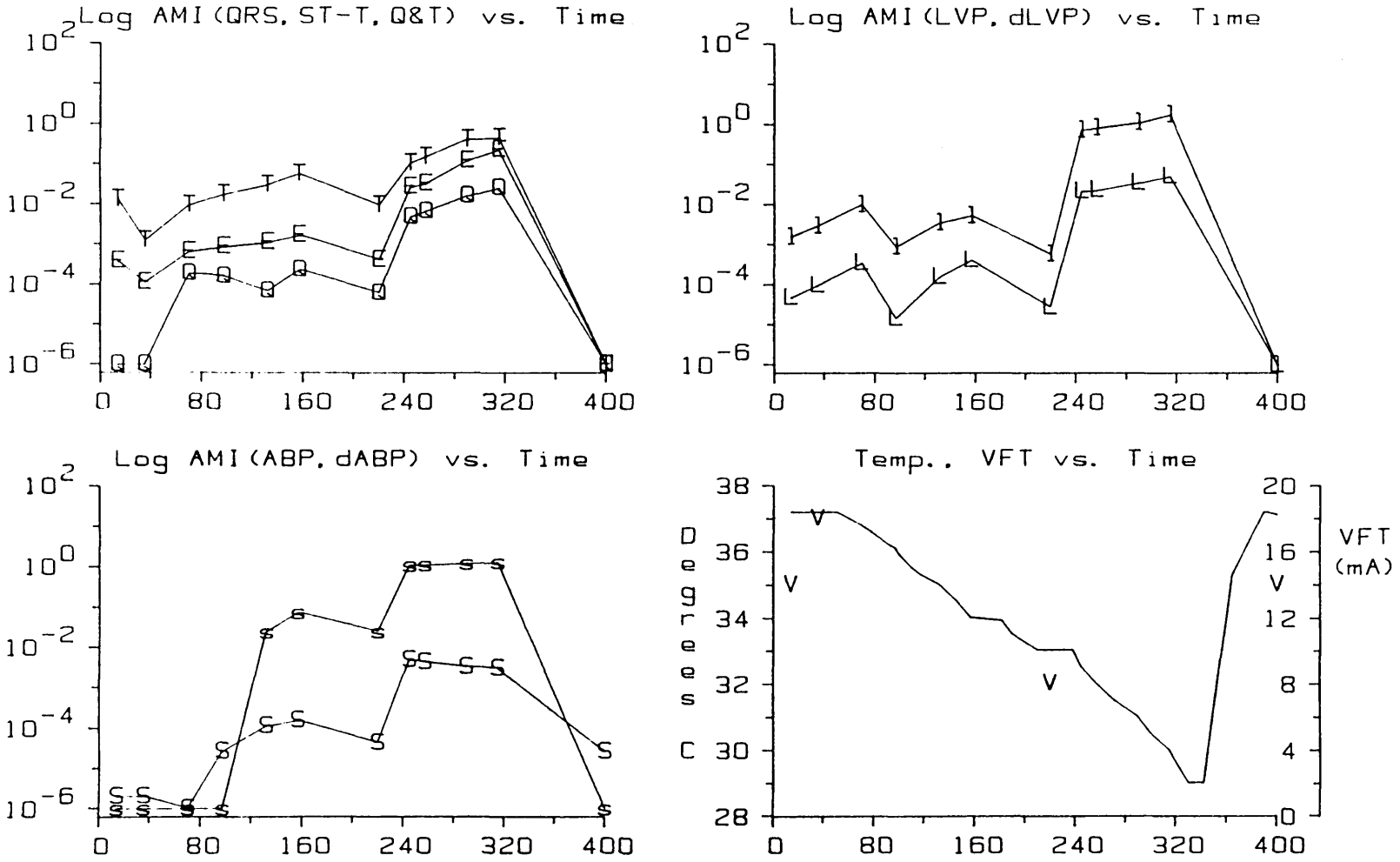

Figure 7.6: AMI, Temperature and VFT Results, 1-30-86, HR=160 bpm

The two upper plots and the lower left plot show log AMI's versus elapsed time in minutes into the experiment. Plotting symbols are defined in the text. Lines are an aid to the eye only. The lower right plot shows temperature (solid line) and VFT determinations versus time.

Data	Experiment 1-28-86,p140 Rank Correl (r)	Sig (p)	Experiment 1-28-86,p160 Rank Correl (r)	Sig (p)	Experiment 1-30-86,p160 Rank Correl (r)	Sig (p)
QRS	-0.821	0.089	-0.878	0.000	-0.896	0.000
ST-T	-0.894	0.041	-0.856	0.000	-0.861	0.000
Q+T	-0.894	0.041	-0.916	0.000	-0.907	0.000
LVP	-0.707	0.182	-0.870	0.000	-0.767	0.004
dLVP	-0.707	0.182	-0.862	0.000	-0.725	0.008
ABP	-0.707	0.182	-0.811	0.001	-0.861	0.000
dABP	-0.707	0.182	-0.853	0.000	-0.959	0.000

Figure 7.7: Rank Correlations of the Various AMI Forms to Temperature

Data from Experiments 1-28-86 (pacing rates of 140 bpm and 160 bpm) and 1-30-86 (pacing rate 160 bpm).

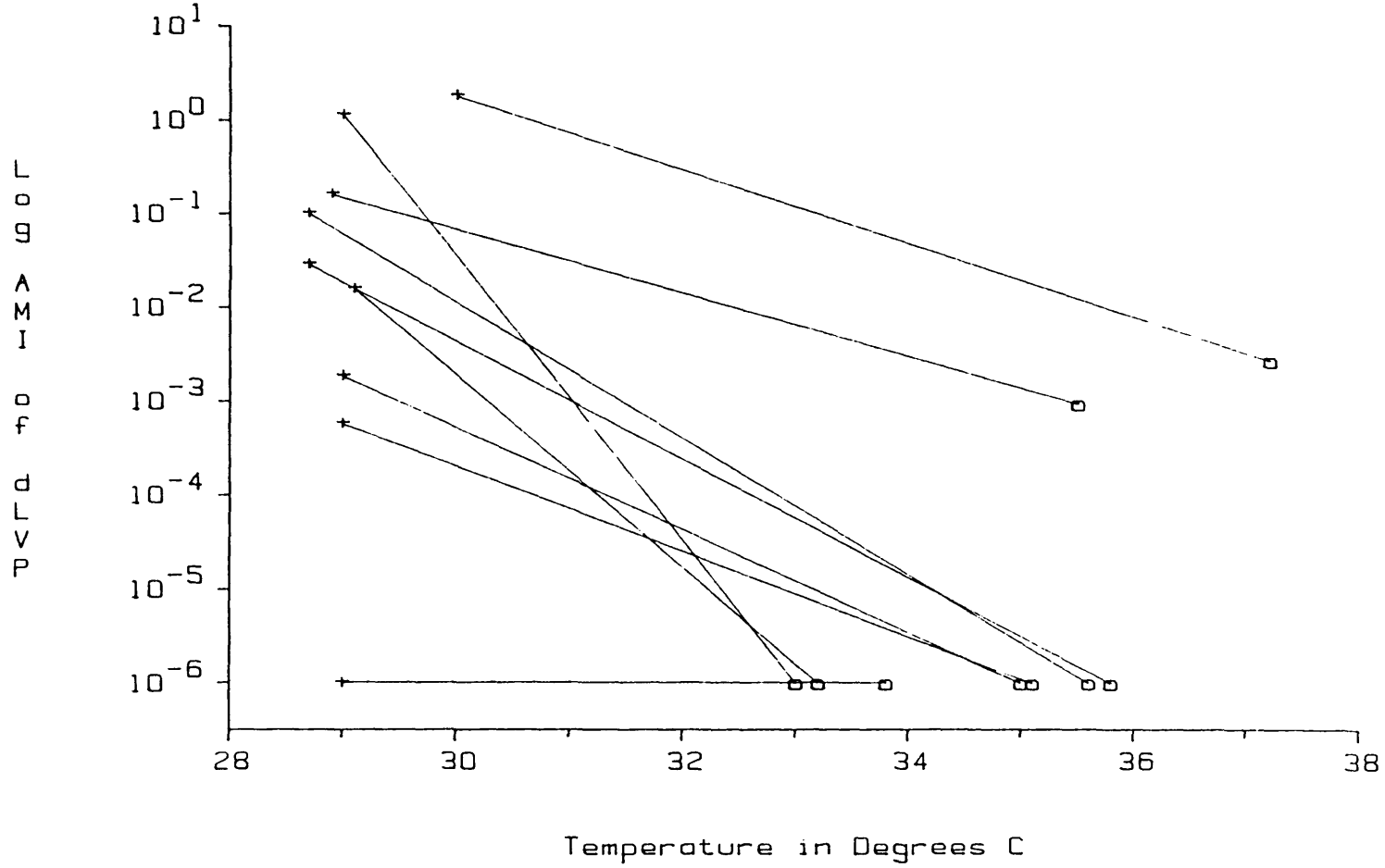

Figure 7.8: Effect of Cooling on Log AMI(dLVP)

Open circles represent log AMI(dLVP) at the normothermic temperature. Plus signs represent log AMI(dLVP) at the hypothermic temperature. Lines connect AMI pairs corresponding to a given heart rate in a given animal.

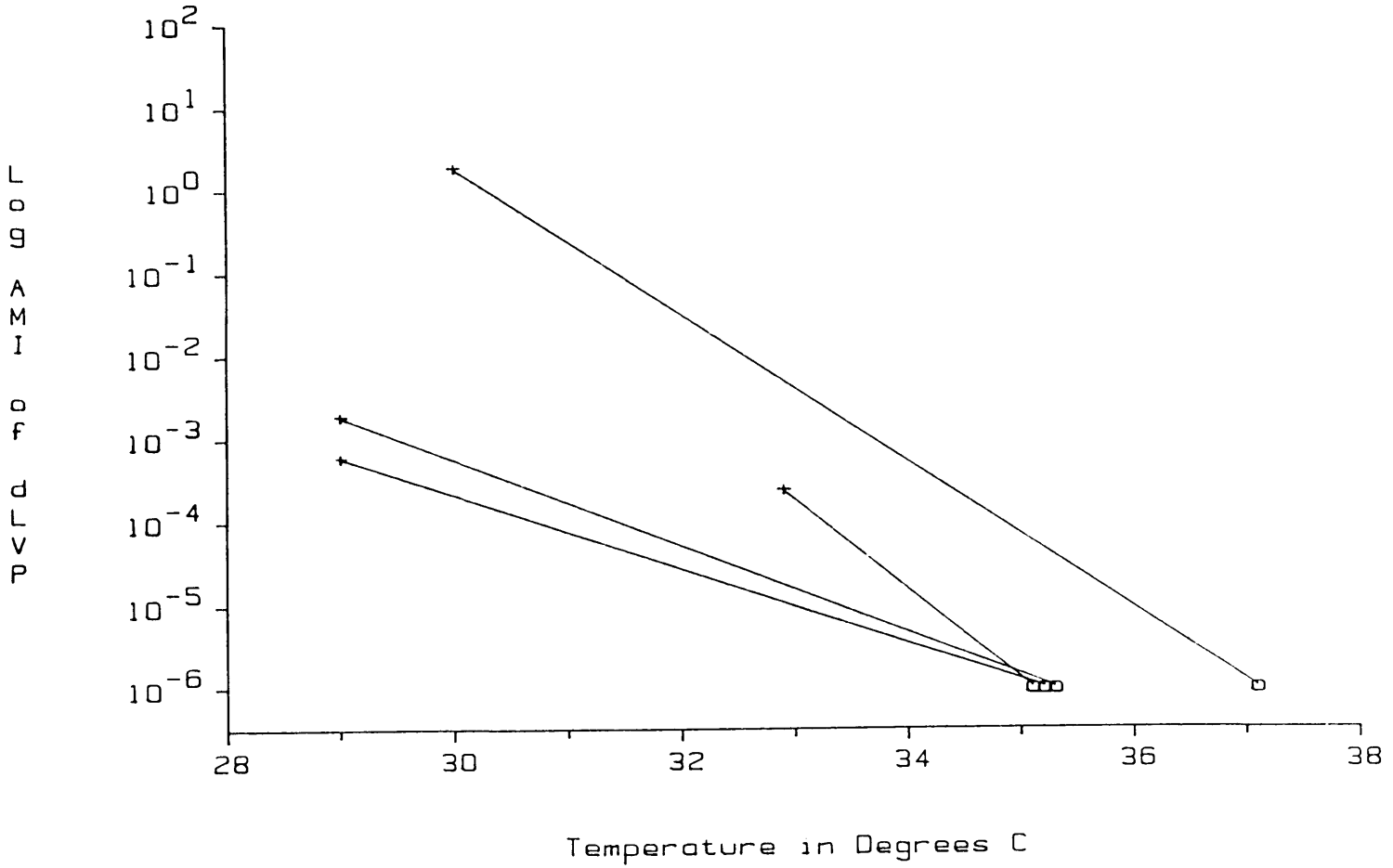

Figure 7.9: Effect of Rewarming on Log AMI(dLVP)

Open circles represent log AMI(dLVP) at the normothermic temperature. Plus signs represent log AMI(dLVP) at the hypothermic temperature. Lines connect AMI pairs corresponding to a given heart rate in a given animal.

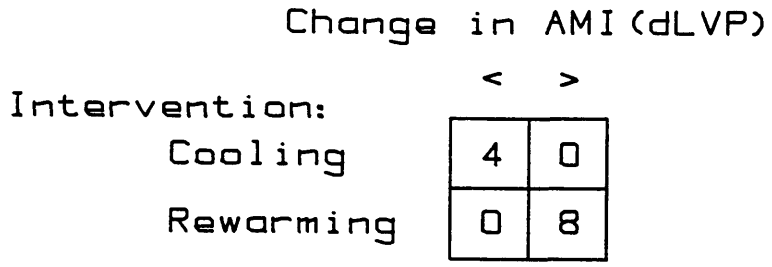

Figure 7.10: Change in AMI(dLVP) During Cooling and Rewarming

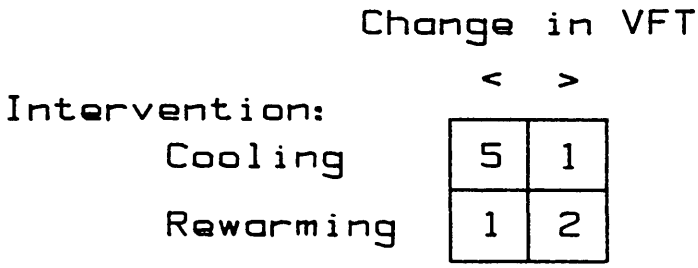

Figure 7.11: Change in VFT During Cooling and Rewarming

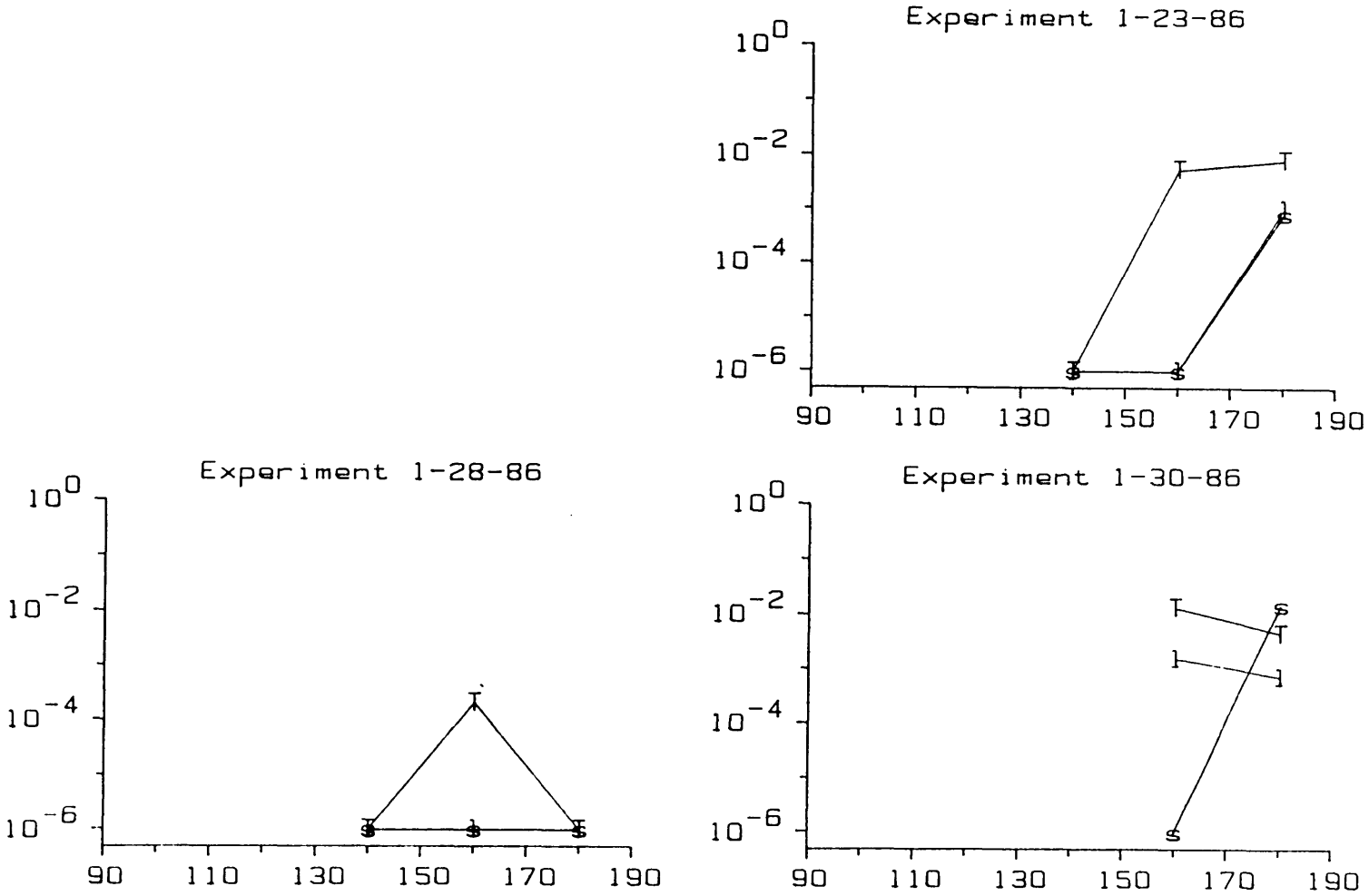

Figure 7.12: Log AMI's versus Heart Rate at Normothermic Temperature

The plots show log AMI's versus heart rate in beats per minute at the normothermic temperature. Plotting symbols are defined in the text. Lines are an aid to the eye only. No data available for Experiment 8-1-85.

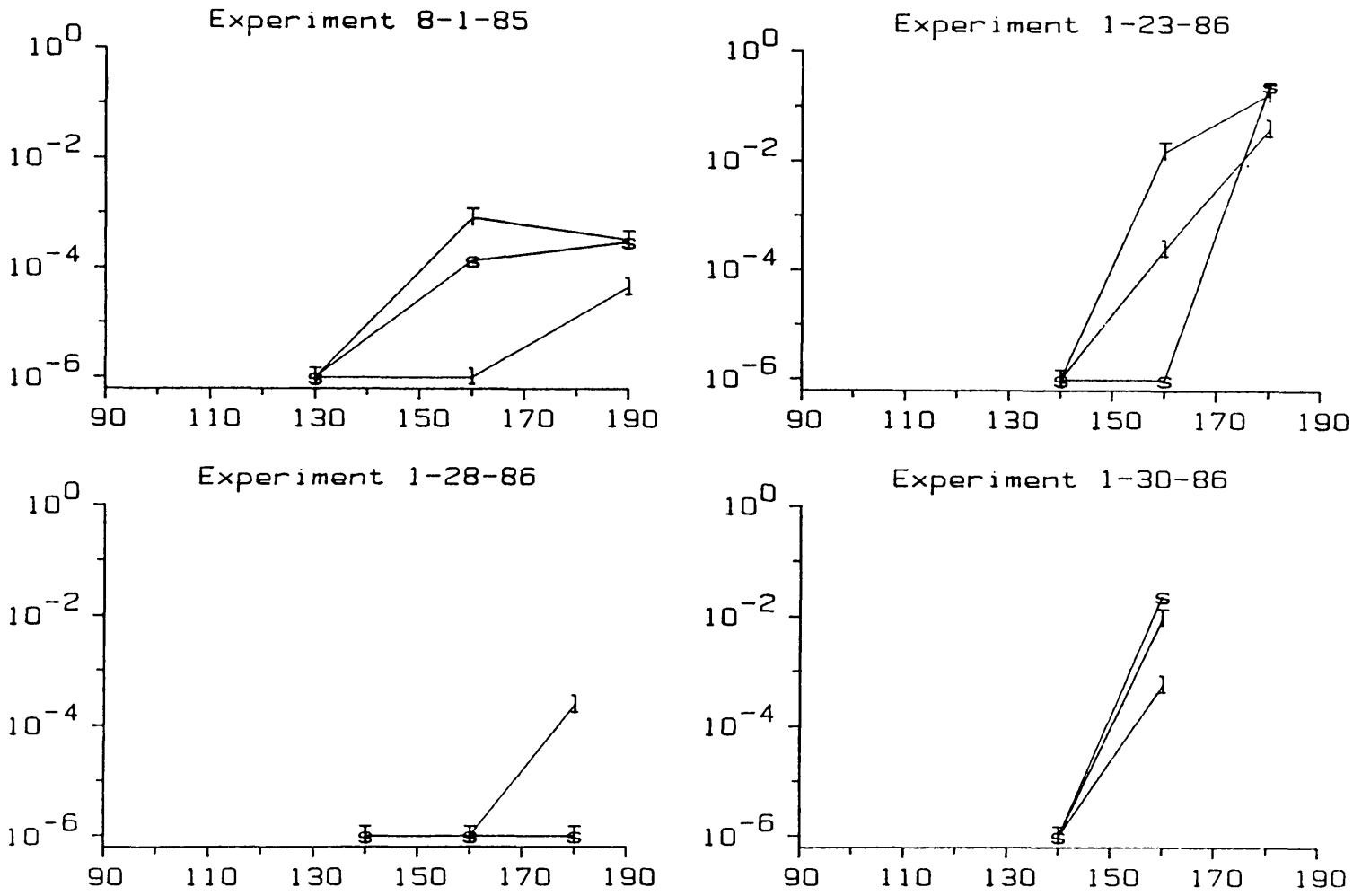

Figure 7.13: Log AMI's versus Heart Rate at 33 Degrees C

The plots show log AMI's versus heart rate in beats per minute at a temperature of 33 degrees C. Plotting symbols are defined in the text. Lines are an aid to the eye only.

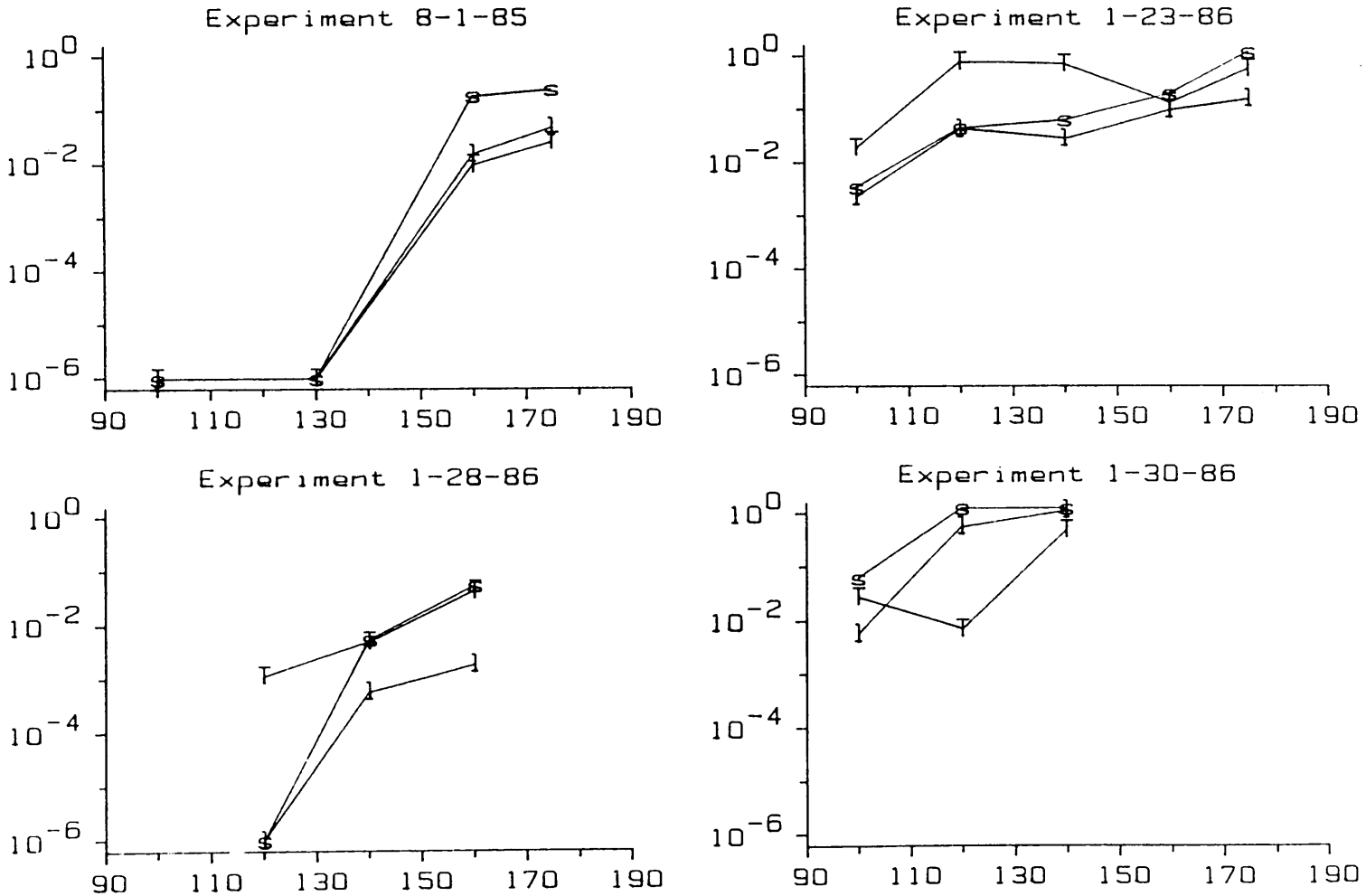

Figure 7.14: Log AMI's versus Heart Rate at 29 Degrees C

The plots show log AMI's versus heart rate in beats per minute at a temperature of 29 degrees C. Plotting symbols are defined in the text. Lines are an aid to the eye only.

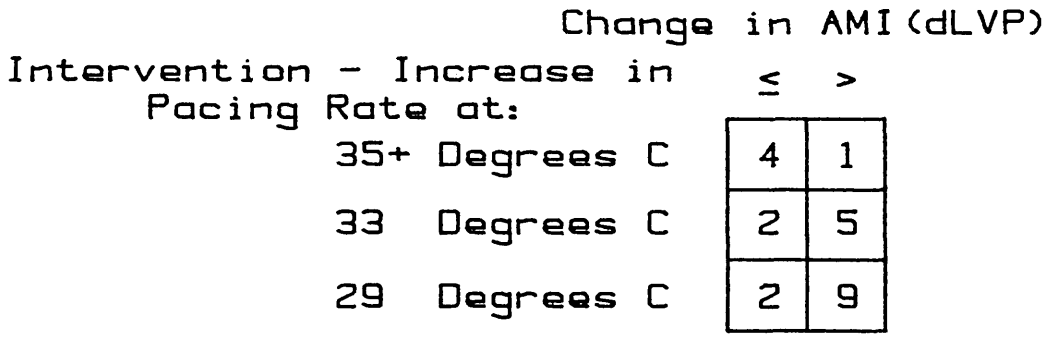

Figure 7.15: Change in AMI(dLVP) versus Heart Rate at Three Temperatures

7.5 Discussion of the Physiologic Model

7.5.1 Overview

The physiologic model provided a complex representation of the heart from which the relationships between electrical alternans, mechanical alternans and the susceptibility of the ventricles to fibrillate could be studied. The results of this model show that electrical-mechanical alternation of the heart provides a reliable measure of ventricular stability. As alternation increases (decreases) the susceptibility to fibrillation likewise increases (decreases). As was the case with the finite-element model three important concepts have been advanced by the model: 1) a regime of alternation was found in both the electrical and mechanical waveforms as the model progressed from a normal rhythm towards a fibrillatory rhythm, 2) the magnitude of the alternation was positively correlated with the susceptibility of the ventricles to fibrillate (as measured by core temperature and the VFT test), and 3) the electrical and mechanical alternans seem to be the result of a single mechanism.

7.5.2 The Effect of Temperature on Myocardial Stability

Numerous investigators (Adam et al., 1984; Covino and D'Amato, 1962; Smith, 1985; Smith et al., 1985; Warner et al., 1970) have shown the ventricle to be more susceptible to fibrillation during the hypothermic state. In the physiologic model, this instability was consistently accompanied by both electrical and mechanical alternans.

Thus, a regime of alternation was once again found during the transition from a normal rhythm towards a chaotic rhythm.

Figures 7.4-7.6 show further that the transition from a normal rhythm towards fibrillation appears to be gradual. At the normothermic temperature, little or no alternation was present in any of the analyzed data forms. As core temperature was decreased, the degree of alternation increased. Alternation peaked at the minimum temperature of 29 degrees C. Upon rewarming, the heart returned to a more stable state and the alternation diminished. Thus, alternation of the heart served as a reliable measure of the relative stability of the heart.

The results of the physiologic model also show that electrical and mechanical alternans seem to provide a similar measure of ventricular stability. Figure 7.7 shows that all of the electrical and mechanical data correlate well with temperature. Any of the physiologic waveforms observed could be used undependently to evaluate ventricular stability. The two forms consistently performed in an analogous fashion. This suggests that a single underlying mechanism was responsible for both the electrical and the mechanical alternation. As in the case of the finite element model data, when alternation was detected in a pressure waveform, the magnitude of the alternans seemed to be amplified in the pressure derivative. This may be due to the fact that the derivative mutes the mean value of the wave, thus providing a smaller mean wave energy by which the alternation is normalized.

7.5.3 The Effect of Hypothermia and Rapid Atrial Pacing on Myocardial Stability

Information in the literature has espoused the independent roles of rapid pacing and hypothermia on ventricular stability. Rapid atrial pacing has been shown to decrease ventricular stability. The decrease in stability can be explained as follows; as the heart rate increases, a concomitant decrease in cellular refractory periods and dispersion is experienced, resulting in increased stability (Han et al., 1966). In the terminology of this thesis, the above is understood as; although T (inverse of the heart rate r) decreases, concomitant decreases in σ and $\bar{\tau}$ cause a net decrease in the F population. Thus, there is less substrate available for reentry and stability is increased. The above relationship was established at a normothermic temperature only.

The results of the physiologic model show that the effect of pacing rate on stability is a function of temperature. This result is shown in Figure 7.15, where changes in AMI(dLVP) are dependent upon increases in heart rate for a given temperature at the $p<0.051$ level of significance (chi-squared statistic). In the normothermic temperature range (35+ degrees C) the trend of the data is precisely that of the literature - an increase in pacing rate results in a decrease (or no change) in vulnerability. Yet, at the extreme hypothermic level (29 degrees C) the opposite trend is observed. If the chi-squared statistic is computed from the two temperature extremes only, then the changes in AMI(dLVP) are dependent upon temperature at the $p<0.018$ level of significance.

The above observations suggest that in the hypothermic state the effect of rapid pacing is to cause a net decrease in ventricular

stability. The interplay between T, σ and $\bar{\tau}$ is such that the F population is increased by rapid pacing. Thus, stability is decreased.

7.5.4 VFT and Myocardial Stability

Although the significance of changes in VFT to changes in temperature was not strong ($p<0.134$), this can be attributed to the small number of VFT determinations. In particular, a single datum point (denoted "X" in Figure 7.5) accounts for both of the off-diagonal entries in the two-by-two contingency table of Figure 7.11. Information from the literature (Adam et al., 1984; Covino and D'Amato, 1962; Smith, 1985; Smith et al., 1985; Warner et al., 1970) suggests that additional observations might prove this datum point to be spurious.

Chapter VIII

Final Discussion

8.1 Alternation and the Susceptibility to Ventricular Fibrillation

Both the finite element computer model and the physiologic model unify the theory that a state of alternation of the heart consistently precurses the fibrillatory state. In the healthy heart, little or no alternation is detected. As the heart is stressed, alternation in both electrical and mechanical activity is observed. The magnitude of the alternans increases as the heart is progressively stressed. Eventually, the heart activity degenerates to fibrillation.

Results from the computer model show that the development of an F population is sufficient to advance the model from the normal stage into the fibrillatory stage. In fact, the relative size of the F population was accurately reflected in the magnitude of alternation. In the animal model, a reduction in core temperature was the sufficient intervention which advanced the model from the normal stage towards the fibrillatory stage. The relative susceptibility of the heart to fibrillation was accurately reflected in the magnitude of alternation. Thus, in the models studied, alternation of the heart provided a reliable graded measure of ventricular stability. As alternation increased, stability decreased, and vice versa.

8.2 Electrical-Mechanical Alternans

The two models of alternation studied within this thesis both show a strong bond between electrical alternation and mechanical alternation. In particular, electrical and mechanical alternation were consistently either both present or both absent. When present, the degree of the two alternans forms tracked each other well. This suggests that a single underlying mechanism is responsible for both the electrical and the mechanical alternation.

From these results, it might be expected that the incidence of combined electrical-mechanical alternation might be a more common phenomenon than is noted in the literature. Two principle arguments support this claim. First, a large portion of investigators limit their study of alternation to either the mechanical or electrical aspect. They do not look for combined alternation. For example, in 1967 Badeer et al. studied the effects of pacing rate on pulsus alternans. They presented a figure, shown in Figure 8.1A, displaying pulsus alternans. No ECG alternans was noted, but ECG data was included with the figure. Figure 8.1B is an enlarged, retraced segment of the figure of Badeer et al. In the enlarged view, electrical alternation in the height of the QRS complex is easily observed. Thus, it is possible that electrical alternans may have accompanied the mechanical alternation.

The second reason why combined electrical-mechanical alternans may not be noted is that a statistically significant alternation can contain only a few parts per million of the total energy of the waveform. Visual observation of such small alternation is not possible. Thus, in the absence of a subtle detection algorithm, alternation may be missed.

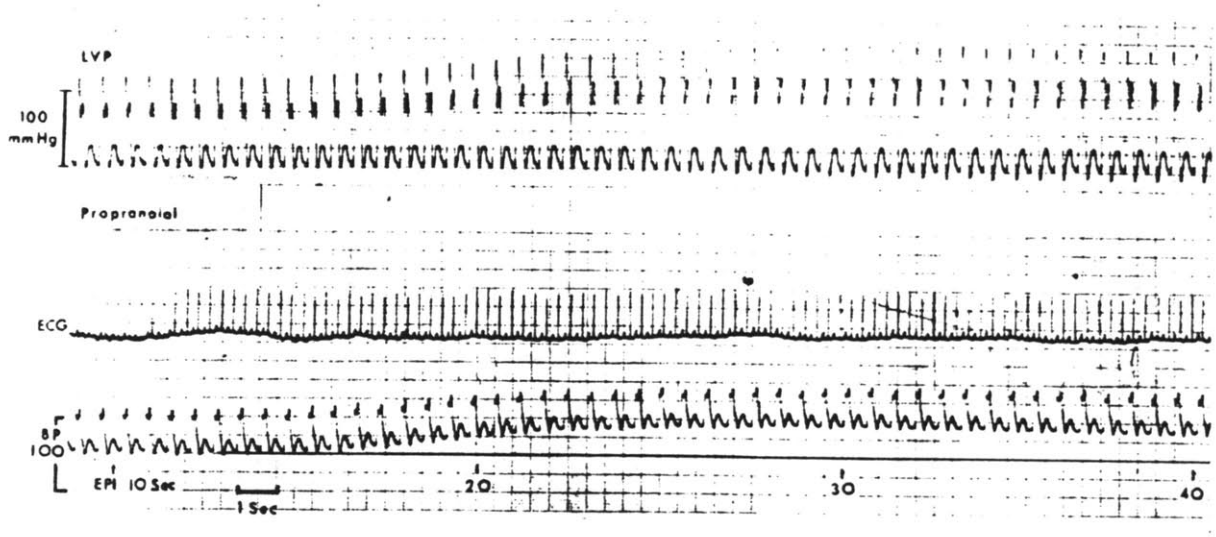

(A)

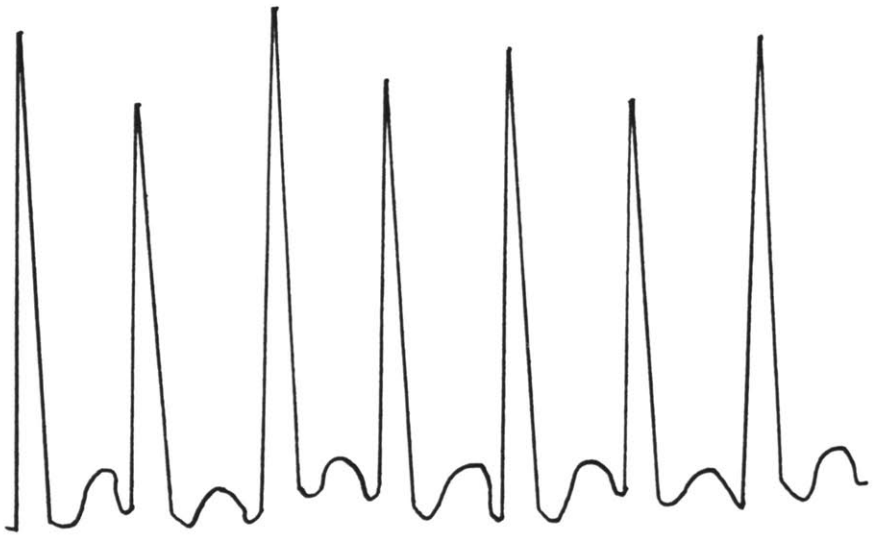

(B)

Figure 8.1: Alternans Data of Badeer et al. (1967)

Figure A shows the results of Badeer et al. (1967) displaying pulsus alternans. An enlarged view of the ECG data, shown in figure B, displays electrical alternans. (From Badeer et al., 1967)

8.3 Mechanism of Alternation of the Heart

This thesis has provided considerable evidence that an alternation in the electrical and mechanical activity of the heart can be the result of a single underlying mechanism - a population of elements which, because of their long refractory periods, cause a spatial-temporal alternation in the contour of the heart beat. According to this theory, the sequencing of depolarization/ repolarization alternates between two different pathways. Thus, both electrical and mechanical alternans result. The finite-element model showed that this mechanism for alternation can produce electrical and mechanical waveforms which contain an identical trend of alternation. Electrical and mechanical alternans were always found together. The degree of the alternation was closely correlated to the intervention. In the physiologic model, electrical and mechanical alternation followed the same trend.

This mechanism for alternation also accounts for the increased susceptibility to fibrillation found during alternation. As the F population increased, the substrate for wavefront fractionation increased. Thus, both the waveform alternation and the susceptibility to fibrillation are expected to increase.

Note that although much evidence has been provided to support populational effects as the mechanism for alternation, other mechanisms for alternation have not been disproved. In the finite-element model, only populational effects were allowed - the individual element response could not change and there was no global movement of the heart. In the physiologic model, global movement of the heart within the chest could not be a result of pericardial effusion since the pericardial sac was

only loosely approximated when the surgical wound was closed. Thus, fluid could not fill the sac.

8.4 Implications to Research and Medicine

The most fundamental question can now be asked: Is alternation of the heart an identifier of the substrate of SCD? A complete solution to this question can not be answered by this thesis. This thesis has, however, provided some insight into the use of alternation of the heart as a marker of ventricular stability. A reduction in the core temperature of the dog, an intervention which is known to increase the susceptibility to VF, was consistently accompanied by electrical and mechanical alternation of the heart. The degree of alternation was related to the degree of hypothermia.

Three major barriers (at least) remain before alternation can be used to identify the individual at risk for SCD. First, hypothermia as a destabilizing intervention may or may not emulate the true substrate of the SCD patient. The use of the alternans technique must be validated on an accurate model of the SCD patient. Second, the alternans quantification process presently requires paced data. As this is an invasive requirement, application of the technique on the general population is impossible. Development of a technique in which unpaced data can be used must progress. Third, alternation was shown to provide a measure of the relative stability of the heart. Stability was shown to increase or decrease. Absolute measures of stability must be developed if the individual at risk for SCD is to be identified.

Further research must continue to evaluate both electrical and mechanical alternation. The models used within this thesis found both forms to be a similar measure of ventricular stability. Other models - most importantly the patient susceptible to SCD - may prove that the

combined evaluation of electrical and mechanical alternans provides the most information as to the stability of the heart.

8.5 Directions For Future Research

The finite element heart model is clearly limited in its ability to emulate the complex electrical and mechanical properties of the in situ cardiovascular system. At the basic level of the element, activity has been modeled by discrete ON/OFF states. Independent, continuous action potential and length-tension relations would be more appropriate. Such a model would allow the investigation of alternation in individual element response to excitation as a mechanism of alternation. The details of the cardiac conduction system have in no way been included in the model. In that the His-Purkinje network is suspected of having longer refractory periods than the remaining ventricular myocardium (Moore et al., 1965), alternation, reentry, and thus VF might be expected to be initiated therein. Mechanically, the anatomic details of ventricular contraction have also been greatly simplified. Recall that contraction was limited to concentric contractions of a given ring with no interplay between adjacent rings. Releasing this constraint, as well as constructing a more anatomically accurate heart contour, would provide a more meaningful mechanical representation of the heart.

The physiologic model can also be advanced. The direct measurement of ventricular volume would allow calculation of the volume-pressure ratio. Also, different interventions must be employed if alternans is to be shown as an identifier of the substrate for fibrillation. Finally, clinical data supporting the relationship between alternation and the susceptibility to fibrillation must be presented.

Chapter IX

Conclusion

This thesis has advanced the body of knowledge which theorizes that a spatial-temporal alternation in the contour of the heart beat may produce a measure of the instability of the cardiac rhythm. The long refractory periods of these elements cause a depolarizing wavefront of excitation to travel around refractory islands of tissue. Wavefront fractionation results. Severe wavefront fractionation can lead to VF. Smith and Cohen (1984) had previously shown in a finite-element model of the heart that electrical alternans consistently preceded any frank rhythm disturbance. In an animal model, Adam et al. (1984), Smith (1985) and Smith et al. (1985) showed an inverse correlation between the degree of alternation present in the ventricular surface ECG and the electrical stability of the heart (as measured by the VFT test). Thus, as alternation increased, stability decreased.

This thesis has proposed that if electrical alternation is the result of a spatial-temporal alternation in the contour of the heart beat, then the mechanical action of the heart should alternate as well. This mechanical alternans will be reflected in the blood pressure, blood volume and contractility waveforms. A finite-element model of the heart, electrically similar to the model of Smith and Cohen (1984), was constructed. This model simulated both the electrical and mechanical activity of the heart. Additionally, a physiologic model of the heart (acute anesthetized dog) was employed. Physiologic signals of blood pressure and ECG were monitored. The degree of alternation in the waveforms of both models were quantified by the subtle detection algorithm of Smith (1985). Both models found 1) a regime of combined electrical-mechanical alternans during the transition from a normal rhythm towards a fibrillatory rhythm, 2) the detected degree of

alternation was correlated with the relative instability of the rhythm, and 3) the electrical and mechanical alternans may be the result of a single underlying mechanism. All of these findings are consistent with the theory of a spatial-temporal alternation in the contour of the heart beat.

Chapter X

References

References

1. Adam, D. R., Akselrod, S., and Cohen, R. J., "Estimation of Ventricular Vulnerability to Fibrillation Through T-Wave Time Series Analysis," Computers in Cardiology, pp. 307-310 IEEE Press, (September, 1981).

2. Adam, D. R., Powell, A. O., Gordon, H., and Cohen, R. J., "Ventricular Fibrillation and Fluctuations in the Magnitude of the Repolarization Vector," Computers in Cardiology, pp. 241-244 IEEE Press, (1982).

3. Adam, D. R., Smith, J. M., Akselrod, S., Nyberg, S., Powell, A. O., and Cohen, R. J., "Fluctuations in T-Wave Morphology and Susceptibility to Ventricular Fibrillation," Journal of Electrocardiology, Vol. **17**, (3) pp. 209-218 (1984).

4. Adler, D., Wong, A. Y. K., and Mahler, Y., "Model of Mechanical Alternans in the Mammalian Myocardium," Journal of Theoretical Biology, Vol. **117**, pp. 563-577 (1985a).

5. Adler, D., Wong, A. Y. K., Mahler, Y., and Klassen, G. A., "Model of Calcium Movements in the Mammalian Myocardium: Interval-Strength Relationship," Journal of Theoretical Biology, Vol. **113**, pp. 379-394 (1985b).

6. Allen, D. G., "On the Relationship Between Action Potential Duration and Tension in Cat Papillary Muscle," Cardiovascular Research, Vol. **11**, pp. 210-218 (1977).

7. Badeer, H. S., Ryo, U. Y., Gassner, W. F., Kass, E. J., Cavaluzzi, J., Gilbert, J. L., and Brooks, C. McC., "Factors Affecting Pulsus Alternans in the Rapidly Driven Heart and Papillary Muscle," American Journal of Physiology, Vol. **213**, (5) pp. 1095-1101 (1967).

8. Berne, R. M. and Levy, M. N, Cardiovascular Physiology, The C. V. Mosby Company, St. Louis, Missouri (1981).

9. Bogen, D. K., Rabinowitz, S. A., Needleman, A., McMahon, T. A., and Abelmann, W. A., "An Analysis of the Mechanical Disadvantage of Myocardial Infarction in the Canine Left Ventricle," Circulation Research, Vol. **47**, pp. 728-741 (1980).

10. Boyett, M. R. and Jewell, B. R., "Analysis of the Effects of Changes in Rate and Rhythm Upon Electrical Activity in the Heart," Prog. Biophys. Molec. Biol., Vol. **36**, pp. 1-52 (1980).

11. Braveny, P., "The Relation of Alternating Contractility of the Heart to the Inotropic Effects of Rhythm," Archives Internationales de Physiologie et de Biochimie, Vol. **72**, (4) pp. 553-566 (1964).

12. Brody, J. G. and Rossman, P. L., "Electrical Alternans: Report of Two Additional Cases," Journal of the American Medical Association, Vol. **108**, (10) pp. 799-802 (March 6, 1937).

13. Carlson, C. J. and Rapaport, E., "Postextrasystolic Pulsus Alternans and Heart Rate," American Journal of Physiology, Vol. **246**, pp. H245-H249 (1984).

14. Caro, C. G., Pedley, T. J., Schroter, R. C., and Seed, W. A., The Mechanics of the Circulation, Oxford University Press, New York, NY (1978).

15. Cohn, K. E., Sandler, H., and Hancock, E. W., "Mechanisms of Pulsus Alternans," Circulation, Vol. **36**, pp. 372-380 (September 1967).

16. Colvin, J., "Electrical Alternans: Case Report and Comments on the Literature," American Heart Journal, Vol. **55**, (4) pp. 513-517 (April 1958).

17. Covino, B. G. and D'Amato, H. E., "Mechanism of Ventricular Fibrillation in Hypothermia," Circulation Research, Vol. **10**, pp. 148-155 (February 1962).

18. Cranefield, P. F., Wit, A. L., and Hoffman, B. F., "Genesis of Cardiac Arrhythmias," Circulation, Vol. **67**, pp. 190-204 (January 1973).

19. D'Amato, H. E., Kronheim, S., and Covino, B. G., "Cardiovascular Functions in the Dog Rewarmed Rapidly and Slowly from Deep Hypothermia," American Journal of Physiology, Vol. **198**, (2) pp. 333-335 (1960).

20. Eisenberg, M. S., Bergner, L., Hallstrom, A. P., and Cummins, R. O., "Sudden Cardiac Death," Scientific American, Vol. **254**, (5) pp. 37-43 (May 1986).

21. Ellis, C. H., "Coexisting Mechanical and Electrical Alternation in Drug-Induced Pulsus Alternans in Dogs," American Journal of Physiology, Vol. **198**, (2) pp. 327-332 (1960).

22. Euler, D. E. and Moore, E. N., "Continous Fractionated Electrical Activity After Stimulation of the Ventricles During the Vulnerable Period: Evidence for Local Reentry," American Journal of Cardiology, Vol. **46**, pp. 783-791 (November 1980).

23. Feigenbaum, M. J., "Universal Behavior in Nonlinear Systems," Los Alamos Science, Vol. **Summer 1980**, pp. 4-27 (1980).

24. Floyd, W. L. and Dillon, M. L., "Observations on Sustained Pulsus Alternans During Hypothermia," American Heart Journal, Vol. **73**, (6) pp. 765-776 (June 1967).

25. Frank, O., Zeitschrift fur biologie, Vol. **37**, p. 483 (1888).

26. Gaffney, F. A., Keller, A. M., Peshock, R. M., Lin, J., and Firth, B. G., "Pathophysiologic Mechanisms of Cardiac Tamponade and Pulsus Alternans Shown by Echocardiography," American Journal of Cardiology, Vol. **53**, pp. 1662-1666 (1984).

27. Gilbert, J. L., Janse, M. J., Lu, H. H., Pinkston, J. O., and Brooks, C. McC., "Production and Abolition of Alternation in Mechanical Action of the Ventricle," American Journal of Physiology, Vol. **209**, (5) pp. 945-950 (1965).

28. Gleason, W. L. and Braunwald, E., "Studies on Starling's Law of the Heart: VI. Relationships between Left Ventricular End-Diastolic Volume and Stroke Volume in Man with Observations on the Mechanism of Pulsus Alternans," Circulation, Vol. **25**, pp. 841-848 (May 1962).

29. Goldberger, A. L., Shabetai, R., Bhargava, V., West, B. J., and Mandell, A. J., "Nonlinear Dynamics, Electrical Alternans, and Pericardial Tamponade," Americal Heart Journal, Vol. **107**, (6) pp. 1297-1299 (June 1984).

30. Grumbach, M. P., "Computer Simulation of Fibrillation Threshold Measurements and Electrophysiologic Testing Procedures," S. B. Thesis, M. I. T. (1986).

31. Guntheroth, W. G., Morgan, B. C., McGough, G. A., and Scher, A. M., "Alternate Deletion and Potentiation as the Cause of Pulsus Alternans," American Heart Journal, Vol. **78**, (5) pp. 669-681 (November 1969).

32. Hada, Y., Wolfe, C., and Craige, E., "Pulsus Alternans Determined By Biventricular Simultaneous Systolic Time Intervals," Circulation, Vol. **65**, (3) pp. 617-626 (1982).

33. Hamburger, W. W., Katz, L. N., and Saphir, O., "Electrical Alternans: A Clinical Study with a Report of Two Necropsies," Journal of the American Medical Association, Vol. **106**, (11) pp. 902-905 (March 14, 1936).

34. Hamer, A., Vohra, J., Hunt, D., and Sloman, G., "Prediction of Sudden Death by Electrophysiologic Studies in High Risk Patients Surviving Acute Myocardial Infarction," American Journal of Cardiology, Vol. **50**, pp. 223-229 (August 1982).

35. Han, J., "Ventricular Vulnerability During Acute Coronary Occlusion," The American Journal of Cardiology, Vol. **24**, pp. 857-864 (December 1969).

36. Han, J., Millet, D., Chizzonitti, B., and Moe, G. K., "Temporal Dispersion of Recovery of Exitability in Atrium and Ventricle as a Function of Heart Rate," American Heart Journal, Vol. **71**, (4) pp. 481-487 (April 1966).

37. Han, J. and Moe, G. K., "Nonuniform Recovery of Excitability in Ventricular Muscle," Circulation Research, Vol. **14**, pp. 44-60 (January 1964).

38. Hashimoto, H., Suzuki, K., Miyake, S., and Nakashima, M., "Effects of Calcium Antagonists on the Electrical Alternans of the ST Segment and on Associated Mechanical Alternans During Acute Coronary Occusion in Dogs," Circulation, Vol. **68**, (3) pp. 667-672 (1983).

39. Hasin, Y., Sarel, O., and Rogel, S., "Electrical and Mechanical Response in Biventricular Mechanical Alternans," Archives Internationales de Physiologie et de Biochimie, Vol. **87**, pp. 19-28 (1979).

40. Hellerstein, H. K. and Liebow, I. M., "Electrical Alternation in Experimental Coronary Artery Occlusion," American Journal of Physiology, Vol. **160**, pp. 366-374 (1950).

41. Hoffman, B. F. and Cranefield, P. F., Electrophysiology of the Heart, McGraw-Hill Book Company, New York, NY (1960).

42. Hogancamp, C. E., Kardesch, M., Danforth, W. H., and Bing, R. J., "Transmembrane Electrical Potentials in Ventricular Tachycardia and Fibrillation," American Heart Journal, Vol. **57**, (2) pp. 214-222 (February 1959).

43. Horowitz, L. N. and Morganroth, J., "Can We Prevent Sudden Cardiac Death?," American Journal of Cardiology, Vol. **50**, pp. 535-538 (1982).

44. -, HST090 Class Notes (Unpublished), Massachusetts Institute of Technology, Cambridge, MA (Spring 1985).

45. Kannel, W. B., Doyle, J. T., McNamara, P. M., Quickenton, P., and Gordon, T., "Factors Related to the Incidence of Sudden Death," Circulation, Vol. **51**, pp. 606-613 (April 1975).

46. Kannel, W. B. and Thomas, H. E. Jr., "Sudden Coronary Death: The Framingham Study," Annals of the New York Academy of Sciences, Vol. **382**, pp. 3-21 (1982).

47. Katz, A. M., Physiology of the Heart, Raven Press, New York, NY (1983).

48. Kavaler, F., "Membrane Depolarization as a Cause of Tension Development in Mammalian Ventricle Muscle," American Journal of Physology, Vol. **197**, (5) pp. 968-970 (1959).

49. Kleinfeld, M. and Stein, E., "Electrical Alternans of Components of Action Potential," Americal Heart Journal, Vol. **75**, (4) pp. 528-530 (April 1968).

50. Kleinfeld, M., Stein, E., and Kossman, C. E., "Electrical Alternans with Emphasis on Recent Observation Made by Means of Single-Cell Electrical Recording," Americal Heart Journal, Vol. **65**, (4) pp. 495-500 (April 1963).

51. Koch-Weser, J., "Effect of Rate Changes on Strength and Time Course of Contraction of Papillary Muscle," American Journal of Physiology, Vol. **204**, (3) pp. 451-457 (1963).

52. Lewis, T., "Notes Upon Alternation of the Heart," Quarterly Journal of Medicine, Vol. **4**, pp. 141-145 (1910).

53. Lown, B., "Sudden Cardiac Death: The Major Challenge Confronting Contempory Cardiology," The American Journal of Cardiology, Vol. **43**, pp. 313-328 (February 1979).

54. Lu, H., Lange, G., and Brooks, C. McC., "Comparative Studies of Electrical and Mechanical Alternation in Heart Cells," Journal of Electrocardiology, Vol. **1**, (1) pp. 7-17 (1968).

55. McGaughey, M. D., Maughan, W. L., Sunagawa, K., and Sagawa, K., "Alternating Contractility in Pulsus Alternans Studied in the Isolated Canine Heart," Circulation, Vol. **71**, (2) pp. 357-362 (1985).

56. McGregor, M. and Baskind, E., "Electric Alternans in Pericardial Effusion," Circulation, Vol. **11**, (6) pp. 837-843 (June 1955).

57. Mitchell, J. H., Sarnoff, S. T., and Sonnenblick, E. H., "The Dynamics of Pulsus Alternans: Alternating End-Diastolic Fiber Length as a Causative Factor," Journal of Clinical Investigation, Vol. **42**, (1) pp. 55-63 (1963).

58. Moore, E. N., Preston, J. B., and Moe, G. K., "Durations of Transmembrane Action Potentials and Functional Refractory Periods of Canine False Tendon and Ventricular Myocardium: Comparisons in Single Fibers," Circulation Research, Vol. **17**, pp. 259-273 (September 1965).

59. Moore, E. N. and Spear, J. F., "Electophysiologic Studies on the Initiation, Prevention, and Termination of Ventricular Fibrillation," Cardiac Electrophysiology and Arrhythmias, Vol. **35**, Grune and Stratton, (1985).

60. Moore, E. N. and Spear, J. F., "Ventricular Fibrillation Threshold," Archives of Internal Medicine, Vol. **135**, pp. 446-453 (1975).

61. Morgan, J. P., Chesebro, J. H., Pluth, J. R., Puga, F. J., and Schaff, H. V., "Intracellular Calcium Transients in Human Working Myocardium as Detected With Aequorin," Journal of the American College of Cardiology, Vol. **3**, (2) pp. 410-418 (February 1984).

62. Nakashima, M., Hashimoto, H., Kanamaru, M., Nagaya, T., Hashizume, M., and Oishi, H., "Experimental Studies and Clinical Report on the Electrical Alternans of ST Segment During Myocardial Ischemia," Japanese Heart Journal, Vol. **19**, (3) pp. 396-408 (May 1978).

63. Navarro-Lopez, F., Cinca, J., Sanz, G., Periz, A., Magrina, J., and Betriu, A., "Isolated T Wave Alternans," American Heart Journal, Vol. **95**, (3) pp. 369-374 (March 1978).

64. Nayler, W. G. and Robertson, P. G. C., "Mechanical Alternans and the Staircase Phenomenon in Dog Papillary Muscle," American Heart Journal, Vol. **70**, (4) pp. 494-498 (October 1965).

65. Patterson, S. W., Piper, H., and Starling, E. H., J. Physiol., Vol. **48**, p. 465 (1914).

66. Patterson, S. W. and Starling, E. H., J. Physiol., Vol. **48**, p. 357 (1914).

67. Puletti, M., Curione, M., Righetti, G., and Jacobellis, G., "Alternans of the ST Segment and T Wave in Acute Myocardial Infarction," Journal of Elecrocardiology, Vol. **13**, (3) pp. 297-300 (1980).

68. Ring, M. E. and Fenster, P. E., "Exercise-Induced ST Segment Alternans," American Heart Journal, Vol. **111**, (5) pp. 1009-1011 (May 1986).

69. Ritzenberg, A. L., Smith, J. M., Grumbach, M. P., and Cohen, R. J., "Precursor to Fibrillation in Cardiac Computer Model," Computers in Cardiology, IEEE Press, (1984).

70. Rosen, M. R., Wit, A. L., and Hoffman, B. F., "Electrophysiology and Pharmacology of Cardiac Arrhythmias. I. Cellular Electrophysiology of the Mammalian Heart," American Heart Journal, Vol. **88**, (3) pp. 380-385 (September 1974).

71. Rozanski, J. J. and Kleinfeld, M., "Alternans of the ST Segment and T Wave. A Sign of Electrical Instability in Prinzmetal's Angina," PACE, Vol. **5**, pp. 359-365 (May-June 1982).

72. Rozanski, J. J., Meller, J., Kleinfeld, M., Castellanos, A., and Kupersmith, J., "Nonmechanical ST-Segment Alternans in Prinzmetal's Angina," Annals of Internal Medicine, Vol. **89**, (1) pp. 76-77 (July 1978).

73. Russell, D. C., Smith, H. J., and Oliver, M. F., "Transmembrane Potential Changes and Ventricular Fibrillation During Repetitive Myocardial Ischaemia in the Dog," British Heart Journal, Vol. **42**, pp. 88-96 (1979).

74. Schwartz, P. J. and Malliani, A., "Electrical Alternation of the T-Wave: Clinical and Experimental Evidence of its Relationship with the Sympathetic Nervous System and with the Long Q-T Syndrome," American Heart Journal, Vol. **89**, (1) pp. 45-50 (January 1975).

75. Seed, W. A., Noble, M. I. M., Walker, J. M., Miller, G. A. H., Pidgeon, J., Redwood, D., Wanless, R., Franz, M. R., Schoettler, M., and Schaeffer, J., "Relationships Between Beat-To-Beat Interval and the Strength of Contraction in the Healthy and Diseased Human Heart," Circulation, Vol. **70**, (5) pp. 799-805 (1984).

76. Sharma, S., Nair, K. G., and Gadekar, H. A., "Romano-Ward Prolonged QT Syndrome with Intermittent T Wave Alternans and Atrioventricular Block," Americal Heart Journal, Vol. **101**, (4) pp. 500-501 (April 1981).

77. Sheperd, J. T. and Vanhoutte, P. M., The Human Cardiovascular System: Facts and Concepts, Raven Press, New York, NY (1980).

78. Sideris, D. A., Nanan, J. N., Papalambrou, J., and Moulopoulos, S. D., "Effect of Pacing Rate and Intensity on Mechanical Alternans Amplitude," Journal of Electrocardiology, Vol. **14**, (3) pp. 289-294 (1981).

79. Smith, J. M., "The Stochastic Nature of Cardiac Electrical Instability: Theory and Experiment," Ph.D. Thesis, M. I. T. (1985).

80. Smith, J. M., Blue, B., Clancy, E., Valeri, C. R., and Cohen, R. J., "Electrocardiographic Morphology as an Indicator of Decreased Cardiac Electrical Stability," Computers in Cardiology, pp. 109-112 (1985).

81. Smith, J. M. and Cohen, R. J., "Simple Finite-Element Model Accounts for Wide Range of Cardiac Dysrhythmias," Proceedings of the National Academy of Science, USA, Vol. **81**, pp. 233-237 (January 1984).

82. Smith, J. M., Ritzenberg, A. L., and Cohen, R. J., "Finite Element Models of Cardiac Dysrhythmias," Proceedings of 1984 Symposium of Mathematics and Computers in Biomedical Applications, National Institute of Health, (1984a).

83. Smith, J. M., Ritzenberg, A. L., and Cohen, R. J., "Simple Computer Model of Cardiac Conduction Disturbances," Computers in Cardiology, pp. 201-204 IEEE Press, (1984b).

84. Sonnenblick, E. H., Braunwald, E., and Morrow, A. G., "The Contractile Properties of Human Heart Muscle: Studies on Myocardial Mechanics of Surgically Excised Papillary Muscles," Journal of Clinical Investigation, Vol. **44**, (6) pp. 966-977 (1965).

85. Spear, J. F. and Moore, E. N., "A Comparison of Alternation in Myocardial Action Potentials and Contractility," American Journal of Physiology, Vol. **220**, (6) pp. 1708-1716 (1971).

86. Spear, J. F., Moore, E. N., and Horowitz, L. N., "Effect of Current Pulses Delivered During the Ventricular Vulnerable Period Upon the Ventricular Fibrillation Threshold," American Journal of Cardiology, Vol. **32**, pp. 814-822 (November 1973).

87. Spodick, D. H., Khan, A. H., and Quarry, V. M., "Systolic and Diastolic Time Intervals in Pulsus Alternans: Significance of Alternating Isovolumic Relaxation," American Heart Journal, Vol. **87**, (1) pp. 5-10 (January 1974).

88. Suga, H. and Sagawa, K., "Instantaneous Pressure-Volume Relationships and Their Ratio in the Excised, Supported Canine Left Ventricle," Circulation Research, Vol. **35**, pp. 117-126 (1974).

89. Suga, H., Sagawa, K., and Shoukas, A. A., "Load Independence of the Instantaneous Pressure-Volume Ratio of the Canine Left Ventricle and Effects of Epinephrine and Heart Rate on the Ratio," Circulation Research, Vol. **32**, pp. 314-322 (March 1973).

90. Sunagawa, K., Burkhoff, D., Lim, K. O., and Sagawa, K., "Impedance Loading Servo Pump System for Excised Canine Ventricle," American Journal of Physiology, Vol. **243**, pp. H346-H350 (1982).

91. Sunagawa, K. and Sagawa, K., "Models of Ventricular Contraction Based on Time-Varying Elastance," CRC Critical Reviews in Biomedical Engineering, Vol. **7**, (3) pp. 193-228 (February 1982).

92. Verrier, R. L., Brooks, W. W., and Lown, B., "Protective Zone and the Determination of Vulnerability to Ventricular Fibrillation," Americal Journal of Physiology, Vol. **234**, (5) pp. H592-H596 (1978).

93. Verrier, R. L. and Lown, B., "Prevention of Ventricular Fibrillation by Use of Low-Intensity Electrical Stimuli," Annals of the New York Academy of Sciences, (1982).

94. Warner, W. A., Anton, A. H., Andersen, T. W., and Swofford, L. J., "Ventricular Fibrillation and Catecholamine Responses During Profound Hypothermia in Dogs," Anesthesiology, Vol. **33**, (1) pp. 43-51 (July 1970).

95. Wayne, V. S., Bishop, R. L., and Spodick, D. H., "Exercise-Induced ST Segment Alternans," Chest, Vol. **83**, (5) pp. 824-825 (May 1983).

96. Wiggers, C. J., "Dynamics of Ventricular Contraction Under Abnormal Conditions," Circulation, Vol. **5**, (3) pp. 321-348 (March 1952).

97. Wiggers, C. J. and Wegria, R., "Ventricular Fibrillation Due to Single, Localized Induction and Condenser Shocks Applied During the Vulnerable Phase of Ventricular Systole," American Journal of Physiology, Vol. **128**, pp. 500-505 (1940).